

**Master's Thesis Report
TVVR 12/5003**

SALINITY INTRUSION INTO THE MAHA OYA ESTUARY AND ASSOCIATED COASTAL WATERWAY



DON CLERANCE DENZIL WEERAKKODY

DIVISION OF WATER RESOURCES ENGINEERING

DEPARTMENT OF BUILDING AND ENVIRONMENTAL TECHNOLOGY

LUND UNIVERSITY



Avdelningen för Teknisk Vattenresurslära

TVVR-12/5003

ISSN-1101-9824

**Salinity Intrusion into the Maha Oya Estuary and Associated
Coastal Waterway**

Author: Don Clerance Denzil Weerakkody

Supervised by: Professor Magnus Larson

Abstract

The Maha Oya (river) originates in the Kandy district of Sri Lanka and travels about 130 km passing four districts to reach the sea at Kochchikade in Sri Lanka. It holds the 3rd largest average annual runoff among the 103 of distinct river basins in Sri Lanka. Its contribution as a fresh water source is of great significance. During year 2004 the river provided five percent of the total production according to the National water supply and drainage board through various intakes along the river. There are many industries located along the river that requires good water quality. The areas in the lower reach of the Maha Oya is urbanized and densely populated. The Maha Oya in the lower reaches has been occupied by many industries, among them, clay mining and sand mining causes adverse effects by changing river morphology in an unfavorable manner. The lower reach of the Maha Oya is in balance with the marine and riverine environmental forcing, though in many situations the river flow dominates over the ocean hydrodynamics. The river connects to the sea through a shallow inlet forming a salt wedge estuary. During low-flow periods, the inlet closes through a sand bar that reduces the open connection to the sea. During average flow conditions, the inlet is about 3-5 m in depth and about 15-30 m in width. Inlet characteristics and river bathymetric conditions vary with time and are highly dependent on the amount of sediments available, because river and inlet dimensions are formed by sand that is transported by the river.

Salinity intrusion in the river seems to be increasing with the human activities and in different climate change scenarios. The development of a salinity intrusion model would be helpful to understand the effect on the river environment from salinity intrusion. Thus, the main objective of the present study was to develop a model of the salinity intrusion in Maha Oya. In order to validate the salinity intrusion model, the hydrodynamics of the estuary and the salinity structure were studied during various field campaigns. Salinity measurements, river flow, tidal inputs, and bathymetry of the river are needed in such validations. The field data showed that the Maha Oya has a stratified salinity structure of wedge type. Being a long narrow channel it may be modeled as a one-dimensional system. The shallowness of the river reasonably well allows for the application of shallow-water wave theories in simulation of tidal waves in the model. Assuming stratification in two layers with sharp interface, the flow equations can be simplified and conveniently solved by finite difference approximations. Vertical mixing at the interface was introduced with a mixing coefficient as a calibration parameter. Two additional calibration parameters are the bottom friction factor and the interfacial friction coefficient. Under the assumptions of densimetric critical flow at inlet, a free upstream boundary with no salt flux, and a river with only fresh water initially, the model simulates the intrusion with the river flow and tidal level as input data. This model is a simple time-varying model that works even in absence of high-tech instruments for data collection.

Key words: Salinity intrusion, the Maha Oya, stratified flow, two-layer model, time-varying model, salt water wedge.

Preface

In estuarine water quality management, salinity intrusion is a major concern that often requires proper solutions to protect the system against deterioration. This natural phenomenon caused by the density difference between sea water and fresh water is governed by hydrodynamic forces induced by tides, wind, ocean waves and current, and river flow, as well as the river bathymetry and the general geomorphology of the area. Surface roughness, water temperature, sediment transport are some other factors that influences the salinity intrusion. Furthermore, the intrusion is often augmented by human activities. If the salinity exceeds a certain level, it does not only damage the estuarine ecosystem but also leads to contamination of the fresh water resources in the vicinity. Solutions can only be achieved by having a good understanding of dominant processes and mechanisms that govern the salinity intrusion. Modeling is one of most popular methods used to organize all gathered information and knowledge in a systematic and objective manner.

Suitable assumptions and simplifications are often necessary in the model development. In this endeavor we tried to develop a conceptual model to simulate salinity intrusion in the Maha Oya, which brings down water from the third largest water basin in Sri Lanka named the Maha Oya basin. The salinity intrusion in the river has reached a critical stage that threatens many aspects, not only the water consumption but also the ecosystem based in and around the river. The effect of salinity intrusion along the river may reach a level that can influence the ground water and cause contamination. Thus, in order to find appropriate solutions to mitigate the present situation and defend the system towards further deterioration, a conceptual salinity intrusion model would be a good tool. For example, through such a model the minimum flow of water to be present in the river to avoid intrusion up to a desired length of the river can be determined, as well as the bathymetric conditions and other relevant morphology to be maintained at the inlet or in the river itself to avoid the intrusion up to pre-specified level.

Acknowledgements

First of all I must pay my gratitude to Sweden for given me an opportunity to follow the Master program in Water Resources through its free education system. Excellent teaching in Lund University was much appreciated.

Special thanks to Professor Magnus Larson who provided technical knowhow and encouragement during the thesis work. Dr Nalin Wikramanayake at the Open University, Colombo, Sri Lanka, devoted his time and directed me in to a successful path concerning the modeling.

Ångpanneföreningen Research Foundation (ÅForsk) is gratefully acknowledged because of their great service by offering scholarships and research grants. Without the scholarship received by ÅForsk I would not have been able to perform this project. They provided me a generous grant promptly.

In the field, the Environmental Foundation Limited in Sri Lanka was the facilitator of the project. Friendly project staff was the members in the field measurement group. Finally I must thank my family for all the encouragement I received.

Contents

1.	Introduction	1
1.1	Background	1
1.2	Objectives.....	3
1.3	Procedure.....	3
2.	Field measurements.....	4
2.1	Salinity measurements.....	4
2.1.1	Sampling methodology	4
2.1.2	Sample collection	4
2.2	River flow and Bathymetry	5
2.2.1	River bathymetry	5
3	Theoretical Bases	6
3.1	Stratified Flows	6
3.2	Salinity Intrusion in Estuaries.....	6
3.3	Salt Water Wedge	7
3.3.1	Densimetric Froude number as a measure of forming salt wedge	8
3.4	Some basic assumptions	8
4.	The Maha Oya Basin	9
4.1	General.....	9
4.1.1	Hydrological characteristics	10
4.1.2	Hydrodynamic conditions	10
4.2	Study Area of the Maha Oya.....	11
4.2.1	Bathymetry of the river.....	11
4.2.2	Salinity structure	11
4.2.3	During high flow season.....	13
4.2.4	Flow data.....	13
4.2.5	Sea level variation and tidal effect.....	14
4.3	Sediment Transport Processes and Morphology of the Maha Oya.....	16
5.	Mathematical Model Development.....	17
5.1	Quasi-steady State	17
5.1.1	Boundary conditions	19
5.2	Unsteady State.....	19

5.3	The Salt Water Layer Dynamics	22
5.3.1	Depth average velocity of the Bottom layer	23
5.4	Entrainment at the interface	24
5.5	Salt transport Equation	25
5.5.1	Density salinity conversion	25
6.	Mathematical Model Implementation	26
6.1	Model Formulation	26
6.1.1	Transformation of Equations	26
6.2	Finite Difference Approximation.....	28
6.3	Discretization	30
6.3.1	River flow	30
6.3.2	Tidal Inputs.....	30
6.3.3	Time steps	31
6.3.4	Length steps	31
6.4	Boundary and initial conditions	31
6.4.1	Downstream.....	31
6.4.2	Upstream	32
6.5	Calibration parameters	32
7.	Model Application.....	33
7.1	Model Testing	33
7.1.1	Simulation of salt wedge propagation of time varying model.....	33
7.1.2	Responds to sudden river discharge variation.....	33
7.1.3	Variation of salt intrusion length with river discharge	34
7.1.4	Variation of salt intrusion length with river depth	35
7.2	Sensitivity Analysis	35
7.2.1	Sensitivity analysis of the steady state model	35
7.2.2	Sensitivity analysis of the time-varying model	36
7.3	Calibration and Validation of the Time Varying Model	37
7.3.1	River flow data used in calibration	37
7.3.2	Calibration results	38
7.3.3	Validation Results.....	40
7.4	Steady-State Model application.....	40

7.4.1 Calibration results	40
8. Discussion.....	42
8.1 Results.....	42
8.1.1 Steady-state model	42
8.1.2 Time-varying model	42
8.2 Problems Related to the Salinity Intrusion in the Maha Oya	42
8.3 Solutions to the Identified Problems	43
8.4 Simulation of Solution.....	43
9. Conclusions	44
Bibliography	46
Appendixes.....	49
Appendix 1: Mat lab codes of the Models.....	49
Appendix 2: Salinity measurements and GPS coordinates (local) of the sampling points	56
Appendix 3: Longitudinal sections of the Maha Oya	64
Appendix 4: Current meter readings and flow calculation at gauge reading 1.62 m.....	67

Figures

Figure 1: Collection of Photographs of the Maha Oya.....	2
Figure 2: Collecting Sample for salinity measurements	5
Figure 3: Schematic structure of saline Wedge with Three major Hydrodynamics Regions described by Sargent and Jirka	8
Figure 4: The Maha Oya Basin.....	9
Figure 5: The Maha Oya at lower section from coastal inlet to salinity barrier:	11
Figure 6: Contour plot of Salinity measurements on 6th April 2011	12
Figure 7: Contour plot of Salinity measurements on 23rd December 2010	13
Figure 8: Hydrograph of the Maha Oya for discharge at Bambukuliya.....	14
Figure 9: Tide chart Colombo.....	15
Figure 10: Seasonal sea level variation at Colombo from October 2005 to August 2006.	15
Figure 11: Schematic diagram showing two-layer counter flow.....	20
Figure 12: Assumed vertical velocity profile in the model	24
Figure 13: Schematic diagram showing discretized tidal input.....	30
Figure 14: Salt wedge propagation with time.....	33
Figure 15: Respond to sudden discharge variation from 25 cum/s to 50 cum/s.....	34
Figure 16: Variation of salt intrusion length with river discharge	34
Figure 17: increases of intrusion length with increases of depth of the River	35
Figure 18: Sensitivity to friction factor.....	36
Figure 19: Sensitivity to bottom friction factor (K_b)	36
Figure 20: Sensitivity to coefficient of interfacial friction factor (c_o)	37
Figure 21: Sensitivity to coefficient of mixing (C_{mix}).....	37
Figure 22: Calibrated model simulation results versus Field condition on day 351 (from 2/10/2011).....	38
Figure 23: Calibrated model simulation results versus field condition on day 366 (from 2/10/2011).....	38
Figure 24: Calibrated model simulation results versus field condition on day 379 (from 2/10/2011).....	39
Figure 25: Calibrated model simulation results versus field condition on day 402 (from 2/10/2011).....	39
Figure 26: Validated model simulation results versus field condition on day 506 (from 2/10/2011).....	40
Figure 27: Validation curve of the Steady-state model	41
Figure 4A: Cross section at the River where current metering was done at Bambukuliya...67	

Tables

Table 1: Hydrological characteristics of the Maha Oya	10
Table 2: Stratification Number (n_s) for salinity measurements.....	12
Table 3: Tidal constituents at locations near the Maha Oya	15

Notations

A = Cross sectional area of the river

B = Width of the river

C_0 = Coefficient of interfacial friction factor

C_{mix} = Coefficient of mixing

F = Froude number

f_i = Interfacial friction factor

i, j = Subset denote space and time

g = Acceleration of gravity

g' = Reduced acceleration due to gravity

h_1, h_2 = Depth of top and bottom layer

h_{1c} = Densimetric critical depth

H = Total height of the water column

H_0 = Amplitude of tidal wave

k = Wave number

K = von Kalman constant

k_h = Eddy diffusivity acting on the stratification

K_i, k_b = Interfacial and bottom friction factor

P = Hydrostatic pressure

q = Lateral inflow per unit area

Q = river discharge

Ri_o = Bulk Richardson number at the interface

S = Salinity

s_0 = Bottom slope

s_b, s_i, s_f = Friction slope due to bottom shear, interfacial shear, and total friction slope, respectively

t = Time

T = Temperature

u, v, w = Velocities in x, y, z directions, respectively

u_1, u_2 = Vertically average velocities of top and bottom layer, respectively

u_b, u_d = Bottom layer velocity at the interface due to tides and density current, respectively

u_∞ = Bottom layer velocity at the interface

w = Width of the inlet mouth

W = Width of the inlet mouth

w_i = Entrainment velocity

x, z = Coordinate along the river and in vertical direction, respectively

z_0 = Bottom roughness length

ρ = Fresh water density

ρ_1, ρ_2 = Density of top and bottom layer, respectively

$\Delta\rho$ = Density difference between salt and fresh water layers

Δu = Velocity difference between layers

μ = viscosity

ω = Angular frequency of tidal wave

τ_i, τ_s, τ_b = Shear stress at the interface, free surface and bottom surface, respectively

1. Introduction

1.1 Background

The Maha Oya river basin is the third largest basin in Sri Lanka in terms of average annual runoff. Starting from Hantane hill of the Kandy district, which is in the upper land area (see chapter 3) with valley slopes and high gradients, it reaches the Indian Ocean in the lower land area that is bounded by a wide floodplain. The Maha Oya is nourished by the First intermonsoon rain (March-April), Southwest monsoon rain (May-September) and Second intermonsoon rain (October-November). The average annual runoff of the Maha Oya is $1.54 \text{ km}^3/\text{year}$ (Amarasinghe and Mutuwatta, 1999). The coastal ecosystem of the Maha Oya comprises estuaries, coastal wetlands, inlets, and beaches. The estuarine ecosystem of the Maha Oya is very important because of its high primary productivity in the coastal food web. The Maha Oya estuary provides breeding ground to many aquatic species. Some sea fish varieties like Caranx and Mullet spawn on mangroves habitat in the estuary.

During the past decades urbanization and industrialization have adversely affected the Maha Oya riverine system. Continuous water quality degradation and changing river morphology by erosion has created a stressful environment among the 1.2 million peoples living by the river. Population density of the lower area of the Maha Oya is $708 \text{ persons}/\text{km}^2$ (Abeywickrama, Lanka Jalani and IWMI2002). Salinity intrusion into the river seems to be increasing as a result of the human activities on the river. Sand mining is one of the major problem causing damage to the river system. There is a risk of contaminating ground water with saline water as well.

The river is often renewed with fresh water during the high flow seasons. River discharge pushes the sea water away from the river. During low flow seasons high concentration of salt water can be found in the bottom of the river, and it decreases towards the free surface. During the driest period (e.g., in January to March, June, July, and December) the inlet may close by a sand bar implying no connectivity with the sea. Inlet dimensions change seasonally in response to the river discharge. The rising and lowering of the water level indicates the response of the river to the tidal variations. Field measurements confirm the existence of stratified salinity structure during average flow conditions. Because of high sediment transport, the sandy river bed changes producing varying river depths.

The study of salinity intrusion would be helpful to prevent future deterioration of the river environment. Salinity intrusion in the Maha Oya estuary can often be described using salt water wedge theory, where two layers of stratified counter flows occur with a sharp interface. Furthermore, the shallowness of the narrow long river corresponds well to one-dimensional conditions. Momentum, continuity, and salt transport equations are the governing equations that describe the situation. Entrainment at the interface has to be included employing appropriate mixing terms. Finite difference approximations can be used to solve the system of equations. Tidal input should be included with shallow water internal wave theory with the assumption that tidally induced velocities are linearly independent with the velocities induced by the density current.

The river is not tidally dominated and upstream it may be described using a boundary condition of no tidal effects and no saline water. At the inlet mouth densimetric critical flow can be assumed. With the absence of lower layer discharge measurements the model needs to be initialized with flood flow conditions. In the Maha Oya this often happens during the high flow period in the months of October to November. A collection of photographs in Figure 1 gives some background information on the Maha Oya.

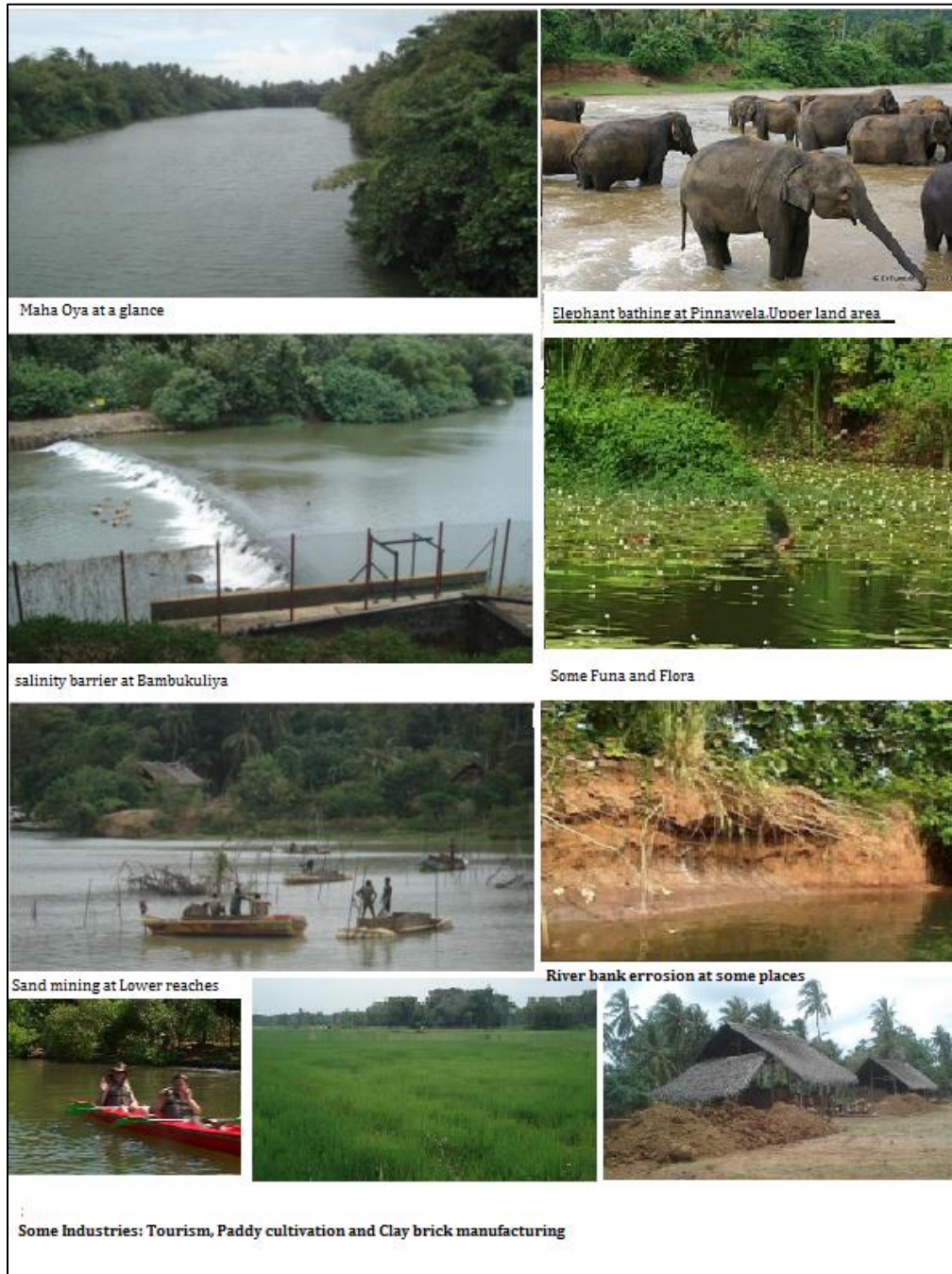


FIGURE 1: COLLECTION OF PHOTOGRAPHS OF THE MAHA OYA

Photographs except *Elephant bathing at Pinnawela* (from *Travelpod* by the courtesy of EFL)

1.2 Objectives

The main objective of the present study is to determine the salinity intrusion from the sea into the Maha Oya estuary, Sri Lanka, and associated coastal waterway, by developing an appropriate mathematical model that works with spatially and timely varying data under reasonable assumptions. In order to develop such a model, a solid understanding of the hydrodynamic characteristics and salinity structure of the system is needed. Possible remedial measures are going to be discussed based on the modeling, compiled information, and field measurements.

1.3 Procedure

A literature review will be performed on stratified flows with focus on salinity intrusion into estuaries and rivers. Two layer counter flow system and salt wedge dynamics are most interesting for the present case. Time-varying river discharge and tidal oscillation are the dynamic components of the input to the model. The basic equations for the shape of a saltwater wedge in a river will be developed. A quasi-steady model is going to be compared with the time varying model, which is developed through an unsteady formulation of the governing equations. Based on the field conditions, suitable assumptions and simplifications may be used in model formulation. A number of simple, schematic cases will first be investigated with the model after which the situation in Maha Oya is going to be simulated. Data on the salinity conditions and river discharge in the Maha Oya and the behavior of the saltwater wedge will be determined through a number of field campaigns. Bathymetric conditions of the river including the inlet area will be recorded and details available from previous surveys are going to be examined. Model simulations will be compared to the observed changes. Past data on discharge conditions are going to be collected from authorities maintaining such records. Finally, the model is going to be developed for the local conditions at the Maha Oya study area.

2. Field measurements

2.1 Salinity measurements

Salinity is the amount of dissolved salt, also known as total dissolved solid (TDS), in a body of water. It is expressed as a weight ratio in part per thousand (ppt) or part per million (ppm). Thus, one ppt means 1 gram of salt in 1 kilogram of water. For practical reasons sometimes salinity is referred to in units of electrical conductivity (EC), because the contribution of charged particles in the solution depends on the amount of salt in the solution. Salinity measurement using a conductivity meter reads salinity in micro Siemens per centimetre ($\mu\text{S}/\text{cm}$). For the comparison of the two units it can be noted that in fresh water salinity is less than 1 ppt or 100 $\mu\text{S}/\text{cm}$ and in sea water it is around 35 ppt or 54000 $\mu\text{S}/\text{cm}$.

During the field measurements salinity were recorded for TDS and EC using CE/TDC/Temperature Tester (Model: HI 98312). Both field temperature and water temperature were recorded using the same tester. This testing apparatus has a maximum measurable range of 20 ppt, hence, the sample at high concentration needs to be diluted with distilled water and the salinity calculated according to dilution ratio. The sampling container should always be cleaned with distilled water after each sampling. All the measurements were recorded in the sample book before proceeding to the next sample. The time is also an important parameter to record in this type of manual sampling. When time passes river flow conditions may change, especially due to tidal variations. In the present study, sampling for salinity were done during the morning during about a six-hour period and some variation may have occurred compared to if simultaneous sampling were done at all locations.

2.1.2 Sampling methodology

Salinity measurements along the river at the sampling points were recorded manually. Looking at the background information and considering the available facilities, sampling points were located a distance of about 250 m apart and fixed with local GPS coordinates (see Annex 2 for the salinity values and point coordinates). Starting from the point at the inlet, measurements proceeded along the river till a sampling point upstream where no salinity was observed. In a sampling day all sampling points were covered. Sampling days were scattered to suit in a wide range of the river flow conditions. At least three set of samples in the surface, middle, and the bottom layer were recorded at each and every location.

2.1.2 Sample collection

A sampler similar to the Bacon Bomb Sampler was used. The sampler has a cylindrical body with plunger at the top (Bacon Bomb sampler has plunger at the bottom) and two wires, one for holding the sampler and another one for pulling to open the plunger to fill the bomb. A wire to hold the sampler is attached to the body of the sampler at the outer surface by means of a frame and a wire used to pull the plunger is attached to the plunger at the end of a metal rod that can be moved along the centre axis of the sampling cylinder. A measuring tape is attached to the holding wire. After positioning the boat at the location, the sampler

is gradually lowered to the prescribed depth by holding the wire while the keeping plunger-opening wire loose. At the sampling depth, the plunger should be opened by pulling the wire in order to allow the filling of the bomb. After the bomb is filled, the plunger opening wire is released to close the plunger by weight of the metal rod, the sample is drawn by wires keeping no tension on the plunger open wire in order to prevent a sudden opening. Figure 2 shows the sampling collection using the sampler.



FIGURE 2: COLLECTING SAMPLE FOR SALINITY MEASUREMENTS

2.2 River flow and Bathymetry

Flow measurements that were employed in generating discharge hydrographs as described in chapter 4.2.4 were done using a current meter at Bambukuliya near to the measuring gauge. The place was selected within the straight reach of the river in order to have straight and parallel stream lines. The bed of the river at the section of measuring was uniform and free of obstacles such as trees and boulders. The river cross section was divided into segments and starting from the left bank current measurements were carried out at several depths. Annex 4 shows the current meter readings and the discharges calculated in the Maha Oya. Figure 4A in the appendix shows the sectioning for the current meter readings. Calculated river discharge at gauge reading 1.62 m was 28.5 cum/s and at 1.78 m it was 40.5 cum/s.

2.2.1 River bathymetry

River bathymetry and other relevant drawings have been provided by the Environmental Foundation limited. Some longitudinal sections for the extent of the study reach are shown in Annex 3.

3 Theoretical Bases

3.1 Stratified Flows

Significant density stratification can be seen in connection with many types of geophysical water flows, for example in lakes and estuaries. These stratified flows with vertical density variations occur mainly due to vertical variation in temperature, chemical composition, suspended particle distribution, and salinity. For stratified flow conditions, the hydrodynamics of the system is governed by the stratification phenomenon. In stratified flows each layer may have different flow conditions controlled by interfacial shear forces between the layers. The flow regime may be in either the laminar or turbulent phase. At low flow rates a smooth interface between the layers can be seen, but with increasing relative velocity between the layers the interface may become unstable. The Richardson number, a dimensionless number defined as ratio of potential to kinetic energy, gives an indication of the stability of stratified flow. In general terms the Richardson number is $Ri = g/\rho (d\rho/dz) / (du/dz)^2$, where g is gravity, ρ is density, u is the velocity, and z is the vertical dimension. In a two-layer flow system the bulk Richardson number, which can be derived by replacing density and velocity gradients by total depth H and the difference between vertically averaged velocities of each layer, is a useful parameter and can be written as $Ri_b = (\Delta\rho/\rho) gH/(\Delta u)^2$. At lower Richardson values, typically below $1/4$, the stratification becomes unstable. With an increase in the flow velocity, turbulent mixing across the stratification lead to a weaker stratification and at higher velocities, the stratification might vanish.

In estuaries having significant tidal influence, an estuarine Richardson number, defined by Fischer (1972a), is more appropriate. It expresses the ratio between the mixing power available from tide and the buoyancy per unit width of the river. In standard notation, the estuarine Richardson number is $Ri = g'Q_f/wur^3$, where g' is $(\Delta\rho/\rho) g$ reduced gravity, Q_f is river flow, w is river width, and u_r is the root-mean-square of the tidal velocity. Again, high values, usually above 0.8, of estuarine Richardson number correspond to strong stratification, whereas small values, below 0.08, represent well-mixed conditions. The degree of stratification due to salinity can also be assessed by a stratification parameter defined as $n_s = (s_b - s_s)/\frac{1}{2}(s_b + s_s)$, where s_b and s_s are the salinity at bottom and top surfaces, respectively. If n_s is less than 0.1 the water column is said to be fully mixed and for n_s in between 1 and 0.1 it is partially mixed. For stratified flow with salt wedge formation the stratification parameter should exceed 1 (Haralambidou, et al 2010). It is clear that mixing and stratification are interdependent. Mixing depends on stratification and flow field, and the stratification in turn depends on mixing.

3.2 Salinity Intrusion in Estuaries

In the simplest form an estuary can be defined as the transition zone between the river environment and the ocean environment, where interaction between salt water and freshwater is taking place. Among the various definitions the most common definition is “an estuary is a semi-enclosed coastal body of water which has a free connection with the open sea and within which sea water is measurably diluted with fresh water derived from

land drainage” (Cameron and Pritchard, 1963). Estuaries are classified according to the topography and salinity structure. According to the topographical classification by Pritchard (1952b) fjords, coastal plain estuaries, and bar built estuaries can be distinguished. Estuaries formed by volcanic eruptions, land slide, and faulting also have different features. Classification of salinity structure is important in order to understand the physical hydrodynamic characteristics of coastal plain estuaries, which are the most common type among the coastal estuaries. Under this category estuaries are classified according to the degree of mixing: “highly stratified or salt wedge type”, “partially mixed” and “well mixed” (Pritchard, 1955; Cameron and Pritchard, 1963). Salinity intrusion in estuaries is governed by their physical hydrodynamic characteristics. River flow, tides, waves, and wind may be the main dominant forcing mechanisms that determine the intrusion and its effects according to the local geomorphology. Tides associate with currents create advection of saline water along the river while improving mixing of saline water. River flow contributes by imposing barotropic longitudinal pressure gradients along the estuary because of its buoyancy. Furthermore, the density difference between fresh and saline water also induce baroclinic pressure gradient along the estuary. River flow is the main opponent against salinity intrusion. It pushes back the salt water front with interfacial shear induced by the river flow. For high flow conditions, the salt water may be washed away. Wind-induced stress also can be a significant local force that prevents salinity intrusion.

Understanding of salinity intrusion by experimental and analytical studies depends on the sea water exchange processes and mixing conditions. Highly stratified, partially mixed with vertical stratification, and fully mixed with no stratification are modeled with different approaches.

3.3 Salt Water Wedge

At estuaries where the river flow dominates over the tidal input there would be high stratification of saline water and fresh water forming a wedge type salt layer. At the mouth of the inlet a thin layer of buoyant fresh water flows on top of the saline water. The saline water moves along the bottom towards the upstream of the river. There will be an interface between the layers and it will touch the bottom of the river at the full length of intrusion. Shear at the interface may create vertical mixing. A salt water wedge can be divided into three subdivisions based on experimental studies to ease the understanding of hydrodynamics of salt water wedge. These are the tip region, quasi-equilibrium region, and exit region (Figure 3). The major portion of the saline wedge, excluding the wedge tip, and the exit regions, is the quasi-equilibrium region in which internal flow properties are nearly similar (Sargent and Jirka, 1987). Although the tip and exit regions are subjected to highly variable conditions, their extension in terms of the intrusion length scale is comparatively small. Therefore the main controlling region for the entire salt water wedge dynamics is the quasi-equilibrium region, where the baroclinic pressure gradient is balanced by the frictional forces.

3.3.1 Densimetric Froude number as a measure of forming salt wedge

The densimetric Froude number is defined as $Fr = u / \sqrt{g'h}$, where g' is the reduced acceleration due to gravity, defined as $g' = g \rho_1 - \rho_2 / \rho$, and u , h are mean velocity and height, respectively. Theoretically, if the densimetric Froude number is larger than 1, no saline wedge will form. In practice it has been shown that salt water wedge will form when densimetric Froude number is less than 0.6. (US Army Corps of Engineers 1993)

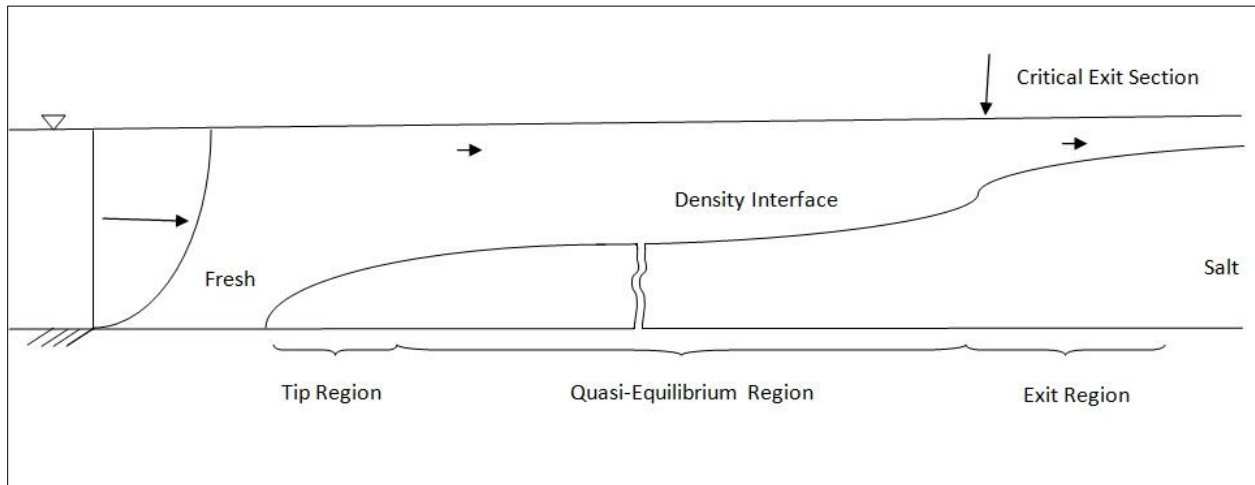


FIGURE 3: SCHEMATIC STRUCTURE OF SALINE WEDGE WITH THREE MAJOR HYDRODYNAMICS REGIONS DESCRIBED BY SARGENT AND JIRKA

3.4 Some basic assumptions

The following listed assumptions are commonly used in developing conceptual models of estuarine hydrodynamics. In the study, Coriolis force can be ignored due to the small extent of the water body being considered. All other assumptions are used to simplify the flow equations in the development of the model.

- Coriolis Effect is negligible.
- No slip at bottom and interface.
- Interfacial shear is equal in magnitude in both layers.
- River bathymetry, inlet characteristics, and other geometrical conditions, as well as environmental conditions that affect the salinity intrusion, remain unchanged, except the river flow during the period of calibration.
- The free surface does not affect the tidal oscillation.
- The river and the inlet mouth have same uniform rectangular cross section
- The flood and ebb tides are symmetrical

4. The Maha Oya Basin

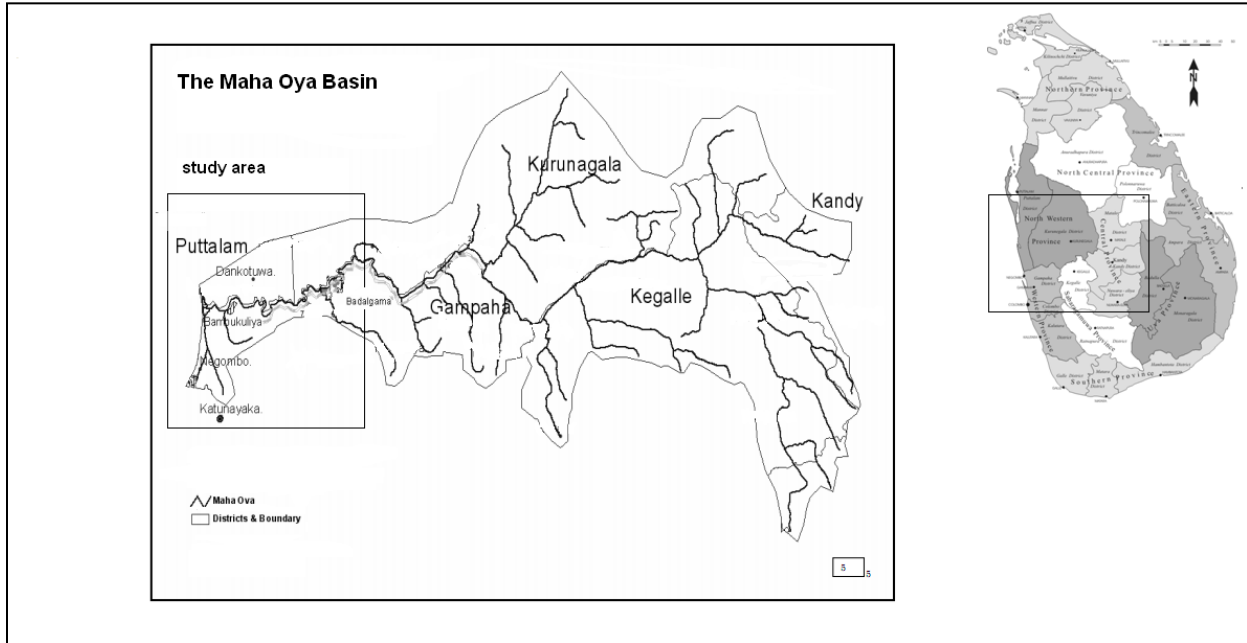


FIGURE 4: THE MAHA OYA BASIN

Source: Fernando (2005). Modified to show study Area

4.1 General

The Maha Oya is the third largest water basin in Sri Lanka. It nourishes the country during its 130 km of journey from upland (at Nawalapitiya, Sri Lanka) to the lower land, where it reaches (at Kochchikade Sri Lanka) the Indian Ocean. It has a drainage area of 1510 square km with an average annual runoff of 1.54 cubic km (Amarasinghe and Mutuwatta, 1999). It provides about 5% of the drinking water production to the country from 17 intakes at various locations established by the National Water Supply and Drainage Board (Fernando, 2005). It provides fresh water for industrial purposes, as well as for agriculture, fisheries, hotels, recreation, and tourism. A valuable aspect of the Maha Oya that needs protection is the biodiversity under a diverse range of ecosystems that comprise riverine, estuarine, and coastal environments. There are many ecologically important natural habitats that can be seen in the ecosystem of the Maha Oya. A variety of lizards, bird species, and fish varieties in the fresh water and lagoon water can be observed. The Maha Oya as a fresh water stream recharges the ground water and helps to keep the water table high in the local areas.

4.1.1 Hydrological characteristics

The Maha Oya is nourished by the First intermonsoon rain (March-April), Southwest monsoon rain (May-September), and Second intermonsoon rain (October-November) as mentioned in the background, but from agricultural perspective the seasonal rainfall consists of two major seasons called Maha season from October to March and Yala season from April to September. Hydrological characteristic in the Maha Oya and other Sri Lankan water basin have been studied using the data source “The Long-term Hydrometeorological Data from Sri Lanka (Nakagawa et al., 1995)”. Seasonal and annual runoffs have been estimated for 75 percent exceedence probability rainfall based on data from 1945 to 1970. It can be shown that 75 percent exceedence probability rainfall can be expected at least three out of every four years in the long run (Amarasinghe, Mutuwatta and Sakthivadivel 1999). The table shows an extract from the study that also includes average value on the annual runoff from the National Atlas of Sri Lanka (Survey Department of Sri Lanka 1988).

TABLE 1: HYDROLOGICAL CHARACTERISTICS OF THE MAHA OYA

Drainage area	Seasonal runoff (P ₇₅)		Estimate annual runoff			Sri Lankan Atlas average
	Maha*	Yala*	P ₇₅	average	P ₅₀	
1510 km ²	0.69 km ³	0.61 km ³	1.31 km ³	1.53 km ³	1.54 km ³	1.61 km ³

* Yala: Season from April to September *Maha: Season from October to March

Source: Amarasinghe, Mutuwatta and Sakthivadivel 1999: Modified to show details of the Maha Oya

4.1.2 Hydrodynamic conditions

The river flow of the Maha Oya reaches its maximum value during the period from October to March usually denoted in Sri Lanka as the “Maha Season” (the country gets maximum rains during the northeast monsoon). This period normally renews the river with fresh water by flushing the salt wedge into the sea.

Stream flow data from 1954 to 1986 at Badalgama has reported the maximum flow in November to be 114.5 cum/s and the minimum flow in February to be 11.4 cum/. The average flow of the Maha Oya is 45.6 cum/s (Ceylon Electricity Board cited in Alwis et al., 1995).

4.2 Study Area of the Maha Oya

The study focuses on the lower part of the stream, because salinity intrusion in the Maha Oya is limited to the lower section of the river. In Sri Lanka, administrative divisions are known as “Divisional secretariat Division”, and the study area covers Negombo, Katana, Wennappuwa, and Dankotuwa Divisional secretariat Divisions. The stream length under the study is about 7 km, because at about 7 km from the inlet there is a salinity barrier that has been built by National Water Supply and Drainage Board to stop salinity intrusion at their water intake.

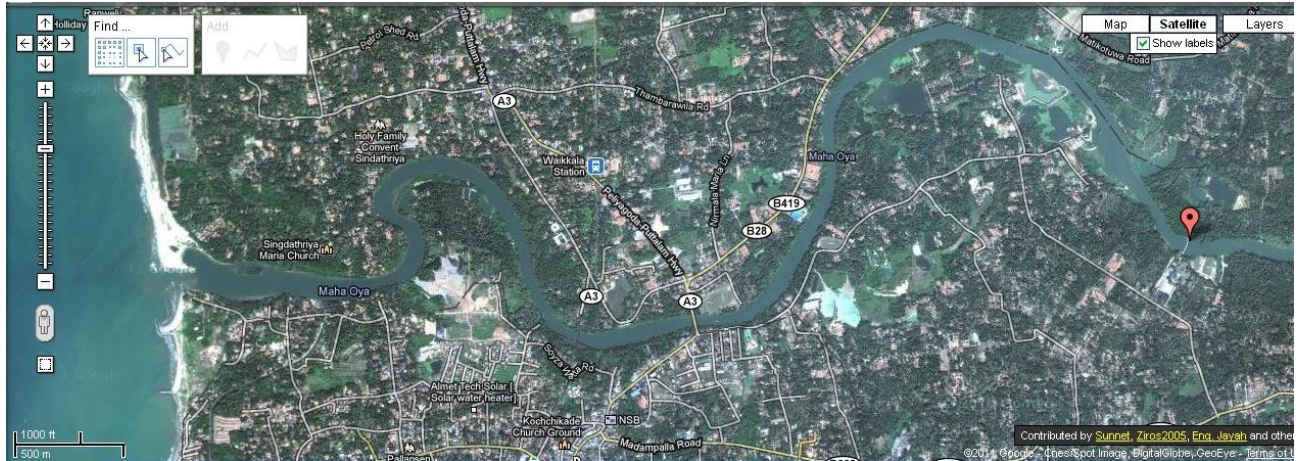



FIGURE 5: THE MAHA OYA AT LOWER SECTION FROM COASTAL INLET TO SALINITY BARRIER:
“  ” Locates salinity barrier at Bambukuliya

Source: Google map

4.2.1 Bathymetry of the river

According to the bathymetric survey data provided by Engineering Foundation Limited (EFL) as attached in Annex4, the average width is 55 m and the average cross-sectional area is 400 sqm. The width at the inlet varies seasonally. It was measured to be 20m on 14th of march 2011, when the salinity measurements were taken. Average depth of the water column in the river was observed to be 3m in this period. Width at free surface can be approximated as 45m on the average, based on the field measurements and the survey data.

4.2.2 Salinity structure

Salinity measurement of the Maha Oya shows the existence of stratification. Table 2 gives the stratification number (n_s) as described in chapter 3.1 at each sampling point for several days of sampling (S_s and S_b are surface and bottom salinity values, respectively). It can be seen that the stratification number on many sampling days exceeded 1, indicating stratified flow conditions. Furthermore, salinity measurements on the 6th of April 2011 have been drawn in Figure 6 as a contour plot in the x-y plane of which the x-axis represents the distance along the river (m) and the y-axis the depth from the free surface (m) with Total Dissolved Solids (TDS) as contours. The stratification is clearly illustrated. The large scale

difference in vertical and horizontal axis of the Figure 6 may mislead, indicating high vertical gradient of salinity. If the plot is drawn in the same scale for both axes the real situation can be observed with small gradients.

TABLE 2: STRATIFICATION NUMBER (n_s) FOR SALINITY MEASUREMENTS

Location	Date:05.01.2011			Date:02.02.2011			Date:14.02.2011			Date:1.03.2011			Date:14.03.2011			Date:06.4.2011			Date:19.07.2011		
	S_s	S_b	n_s	S_s	S_b	n_s	S_s	S_b	n_s	S_s	S_b	n_s	S_s	S_b	n_s	S_s	S_b	n_s	S_s	S_b	n_s
P1	1.75	24.78	1.7	2.26	20.13	1.6	1.03	23.49	1.8	0.8	24.99	1.9	0.58	3.24	1.4	2.37	22.47	1.6	Na		
P2	1.23	16.53	1.7	1.9	21.81	1.7	1.05	18.99	1.8	0.45	21.9	1.9	0.55	18.54	1.9	2.47	24.66	1.6	0.69	20.55	1.9
P3	1.05	26.79	1.8	1.95	12.9	1.5	0.92	27.63	1.9	0.66	23.61	1.9	0.51	19.62	1.9	2.61	22.56	1.6	0.58	21.9	1.9
P4	0.88	25.77	1.9	1.7	23.01	1.7	0.81	29.25	1.9	0.62	18.84	1.9	0.55	16.92	1.9	1.69	24.6	1.7	0.6	24.27	1.9
P5	0.61	27.39	1.9	1.51	26.88	1.8	0.87	26.04	1.9	0.65	24	1.9	0.37	22.26	1.9	1.26	20.49	1.8	0.61	22.17	1.9
P6	0.26	12.81	1.9	0.98	21.06	1.8	0.57	19.77	1.9	0.43	21.96	1.9	0.34	21.06	1.9	0.75	24.42	1.9	0.44	23.04	1.9
P7	0.14	11.79	2.0	0.76	21.45	1.9	0.52	29.16	1.9	0.34	20.01	1.9	0.23	0.69	1.0	0.5	15.39	1.9	0.39	21.33	1.9
P8	0.09	8.69	2.0	0.41	27.33	1.9	0.32	26.46	2.0	0.28	22.5	2.0	0.2	17.64	2.0	0.35	21.51	1.9	0.35	22.98	1.9
P9	0.13	1.11	1.6	0.36	20.37	1.9	0.18	26.22	2.0	0.21	21.81	2.0	0.2	17.16	2.0	0.1	18.96	2.0	0.26	22.26	2.0
P10	0.06	0.06	0.0	0.11	0.26	0.8	0.1	0.75	1.5	0.15	19.35	2.0	0.12	19.56	2.0	0.11	0.1	0	0.21	20.61	2.0

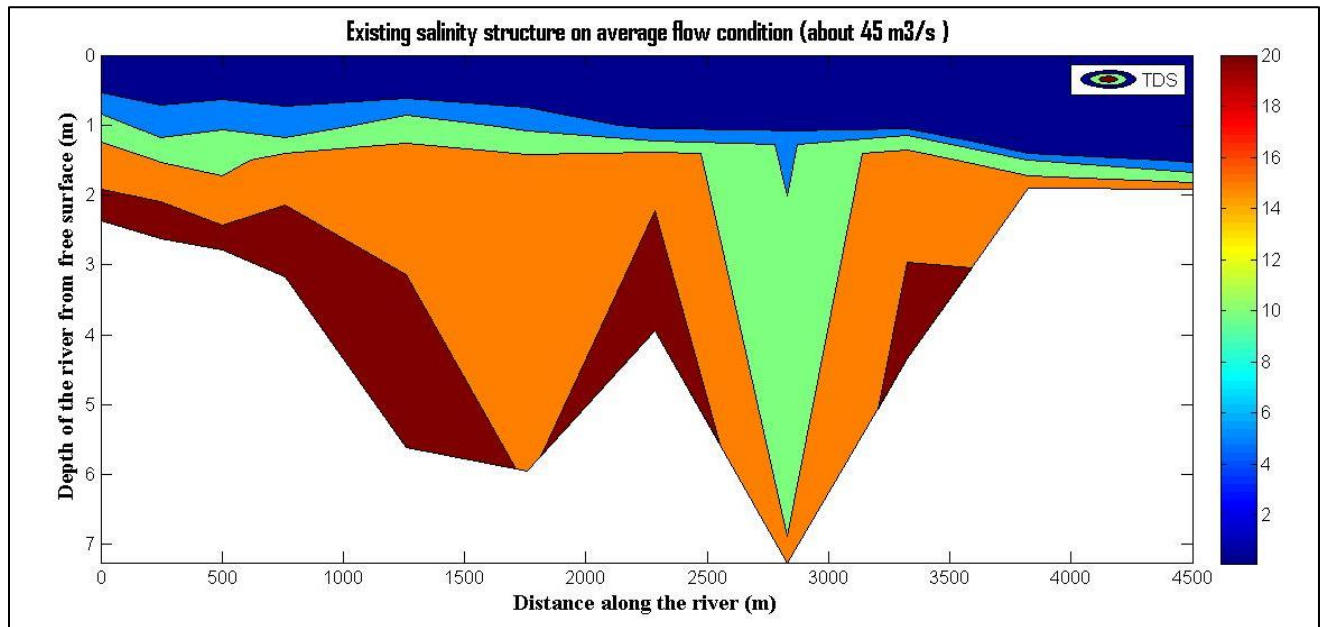


FIGURE 6: CONTOUR PLOT OF SALINITY MEASUREMENTS ON 6TH APRIL 2011

4.2.3 During high flow season

During high flow season, the saline layer is flushed out by the river flow as shown in the Figure 7. Hence, the requirement on the initial condition in the model, implying fresh water in the river, should be fulfilled.

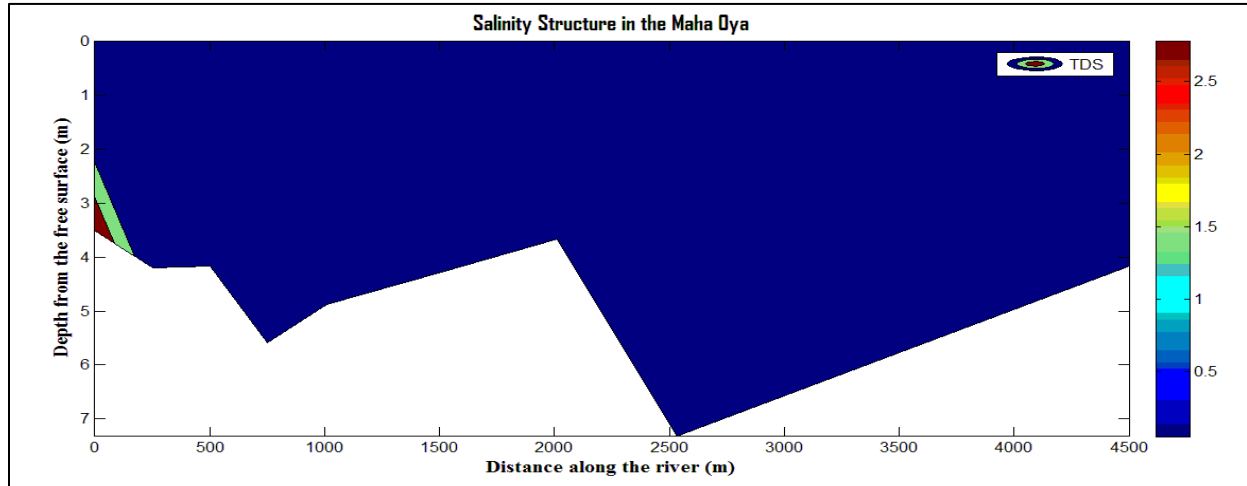


FIGURE 7: CONTOUR PLOT OF SALINITY MEASUREMENTS ON 23RD DECEMBER 2010

4.2.4 Flow data

River flow has been calculated using the gauge reading at Bambukuliya, where no salt water is present. These data are recorded by the National Water Board. Weir height at Bambukuliya (daily measurements of height of the water column above the weir crest) and corresponding current meter readings in the river upstream Bambukuliya were used to establish the discharge characteristic curve for the weir at the Bambukuliya, as described below.

Range of levels in gauge readings has been observed to be between 1.3 m and 3 m. The weir crest level is 1.29 m. The relationship between discharge and gauge height may be expressed as

$$Q = k(H - H_0)^n \quad (4.2.4)$$

Where

Q = Discharge

H = Gauge reading

H_0 = Height of the weir

k , and n = parameters that varies with the local conditions in the river.

With a minimum of two sets of discharge measurements (by current meter readings) for known gauge readings, k and n can be determined.

The discharge generated for the period of 1st September 2010 - 31st August 2011 is displayed in Figure 8. The days when discharge and salinity measurements were carried out are also shown in the figure.

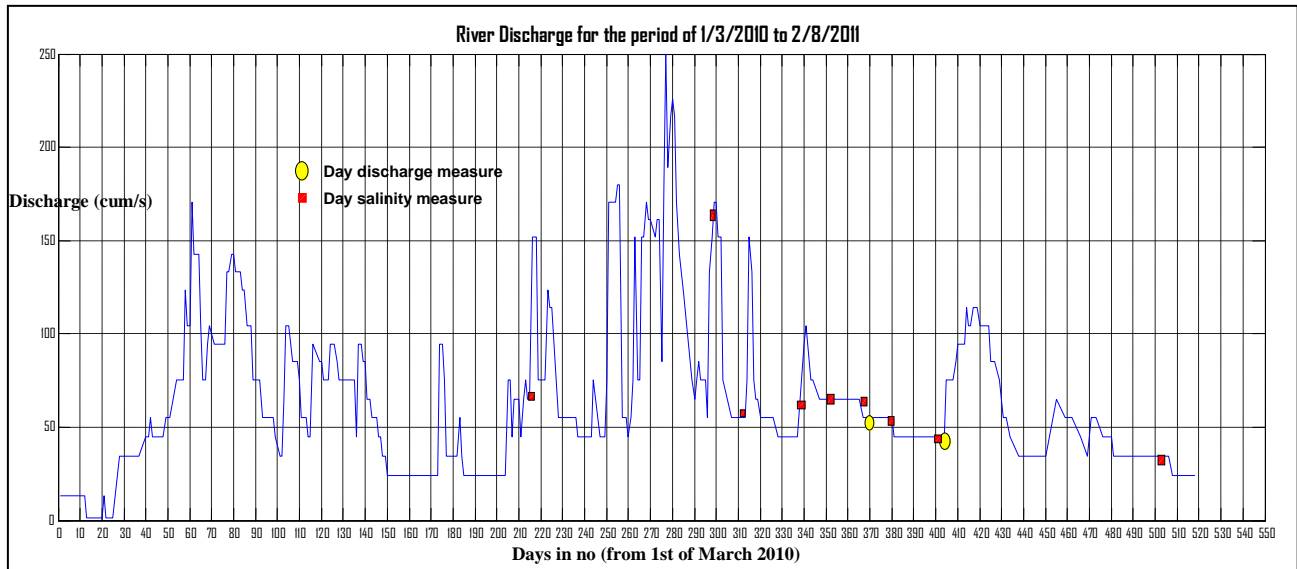


FIGURE 8: HYDROGRAPH OF THE MAHA OYA FOR DISCHARGE AT BAMBUKULIYA

4.2.5 Sea level variation and tidal effect

Sri Lanka is positioned in the northern Indian Ocean between latitudes 5-10 °N and longitude 79-82 °E. It is separated from the Indian continent by the narrow and shallow Palk Strait, and the oceanic waters have low salinity in the Bay of Bengal on the eastern side and high salinity in Arabian Sea on the western side. In the Arabian Sea, the net freshwater supply (precipitation +river runoff- evaporation) is strongly negative (about 1 m yr⁻¹), whereas it is strongly positive (about 0.4 m yr⁻¹) in the Bay of Bengal (Delaygue et al., 2001). The salinities of the Bay of Bengal are generally lower than the oceanic mean salinity (35), while the salinities of the Arabian Sea is high up to 36.5, which is due to high evaporation and hardly no freshwater input (Wijeratne and Pattiaratchi, n.d) .The continental shelf in Sri Lanka is narrow and very shallow. It is shallower than the average depth of the shelves around the world (Wijeratne and Pattiaratchi, n.d).

The above conditions affect the sea level variation in Sri Lanka. As far as the daily sea level variation is concerned tides caused by astronomical forcing is more interesting than the sea level variation due to meteorological and hydrological forcing. The most pronounced tidal constituent is the semidiurnal tidal constituents that has 12 hours and 25 minutes period (two high waters and two low waters per tidal day). The main components of the semidiurnal tides are the principal lunar semidiurnal (M2) and the principal solar semidiurnal (S2) constituents. The tides in Sri Lanka are mixed semidiurnal and the spring tidal range (2(M2+S2)) is between 0.40-0.60 m. In Colombo the spring tidal range is 0.6 m (Wijeratne and Pattiaratchi, n.d). Colombo is 42 km away from the site but in the same coastal belt. Some tidal constituents at the station Kochchikade, where the Maha Oya inlet

is located, are shown in Table 3 (where a is tidal amplitude and g is phase angle referred to local time).

TABLE 3: TIDAL CONSTITUENTS AT LOCATIONS NEAR THE MAHA OYA

Station	M2 (principal lunar semi-diurnal)		K1 (luni-solar declinational diurnal)	
	a (m)	g^0	a (m)	g^0
Kochchikade	0.17	45	0.06	61
Colombo ¹	0.18	45	0.07	32
Chilaw ²	0.18	45	0.09	43

¹ Approximately 42km away to Southern direction

² Approximately 40km away to Northern direction

Source: Wijeratne 2003 cited in Wijeratne and Pattiaratchi (n.d) modified to show nearest stations

In order to illustrate the semi diurnal tidal pattern in Colombo during a tidal day, Figure 9 shows the tides between 17-19 February 2012. Peak tidal amplitude also varies due to the moon's rotation around the earth. Spring tides occur when the sun and the moon are in line, whereas neap tides occur when they are at 90° viewed from the earth. There is a 7-day interval between neap and spring tide.

Other than the tidal variation, seasonal sea level variation can occur due to salinity variations, shifting winds, and currents along the coast (Schott et al., 1994 cited in Wijeratne, 2007). Seasonal sea level variations in Colombo from October 2005 to August 2006 is shown in Figure 10. The seasonal range of sea level variation is 0.2-0.3 m (Wijeratne and Pattiaratchi, n.d).

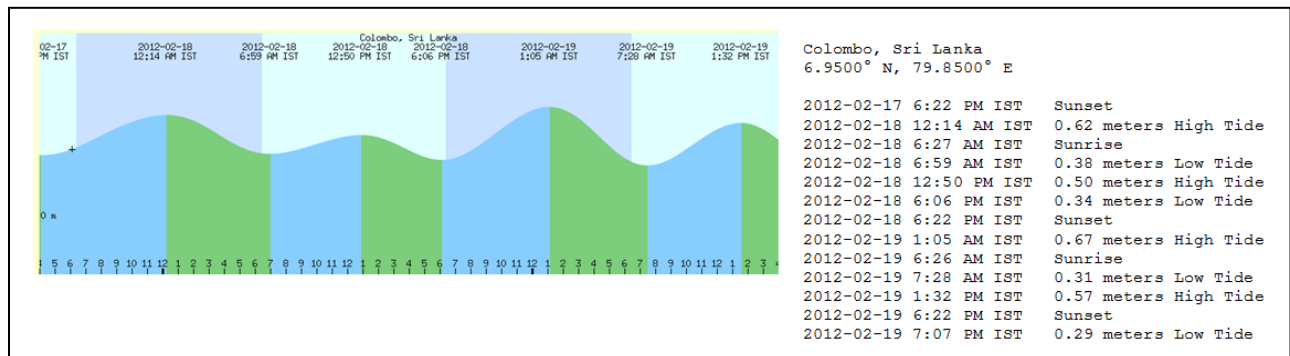


FIGURE 9: TIDE CHART COLOMBO

Source: Mobile Geographics LLC.2005

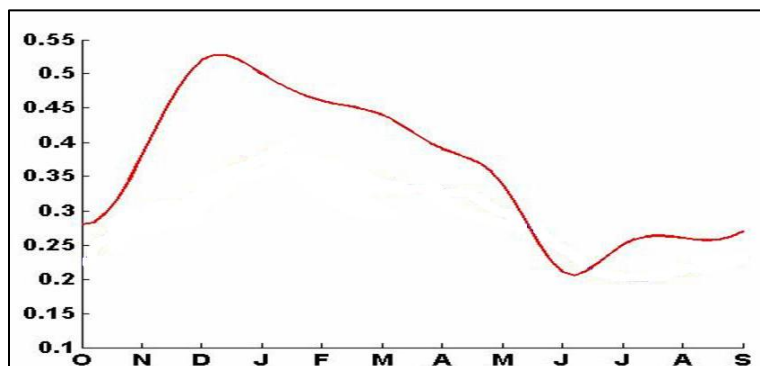


FIGURE 10: SEASONAL SEA LEVEL VARIATION AT COLOMBO FROM OCTOBER 2005 TO AUGUST 2006.

Source: Wijeratne; 2007

4.3 Sediment Transport Processes and Morphology of the Maha Oya

Sediment that is being transported by the river is mainly defined by the upstream lithology. Fractionation of sediment is governed by climate, morphology, and the nature of the sedimentological process such as soil erosion. According to the geological region classification in Sri Lanka, the country may be divided into four major lithotectonic subdivisions, that is, the highland complex, the Vijayana complex, the Wannu complex, and the Kadugannawa complex. The Maha Oya is in the Kadugannawa complex and Wannu complex regions. These complexes are made up of highly crystalline, non fossiliferous rocks since Precambrian age (Institute of Fundamental Studies Sri Lanka 2010). Thus, migmatitic hornblende biotite gneiss, charnockitic gneiss, granitic gneiss, and minor metasedimentary rock units are the main lithologies of the Maha Oya basin (Geological Survey and Mines Bureau, 1966b; cited in Ranasinghe et al., 2007).

The island can be divided into three main morphological regions based on the topography, where elevation and slope are the main characteristic parameters (Vitanege, 1972). The morphological regions consist of the coastal Lowlands within the elevations ranging from sea level to 305 m above mean sea level, the Upland from 305m to 915m, and the Highlands above 915m up to maximum of 2420m (Ranasinghe et al., 2007). The Highlands have well defined high plains and plateaus rimmed with high mountain peaks. Slopes are ranging up to 15° for the Lowlands, whereas they vary between 10° and 35° for the Upland areas.

As far as the climate is concerned, Sri Lanka is divided into three climate zones, which are the dry zone, intermediate zone, and wet zone. This classification is based on the annual average rainfall in the zones. Annual average rainfall of the dry zone is less than 1750 mm, it is between 1750 and 2500 mm in the intermediate zone, and larger than 2500 mm in the wet zone (Punyawardena, n.d). The Maha Oya basin is in intermediate climatic zone and it is often experiencing intense rainfall events.

The Maha Oya brings down weathered rock as sand from the upland that is 700 m high above mean sea level to the lower land area, where the sediment may be trapped at various locations during its transport to the sea. Channel bed morphology and bank slopes of the Maha Oya have strongly influenced the sorting of the sediments. The large energy slope of the river also induces forces for the initiation and transport of sediment. The intense rainfalls in the lower land area contribute as an extra force to the sediment transport. Because of the well-sorted clean sand, the demand in the market for the sand extracted from the Maha Oya River is very high. The absence of regulations for sand mining makes it difficult to protect the Maha Oya and its ecosystem.

5. Mathematical Model Development

5.1 Quasi-steady State

The term quasi-steady state may be more relevant than steady state in salt wedge analysis. Bottom layer dynamics are changing slowly at the quasi-steady state. Rate of change of matter is nearly zero in quasi-steady state, whereas it is zero in steady state. In quasi-steady state flow condition, arrested salinity wedge theory can be applied. The major portion of the salt wedge is governed by a quasi-equilibrium range with nearly self-similar distributions of velocity and density (Arita and Jirka, 1987).

As previously mentioned, the position of the salt water wedge in the quasi-equilibrium region is sought. Longitudinal diffusion is not of interest because interfacial shear control the quasi-equilibrium region. The developed quasi-equilibrium region at its maximum length under a particular flow is considered. Hence, the dynamic of the salt layer is negligible and the effects of bottom friction can be ignored. For a rectangular channel section the governing equations are as follows.

For the fresh water layer:

The one-dimensional laterally integrated continuity equation (with lateral inflow)

$$\frac{\partial q}{\partial x} = q \quad (5.1.1)$$

The one-dimensional laterally integrated momentum equation using Boussinesq approximation

$$\frac{\partial(h_1+h_2)}{\partial x} + u/g \frac{\partial u}{\partial x} + \frac{\tau_i}{\rho g h_1} - s_0 = 0 \quad (5.1.2)$$

For the salt water layer:

The one-dimensional laterally integrated momentum equation using Boussinesq approximation

$$\left(1 - \frac{\Delta\rho}{\rho}\right) \frac{\partial h_1}{\partial x} + \frac{\partial h_2}{\partial x} - \frac{\tau_i}{\rho g h_2} - s_0 = 0 \quad (5.1.3)$$

$$\tau_i = \frac{f_i \rho u^2}{8} \quad (5.1.4)$$

Where

- x = Distance along the river
- u = Lateral average velocity in the x direction
- q = Lateral inflow per unit lateral area

- h_1 = Depth of fresh water layer from interface to top surface
 h_2 = Depth of salt water layer from bottom to interface
 g = Acceleration due to gravity
 ρ = density of fresh water
 τ_i = Interfacial shear
 s_0 = Bottom slope
 $\Delta\rho$ = Density difference between salt and fresh water layers
 f_i = Interfacial friction factor

Lateral flow may be significant when the river is having water crossings. In the Maha Oya lateral flow can be assumed negligible within the study area. The influence of the Dutch canal that meets the Maha Oya within the area can be ignored. So the fresh water flow Q is assumed to have the same value as at the measurement point.

Combining equations 5.1.1, 5.1.2, 5.1.3, and 5.1.4 the governing equation can be written in non-dimensional form as in Equation 5.1.3. Parameters can be non-dimensionalized by dividing any linear dimensions by total depth H and the velocities by the baroclinic long wave speed $\sqrt{(g'H)}$, where $g' = (\Delta\rho/\rho) g$ is the reduced acceleration due to gravity

$$\frac{\partial h}{\partial X} + u \frac{\partial U}{\partial X} + f_i \left(\frac{U^2}{8} \right) \left\{ \frac{1}{h} + \frac{1}{(1-h)} \right\} = 0 \quad (5.1.5)$$

Assuming a rectangular channel cross section, the velocity can be replaced by river discharge and the equation becomes

$$\left(1 - \frac{\phi^2}{B^2 h^3} \right) \frac{\partial h}{\partial x} + \frac{f \phi^2}{8 B^2 h^2} \left(\frac{1}{h} + \frac{1}{1-h} \right) = 0 \quad (5.1.6)$$

Where B , h , and ϕ are the non-dimensional form of width, distance to interface from free surface, and river discharge respectively.

Introducing finite difference as the solution method, the final equation becomes

$$h_{(i+1)} = h_{(i)} - \frac{\frac{f \phi^2}{8 B^2 h_{(i)}^2} \left(\frac{1}{h_{(i)}} + \frac{1}{1-h_{(i)}} \right) \Delta X}{\left(1 - \frac{\phi^2}{B^2 h_{(i)}^3} \right)} \quad (5.1.7)$$

- h_i = non-dimensional depth to interface from free surface at station i
 h_{i+1} = non-dimensional depth to interface from free surface at station $i+1$ (Δx from i)
 ϕ = $Q/\sqrt{(g'H)} * H^2$ where Q is Fresh water discharge of the river
 B = b/H where b is width of the river at point i
 f = friction factor

$X = x/H$ where x is distance measured from inlet mouth towards upstream of the river against the flow.

3.1.1 Boundary conditions

At the inlet mouth, densimetric critical flow can be assumed (Balloffet and Borah 1985). Critical depth is then expressed as

$$h_{1c} = \sqrt[3]{\left(\frac{Q^2}{g'W^2}\right)} \quad (5.1.8)$$

h_{1c} = Densimetric critical depth

W = Width of the inlet mouth

The starting value of iteration h_i is taken as $1.2 h_{1c}$ to avoid solution instabilities in the reach adjacent to theoretical critical flow section (Balloffet and Borah, 1985).

5.2 Unsteady State

If the salt wedge is long, changes in discharge during hydrograph recession are gradual and tides are low, consequently a quasi-steady state condition may be assumed where the friction factor has a predominant role for the salinity intrusion (Balloffet and Borah, 1985). Existence of the quasi-steady state depends on the ability to adjust the baroclinic flow against the tidal variation, because higher frequency waves vary before the baroclinic wave can settle. When tidal flow dominates the hydraulic control, time-dependent solutions may give a better description than the quasi-steady solution where the tidal influence is assumed small. Time-varying river conditions, including variation in the free surface, interface or salt, and fresh water flux may also require a time-dependent solution.

In the unsteady state, the governing equations can be obtained by applying the continuity equation and shallow water equation to the upper fresh water layer and lower saline layer. The salt transport equation with consideration of mixing at the interface is also important in understanding variations in salinity. Figure 11 shows a schematic of a two-layer counter flow system. The layers are assumed to have constant density with a velocity as a function of time and horizontal position only. It is assumed that the velocities of both layers do not change with the vertical positions, that is, $u=u(x,t)$, and that the channel has a rectangular cross section.

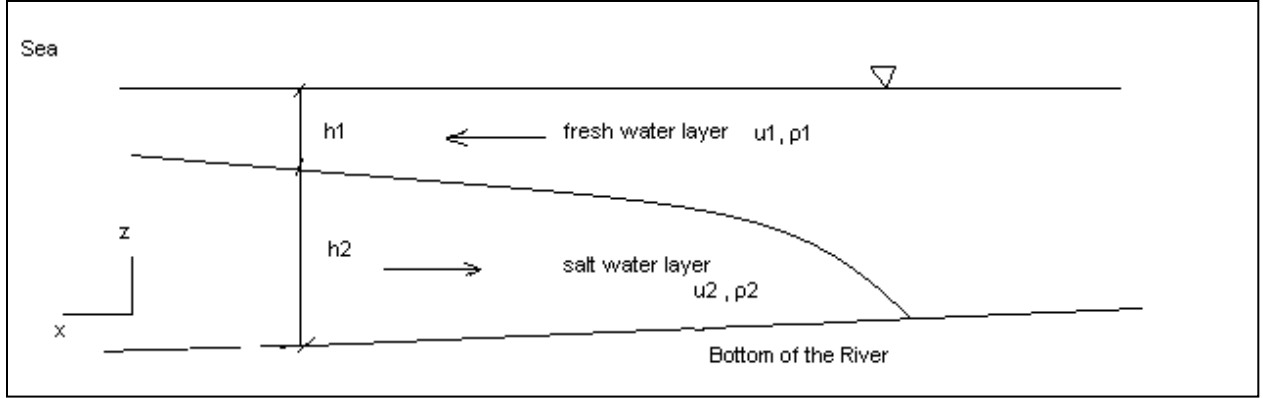


FIGURE 11: SCHEMATIC DIAGRAM SHOWING TWO-LAYER COUNTER FLOW

The Navier-Stokes equation is

$$\frac{\partial u}{\partial t} + u \frac{\partial u}{\partial x} + v \frac{\partial u}{\partial y} + w \frac{\partial u}{\partial z} = \left(-\frac{1}{\rho}\right) \frac{\partial P}{\partial x} + \frac{\mu}{\rho} \left(\frac{\partial^2 u}{\partial x^2} + \frac{\partial^2 u}{\partial y^2} + \frac{\partial^2 u}{\partial z^2}\right) - gS_0 \quad (5.2.1)$$

Where u , v and w are the velocity components in x , y and z directions, respectively, and μ and ρ are the viscosity and the density of the fluid, respectively.

For a long river $x \gg z, y$, and v and w are negligible. Furthermore, it can be shown that second-order terms with x and y components are negligible compared to z . So the simplified equation becomes

$$\frac{\partial u}{\partial t} + u \frac{\partial u}{\partial x} = \left(-\frac{1}{\rho}\right) \frac{\partial P}{\partial x} + \frac{\mu}{\rho} \left(\frac{\partial^2 u}{\partial x^2}\right) - gS_0 \quad (5.2.2)$$

For fresh water layer:

The one-dimensional laterally integrated continuity equation is

$$\frac{\partial A}{\partial t} + \frac{\partial Q}{\partial x} = 0 \quad (5.2.3)$$

For a rectangular channel with width b , then,

$$\frac{\partial(h_1 b)}{\partial t} + \frac{\partial(b h_1 u_1)}{\partial x} = 0 \quad (5.2.4)$$

Hydrostatic pressure P at x equals

$$P = (H - z)\rho_1 g \quad (5.2.5)$$

Where $H = h_1 + h_2$

Applying Equation 3.2.2 to the top layer, substituting P and laterally integrating the equation using Leibniz integral rule yield

$$\frac{\partial u_1}{\partial t} h_1 + u_1 \frac{\partial u_1}{\partial x} h_1 = -\rho_1 g \frac{\partial}{\partial x} \left(\frac{(H-h_2)^2}{2} + h_1 \frac{\partial h_2}{\partial x} \right) + \frac{1}{\rho_1} \mu_1 \frac{\partial u}{\partial z} \Big|_{h_2}^H - h_1 g S_0 = 0 \quad (5.2.6)$$

$$\mu_1 \frac{\partial u_1}{\partial z} \Big|_{h_2}^H = \tau_s - \tau_i \quad (5.2.7)$$

Where τ_s is the shear stress at the free surface, u_1 and u_2 is the vertically averaged horizontal velocity of top and bottom layer respectively.

From Equation 5.2.6 and 5.2.7

$$\frac{1}{g} \frac{\partial u_1}{\partial t} + \frac{u_1}{g} \frac{\partial u_1}{\partial x} + \frac{\partial(h_1+h_2)}{\partial x} + \frac{\tau_i}{\rho g h_1} - S_0 = 0 \quad (5.2.8)$$

For salt water layer:

Similarly continuity can be written

$$\frac{\partial(h_2 b)}{\partial t} + \frac{\partial(b h_2 u_2)}{\partial x} = 0 \quad (5.2.9)$$

Hydrostatic pressure P at x is assumed,

$$P = h_1 \rho_1 g + (h_2 - z) \rho_2 g \quad (5.2.10)$$

$$\mu_2 \frac{\partial u_2}{\partial z} \Big|_0^{h_2} = \tau_i - \tau_b \quad (5.2.11)$$

Applying Equation 5.2.2 to the bottom layer, the flow equation can be derived by integrating the equation from 0 to h_1 , as for the fresh water layer. Using the Boussinesq approximation in the flow equation for the salt layer gives

$$\frac{1}{g} \frac{\partial u_2}{\partial t} + \frac{u_2}{g} \frac{\partial u_2}{\partial x} + \left(1 - \frac{\Delta \rho}{\rho} \right) \frac{\partial h_1}{\partial x} + \frac{\partial h_2}{\partial x} + \frac{(\tau_b + \tau_i)}{\rho g h_2} + S_0 = 0 \quad (5.2.12)$$

$$\tau_b = k_b \rho u_2^2 \quad (5.2.13)$$

Where k_b is defined as bottom friction factor

(The Manning formulae $u_2 = \frac{1}{n} R^{2/3} S_f^{1/2}$ also can be used to find the bottom friction τ_b)

$$\tau_i = k_i \rho (u_1 - u_2) |u_1 - u_2| \quad (5.2.14)$$

Where k_i is the interfacial friction factor.

5.3 The Salt Water Layer Dynamics

The dynamics of the bottom layer is governed by tidal strain and density currents. Tidal wave propagation and associated currents along the river can be described with shallow water wave theory, because tidal waves are very long compared to the depth of the river. Tidal wave length λ can be express in terms of the wave celerity c and the tidal wave period T as $\lambda=cT$. For shallow water waves $c = [g (D + 3/2 \xi)]^{1/2}$ (Pugh, 1996), where ξ is the instantaneous level increment by tidal oscillation at the point of interest, D is the depth. For the simplicity of the model it may be simplified to $c = \sqrt{Dg}$. For a stratified two-layer system internal wave theory is more appropriate and g is replaced with the reduced gravity g' , whereas D is replaced with $(h_1 h_2 / (h_1 + h_2))$. For the Maha Oya River it can be shown that the calculated tidal wavelength for a semi-diurnal tidal wave exceeds the salinity intrusion length. For example, if the depth of the river is 5m then c becomes 7 m/s and λ would be 151 km for a 6-hour period. Salinity intrusion lengths have been observed for much smaller values than this. So the wave number k can be assumed to be 1.

Based to the above observations, the horizontal velocity due to tides u_t at the interface by

internal wave theory can be express as $u_t = \xi \left(\frac{g'}{\left(\frac{h_1 h_2}{h_1 + h_2} \right)} \right)^{\frac{1}{2}}$ (Bowden, 1983 cited in Pugh 1987)

and $\xi = H_0 \cos(kx - wt)$ ($k=1$). Thus,

$$u_t = H_0 \left(g' / \left(\frac{h_1 h_2}{h_1 + h_2} \right) \right)^{\frac{1}{2}} \cos(x - wt) \quad (5.3.1)$$

Where k is the wave number and it was assumed that the current is in phase with surface elevation.

The bottom layer horizontal velocity mainly has two components. One contributor is the velocity component induced by the barotropic tidal oscillation, as described above. The second component is the density current. Density current, or gravity current is described through an advancing front of the salt wedge rather than mean velocity of the salt layer. Here the gravity wave is advancing towards the upstream direction against the slope by a motive force due to extra weight of the denser fluid that creates a larger piezometric pressure inside the current than in the fluid ahead. As the motive force of the gravity current is governed by hydrostatic pressure, the extra weight of the denser fluid that contribute to the motive force due to slop can be assumed negligible for mild slopes. (Benjamin, 1967). This assumption is reasonable in the Maha Oya estuary. The velocity component due to the density current u_d is (Von Karman, 1940; cited in Benjamin, 1967)

$$u_d = \sqrt{2g'h_2} \quad (5.3.2)$$

Assuming these components are linearly independent (Cheng et al., 2010), it can be written

$$u_{\infty} = u_t + u_d \quad (5.3.3)$$

Where u_{∞} is the velocity of the bottom layer at the interface,

5.3.1 Depth average velocity of the Bottom layer

To determine the depth-averaged velocity of the bottom layer, the assumption is made that it resembles a boundary layer region and can be described by boundary layer theory (Seim et al., 2006). This simulation is reasonable in a shallow estuary like the Maha Oya. Hence the variation in the velocity of the bottom layer with depth z can be described by a logarithmic profile as (Seim et al., 2006)

$$u = \frac{u_{\infty}}{k} \log\left(\frac{z}{z_0}\right) \quad (5.3.4)$$

Where u is the horizontal velocity of the bottom layer at depth z , K is the von Karman constant, usually takes as 0.4, and z_0 is the roughness length defined in boundary layer theory. Then the depth average velocity of the bottom layer can be found by integrating the velocity profile across the layer to yield

$$\frac{1}{z} \int_{z_0}^z \frac{u_{\infty}}{k'} \log\left(\frac{z}{z_0}\right) dz \approx \frac{u_{\infty}}{k'} \left\{ \log\left(\frac{z}{z_0}\right) - 1 \right\}$$

$$u_2 = \frac{u_{\infty}}{k'} \log\left(\frac{h_2}{10z_0}\right) \quad (5.3.5)$$

Logarithmic velocity variation with vertical distance from the bottom and assumed constant velocity over the upper layer, as shown in the Figure 12, describe the depth-averaged velocity profile of the system.

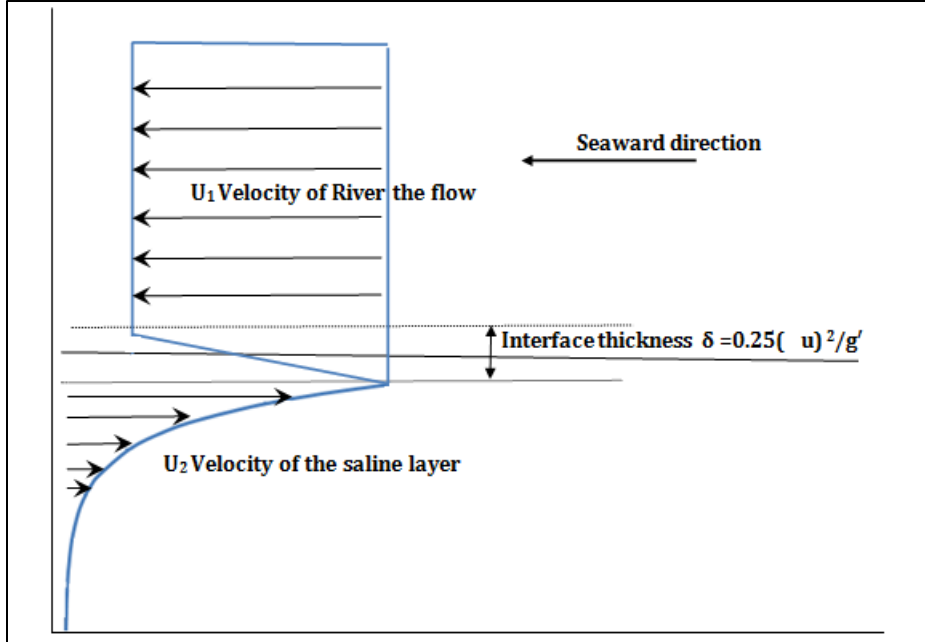


FIGURE 12: ASSUMED VERTICAL VELOCITY PROFILE IN THE MODEL

5.4 Entrainment at the interface

Entrainment transfer is the transfer of net volume flux of water across the interface taking salt or heat with it. Ignoring diffusive transfer due to turbulent diffusion and molecular diffusion, net flux of salt transfer T at the interface can be given as $T = \Delta\rho w_i$ where w_i is the entrainment velocity due to turbulent motion of the water (Karelse , Vreugdenhil , Delvigne and Breusers , 1974). Values on w_i can be found from many experimental studies carried out by various scientists. Among them the best fit for two-layer stratified counter flows with shear is the following expression (Long and Moore 1971 cited in Karelse , Vreugdenhil , Delvigne and Breusers , 1974)

$$w_i = 2\Delta u/Ri_o \quad (5.4.1)$$

Ri_o = overall Richardson number at the interface $\{ Ri_o = g'H/(\Delta u)^2$ where $\Delta u = (u_1 - u_2)$ velocity at the interface}. Further development gives

$$w_i = 2\Delta u^3/g'H \quad (5.4.2)$$

5.5 Salt transport Equation

Salt transport is governed by horizontal advection and entrainment at interface. The governing equation with mixing due to turbulent diffusion is

$$\frac{\partial \rho}{\partial t} + \frac{\partial \rho u}{\partial x} = w_i \frac{\partial \rho}{\partial z} + \frac{\partial}{\partial z} \left(k_n \frac{\partial \rho}{\partial z} \right) \quad (5.5.1)$$

Integrating over the depth (Vreugdenhil, 1970 cited in Karelse , Vreugdenhil , Delvigne and Breusers , 1974) and ignoring diffusive mass transfer yields for the salt layer

$$\frac{\partial \rho_2}{\partial t} + u_2 \frac{\partial \rho_2}{\partial x} = w_i \frac{\partial \rho}{\partial z} \quad (5.5.2)$$

Introduce the mixing coefficient C_{mix} , $w_i = C_{mix} 2\Delta u^3 / g'H$, $\frac{\partial \rho}{\partial z} = \frac{\Delta \rho}{H}$ and neglect second-order terms in the turbulent diffusion equation leads to

$$\frac{\partial \rho_2}{\partial t} + u_2 \frac{\partial \rho_2}{\partial x} = C_{mix} \frac{2\Delta u^3 \Delta \rho}{g'H^2} \quad (5.5.3)$$

Similarly for the top layer

$$\frac{\partial \rho_1}{\partial t} + u_1 \frac{\partial \rho_1}{\partial x} = C_{mix} \frac{2\Delta u^3 \Delta \rho}{g'H^2} \quad (5.5.4)$$

The ratio $\Delta \rho / \rho$ is assumed to be constant at the inlet to determine the density of top layer at the inlet.

Initial and boundary values of densities for both top and bottom layers are required at the upstream and downstream in solving salt transport equation.

At the inlet density of the bottom layer is assumed to be the same as sea water. In the top layer it can be determined by assuming a suitable constant value for the ratio between density differences as described before. This ratio at the inlet can be found experimentally. At the first time step both layers have densities equal to fresh water.

5.5.1 Density salinity conversion

As the field measurements are salinity values, a conversion from salinity to density is required. The density can be converted to the salinity (ppt) according to the formulae

$$\rho = 9.992057 \cdot 10^{+02} + S \cdot 7.99992230 \cdot 10^{-01} + T \cdot 9.5390097 \cdot 10^{-02} - S \cdot T \cdot 2.40936500 \cdot 10^{-03}$$

(McCutcheon S.C, Martin J.L, Barnwell T.O.Jr 1993)(ρ, S and T denotes density, salinity and temperature, respectively, in the equation)

6. Mathematical Model Implementation

6.1 Model Formulation

Recalling Equations 5.2.4, 5.2.8, 5.2.9 and 5.2.12, by introducing appropriate components due to the entrainment at the interface a new set of equations can be written as

$$\frac{1}{g} \frac{\partial u_1}{\partial t} + \frac{u_1}{g} \frac{\partial u_1}{\partial x} + \frac{\partial(h_1+h_2)}{\partial x} + \frac{\tau_i}{\rho g h_1} + s_0 - w_i u_1 = 0 \quad (6.1.1)$$

$$\frac{1}{g} \frac{\partial u_2}{\partial t} + \frac{u_2}{g} \frac{\partial u_2}{\partial x} + \left(1 - \frac{\Delta\rho}{\rho}\right) \frac{\partial h_1}{\partial x} + \frac{\partial h_2}{\partial x} + \frac{(\tau_b + \tau_i)}{\rho g h_2} - s_0 + w_i u_2 = 0 \quad (6.1.2)$$

$$\frac{\partial h_1}{\partial t} + u_1 \frac{\partial h_1}{\partial x} + h_1 \frac{\partial u_1}{\partial x} = w_i \quad (6.1.3)$$

$$\frac{\partial h_2}{\partial t} + u_2 \frac{\partial h_2}{\partial x} + h_2 \frac{\partial u_2}{\partial x} = w_i \quad (6.1.4)$$

6.1.1 Transformation of Equations

To transform the differential equations and solve them by finite difference approximation, the friction slope should be determined. Using the general equation of gradually varied flow gives

$$\frac{dy}{dx} = \frac{s_0 - S_f}{1 - F^2} \quad (6.1.5)$$

Where S_f is the total friction slope, s_0 is the slope of the river bed, F is the Froude number, x is the horizontal distance, and y is the depth measured from bottom to free surface. Here it has been assumed that long tidal wave at interface does not influence the above relationship.

Under low flow conditions when the Froude number is small, the denominator is close to 1 and the following equation is obtained

$$\frac{\partial(h_1+h_2)}{\partial x} = \frac{\partial H}{\partial x} = s_0 - S_f \quad (6.1.6)$$

Where the overall friction slope S_f can be defined by considering interfacial friction loss as well as bottom friction loss (Li and Lawrence, 2005). Here friction loss due to river banks has been ignored.

$$S_f = S_b + S_i \quad (6.1.7)$$

Where S_b is the friction slope due to bottom shear and S_i is the friction slope due to interfacial shear. These terms can be written using appropriate Froude numbers defined as

$$F_2 = \frac{u_2}{\sqrt{g'h_2}} \quad (6.1.8)$$

$$F_i = \frac{u_2 - u_1}{\sqrt{g'H}} \quad (6.2.9)$$

$$S_b = k_b F_2 | F_2 | \quad (6.1.10)$$

$$S_i = k_i F_i | F_i | \frac{H^2}{h_1 h_2} \quad (6.1.11)$$

Therefore

$$S_f = k_b F_2 | F_2 | + k_i F_i | F_i | \frac{H^2}{h_1 h_2} \quad (6.1.12)$$

From Equation 6.1.8 and 6.1.9

$$u_2^2 = \frac{S_b}{k_b} g' h_2 \quad (6.1.13)$$

Differentiating Equation 6.1.13 with respect to x gives

$$2u_2 \frac{\partial u_2}{\partial x} = \frac{S_b}{k_b} g' \frac{\partial h_2}{\partial x} + \frac{g'}{k_b} h_2 \frac{\partial S_b}{\partial x} \quad (6.1.12)$$

Assuming $\frac{\partial b_s}{\partial x}$ is small in Equation 4.1.12 and substituting in Equation 6.1.4

$$\frac{\partial h_2}{\partial t} + \left(u_2 + \frac{g' h_2 k_b u_2^2 / g' h_2}{2u_2} \right) \frac{\partial h_2}{\partial x} = C_{mix} \frac{2\Delta u}{R_i} \quad (6.1.13)$$

Rearranging equation 6.1.1

$$\frac{\partial u_1}{\partial t} + u_1 \frac{\partial u_1}{\partial x} + g' S_i \frac{h_2}{H} - g S_f = 0 \quad (6.1.14)$$

Rearranging equation 6.1.2

$$\frac{\partial u_2}{\partial t} + u_2 \frac{\partial u_2}{\partial x} + g' \left(S_b + S_i \frac{h_1}{H} \right) + g(2s_0 - S_f) = 0 \quad (6.1.15)$$

Here it is assumed that $1 - \Delta\rho/\rho \approx 1$

The two equations above are in the form of $\partial u/\partial t + \alpha \partial u/\partial x + \beta = 0$ (Keskin, 1997)

$$\frac{\partial u_1}{\partial t} + u_1 \frac{\partial u_1}{\partial x} + \beta = 0 \quad (6.1.16)$$

$$\frac{\partial u_2}{\partial t} + u_2 \frac{\partial u_2}{\partial x} + \lambda = 0 \quad (6.1.17)$$

Where

$$\beta = g' S_i \frac{h_2}{H} - g S_f \text{ and } \lambda = g' \left(S_b + S_i \frac{h_1}{H} \right) + g(-S_f + 2s_0)$$

$$\frac{\partial h_2}{\partial t} + \eta \frac{\partial h_2}{\partial x} + \Psi = 0 \quad (6.1.15)$$

Where

$$\eta = 3/2 u_2 \text{ and } \Psi = -C_{mix} \frac{2\Delta u}{R_i}$$

Rearranging Equations 5.5.3 and 5.5.4 gives

$$\frac{\partial \rho_1}{\partial t} + u_1 \frac{\partial \rho_1}{\partial x} = \sigma \quad (6.1.16)$$

$$\frac{\partial \rho_2}{\partial t} + u_2 \frac{\partial \rho_2}{\partial x} = \sigma \quad (6.1.17)$$

Where

$$\sigma = c_{mix} \frac{2\Delta u^3 \Delta \rho}{g'H^2}$$

6.2 Finite Difference Approximation

Finite difference approximations can be written with subscript i and j for space and time. Δx is the size of each equal length step.

$$\frac{u_{1i+1}^{j+1} - u_{1i+1}^j}{\Delta t} + u_{1m} \frac{u_{1i+1}^{j+1} - u_{1i}^{j+1}}{\Delta x} + \beta_m = 0 \quad (6.2.1)$$

$$u_{1i+1}^{j+1} = \frac{u_{1i+1}^j + \frac{\Delta t}{\Delta x} u_m u_{1i}^{j+1} - \beta_m \Delta t}{1 + u_{1m} \frac{\Delta t}{\Delta x}} \quad (6.2.2)$$

Where

$$u_{1m} = \left(\frac{u_{1i}^{j+1} + u_{1i+1}^j}{2} \right) \text{ and } \beta_m = \left(\frac{\beta_i^{j+1} + \beta_{i+1}^j}{2} \right)$$

For u_2 , the following equation is obtained

$$\frac{u_{2i+1}^{j+1} - u_{2i+1}^j}{\Delta t} + u_{2m} \frac{u_{2i+1}^{j+1} - u_{2i}^{j+1}}{\Delta x} + \lambda_m = 0 \quad (6.2.3)$$

$$u_{2i+1}^{j+1} = \frac{u_{2i+1}^j + \frac{\Delta t}{\Delta x} u_{2m} u_{2i}^{j+1} - \lambda_m \Delta t}{1 + u_{2m} \frac{\Delta t}{\Delta x}} \quad (6.2.4)$$

Where

$$u_{2m} = \left(\frac{u_{2i}^{j+1} + u_{2i+1}^j}{2} \right) \text{ and } \lambda_m = \left(\frac{\lambda_i^{j+1} + \lambda_{i+1}^j}{2} \right)$$

The layer thickness h_2 is given by

$$h_{2i+1}^{j+1} = \frac{h_{2i+1}^j + \frac{\Delta t}{\Delta x} \eta_m h_{2i}^{j+1} + \psi_m \Delta t}{1 + \eta_m \frac{\Delta t}{\Delta x}} \quad (6.2.5)$$

Where

$$\eta_m = \left(\frac{\eta_i^{j+1} + \eta_{i+1}^j}{2} \right) \text{ and } \psi_m = \left(\frac{\psi_i^{j+1} + \psi_{i+1}^j}{2} \right)$$

The layer thickness h_1 is calculated as

$$h_{1i}^j = H_i^j - h_{2i}^j \quad (6.2.6)$$

The densities ρ_1 and ρ_2 is given by

$$\rho_{2i+1}^{j+1} = \frac{\rho_{2i+1}^j + \frac{\Delta t}{\Delta x} u_{2m} \rho_{2i}^{j+1} + \sigma_m \Delta t}{1 + u_{2m} \frac{\Delta t}{\Delta x}} \quad (6.2.7)$$

$$\rho_{1i+1}^{j+1} = \frac{\rho_{1i+1}^j + \frac{\Delta t}{\Delta x} u_{1m} \rho_{1i}^{j+1} + \sigma_m \Delta t}{1 + u_{1m} \frac{\Delta t}{\Delta x}} \quad (6.2.8)$$

Where

$$\sigma_m = \frac{\sigma_i^{j+1} + \sigma_{i+1}^j}{2}$$

To derive h_1 , the gradually varying flow equation is used. The total depth at any point is equal to total depth at the inlet and head loss at the point. To calculate the head loss, the friction slope is assumed as constant during a given time interval

$$H_i^j = H_{i=1}^j + s_f \Delta x_i \quad (6.2.9)$$

6.3 Discretization

6.3.1 River flow

Time series flow data can be calculated from daily gauge readings as mentioned in Section 3.2.4 and an appropriate set of data that fulfill the initial conditions should be selected for the simulation.

Discharge can vary along the river depending on the location and the velocity of the flow. Thus, discharge values pertaining to any length step at any time step is assigned based on the assumption that the existing flow is prevailing until the next flow occurs. The flow is determined by its travel time to the point from the upstream boundary. Only two consecutive flows are considered at a time.

For any distance step Δx at a time equals to $\Sigma \Delta t$

if $\Sigma \Delta t < T + (L - \Sigma \Delta x)/U_i^{j+1}$

$$Q = Q^j$$

Otherwise

$$Q = Q^{j+1}$$

6.3.2 Tidal Inputs

The tidal velocity component is simulated using the root-mean-square (rms) value for both flood and ebb tides. The schematic variation is shown graphically in Figure 13.

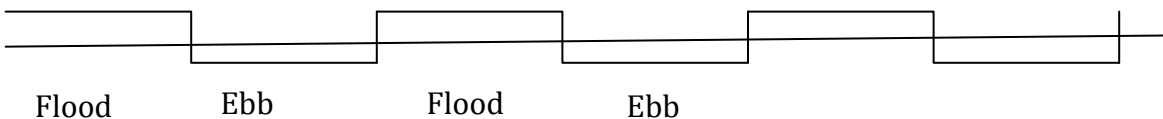


FIGURE 13: SCHEMATIC DIAGRAM SHOWING DISCRETIZED TIDAL INPUT

The rms value of the tidal velocity component can be written as

$$U_{tide} = \frac{H_0}{\sqrt{2B}} (g' / (h_1 h_2 / (h_1 + h_2)))^{1/2} \quad (6.3.2)$$

Principle lunar semidiurnal tide with semi-monthly variations is distributed uniformly from the maximum value to the minimum value during a quarter month and vice versa. The model can easily be modified to cope with input time series tidal data, if it is of interest.

6.3.3 Time steps

Time step is in the form of fractions of half of the tidal period. For the semidiurnal tides it can be 6.25 hrs, 3.125 hrs etc. Thus, the effects of the tidal variation can be included into the model.

6.3.4 Length steps

It has been demonstrated that with a 250 m length step using a 3.125 hrs time step, the model shows convergence with reasonable accuracy. Using smaller steps, higher accuracy could not be expected due to limitations of the sampling techniques employed.

6.4 Boundary and initial conditions

6.4.1 Downstream

The salt water wedge is assumed to have been fully flushed at the beginning of the calculations. This happens in the Maha Oya normally during periods of heavy rainfall. Thus, model calibration has to be done based on this situation.

The boundary conditions are as follows:

$$j=1$$

$$u_{1i}^1 = \frac{Q}{bH} \quad (6.4.1)$$

H = initial total water depth with no salt wedge (steady state river flow assumed)

$$u_{2i}^1 = 0 \quad (6.4.2)$$

$$h_{2i}^1 = 0 \quad (6.4.3)$$

$$h_{1i}^1 = H \quad (6.4.4)$$

$$i=1$$

$$h_{2i}^1 = d + a \quad (6.4.4)$$

d = depth of river at the mouth from mean sea level and a = tidal amplitude.

Densimetric critical flow is assumed at the river mouth:

$$h_{11}^j = 1.2h_{1c} = 1.2 \sqrt[3]{\frac{Q^2}{g'B^2}} \quad (6.4.5)$$

$$u_{11}^j = \sqrt{g'h_{1c}} \quad (6.4.6)$$

u_{21}^j can be found by applying appropriate boundary values using Equation 5.3.2, 5.3.3, 5.3.5 and 6.3.2.

6.4.2 Upstream

The assumption is made that there are no tidal effects at the upstream boundary, as well as no salinity present at this boundary:

$$U_1(L, T) = U \quad (6.4.2)$$

$$U_2(L, T) = 0 \quad (6.4.3)$$

$$h_1(L, T) = H \quad (6.4.4)$$

$$h_2(L, T) = 0 \quad (6.4.5)$$

6.5 Calibration parameters

The main calibration parameters are the interfacial friction factor, the bottom friction factor, and the mixing coefficient of salt due to entrainment at the interface. The entrainment is assumed to be mainly from velocity shear induced at the interface. The interfacial friction factor is highly dependent on the velocities at the interface. Thus, the model was designed to have a variable friction factor instead of a constant value. Because most of the dynamics are highly dependent on the river flow, it is reasonable to keep the interface friction factor as a function of the river flow alone,

$$k_i = c_0 \left(\frac{Q}{Q_0} \right)^w \quad (6.5.1)$$

Where k_i = interface friction factor

c_0 = coefficient of interface friction factor (the calibration parameter)

w = empirical power that may take the value 1, 2, or 3, but for Maha Oya it is set to 2

Q = river flow at the step being considered

Q_0 = mean value of discharge data

Model has two more parameters to specify, that is, von Karman's constant K and z_0 , which is similar to the friction length scale in boundary layer theory.

7. Model Application

7.1 Model Testing

7.1.1 Simulation of salt wedge propagation of time varying model

The model was tested regarding the evolution towards the maximum intrusion length, and an example of the result is shown in Figure 14. The calculations were performed for a constant river discharge of 25 cum/s over a substantial period of time under no tidal influence following after initial fresh river condition. Under this condition, plot of salt wedge at each time step (3.125 hrs interval) has drawn in Figure 14. It shows salt wedge propagation has reached to maximum limit in one and half day (10 time steps).

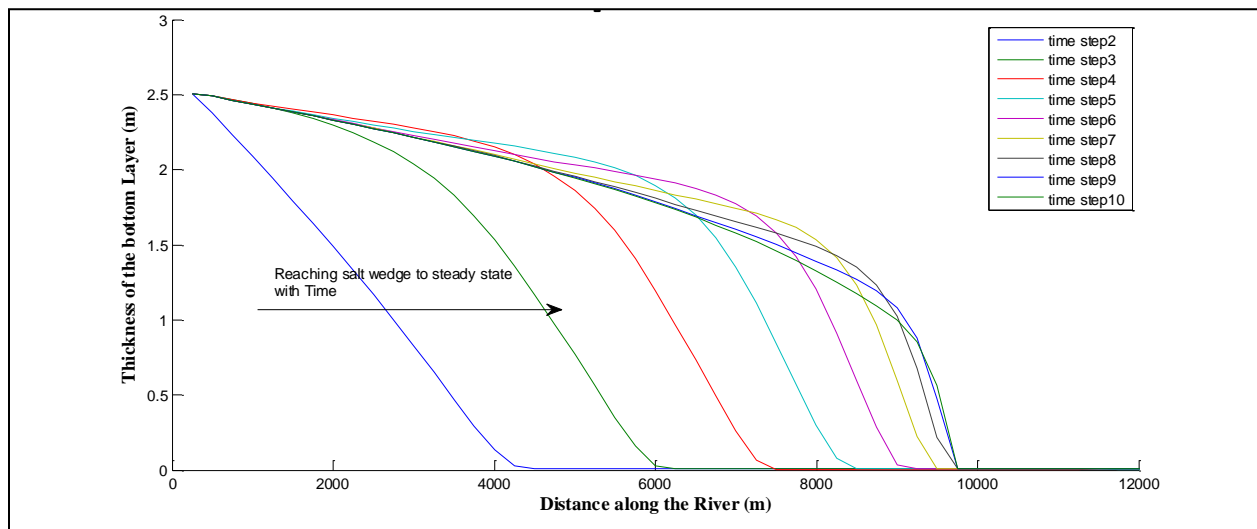


FIGURE 14: SALT WEDGE PROPAGATION WITH TIME

7.1.2 Responds to sudden river discharge variation

Figure 15 shows the variation in the salt layer thickness responds to sudden discharge variation from 25 cum/s to 50 cum/s at a distance of 2.5 km along the river. Model was run with the discharge of 25 cum/s initially and in the second day 50 cum/s of discharge introduced at the upstream end. The variation in bottom layer thickness 2.5 km upstream from the inlet was plotted with time. It can be seen from the Figure 15 at 37.5 hrs (after half a day) a decrease in thickness begins and continue until about 50 hrs, taking almost one day to adjust towards new conditions.

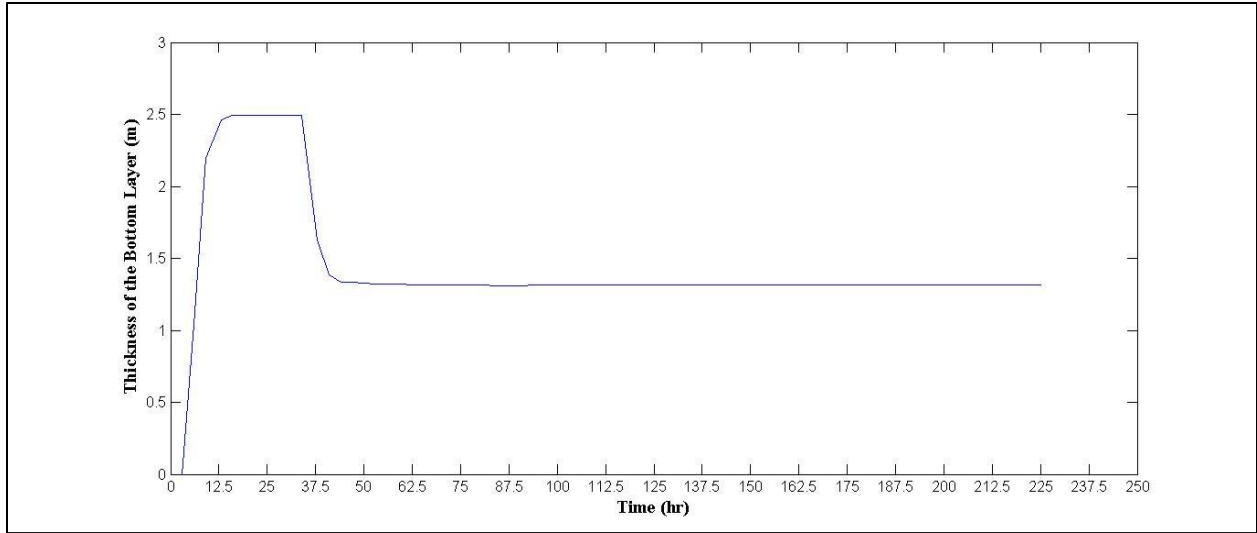


FIGURE 15: RESPOND TO SUDDEN DISCHARGE VARIATION FROM 25 CUM/S TO 50 CUM/S

7.1.3 Variation of salt intrusion length with river discharge

Model was run repeatedly for constant river discharge from 10 cum/s to 90 cu/s, as shown in the figure 16. Maximum intrusion length at each simulation were plotted against the corresponding discharge.

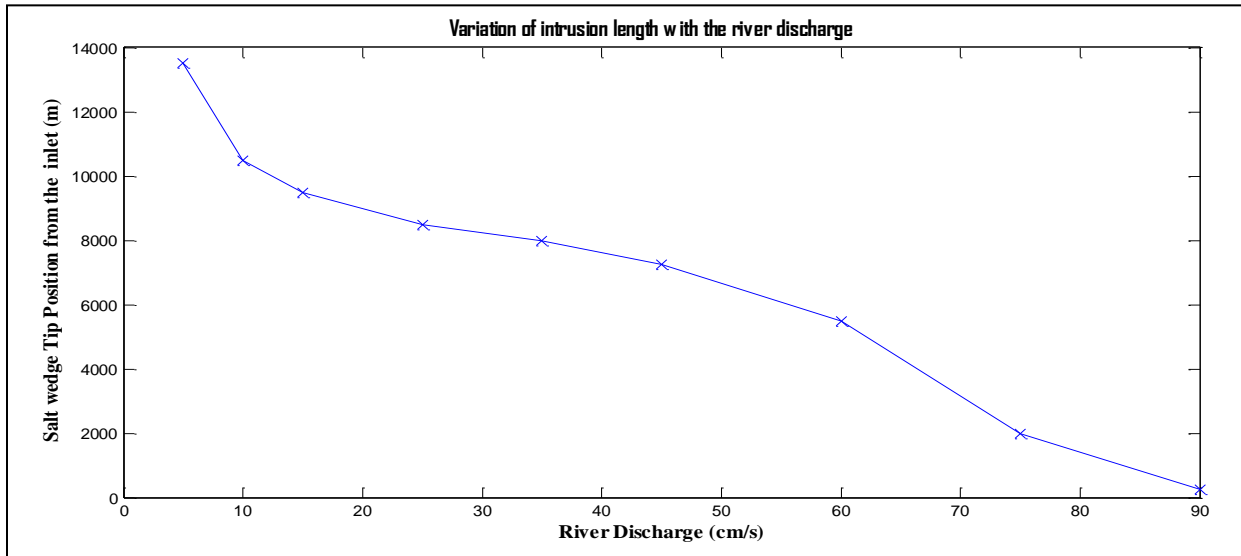


FIGURE 16: VARIATION OF SALT INTRUSION LENGTH WITH RIVER DISCHARGE

Figure 16 shows the decrease of the intrusion length with an increase in river discharge. Under the existing bathymetry, the salt wedge does not exist if the discharge increases beyond 90 cum/s.

7.1.4 Variation of salt intrusion length with river depth

When the depth of the water column increases it can be shown that the bulk Richardson number is increasing and the stratification becomes more stable. It means that the vertical mixing becomes less. So simulation of intrusion with depth variation needs some adjustment concerning the mixing coefficient. The model has been run for a number of cases with a mixing coefficient that is reduced with increases in depth, whereas other parameters are kept fixed, and the result is shown in Figure 17.

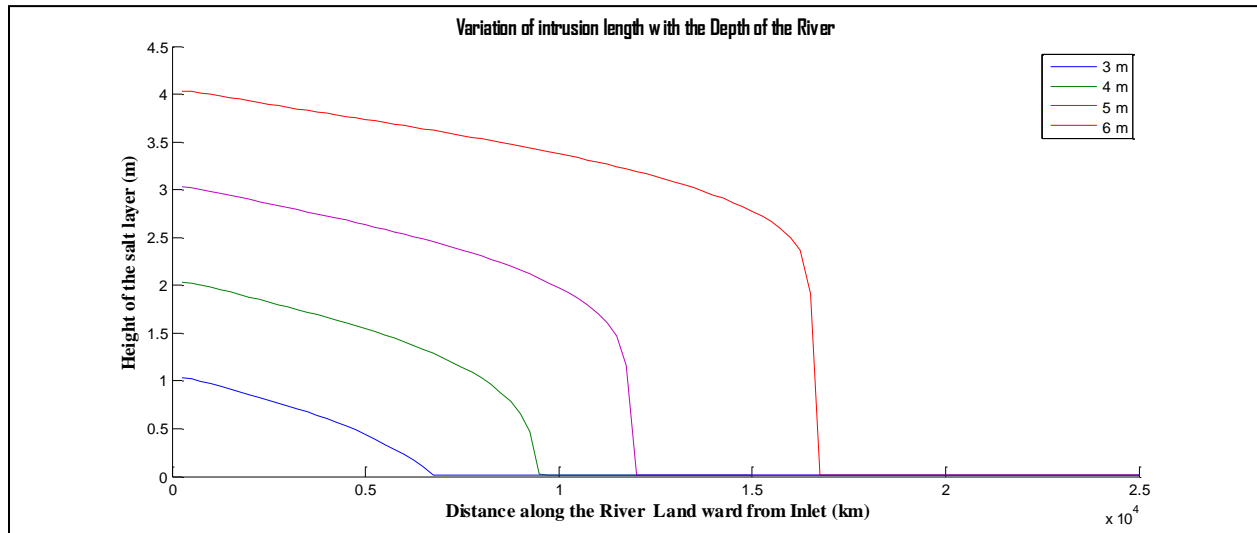


FIGURE 17: INCREASES OF INTRUSION LENGTH WITH INCREASES OF DEPTH OF THE RIVER

7.2 Sensitivity Analysis

7.2.1 Sensitivity analysis of the steady state model

Suitable value for the friction factor lies in the range of 10^{-4} - 10^{-5} . Increases up to 10^{-3} give unsatisfactory results when comparing to actual field data. Decreases towards 10^{-6} also show that salinity goes beyond the maximum limit. From the figure, variation by a fraction shows significant movement of intrusion length. Hence it can be concluded that the model is highly sensitive to the friction factor.

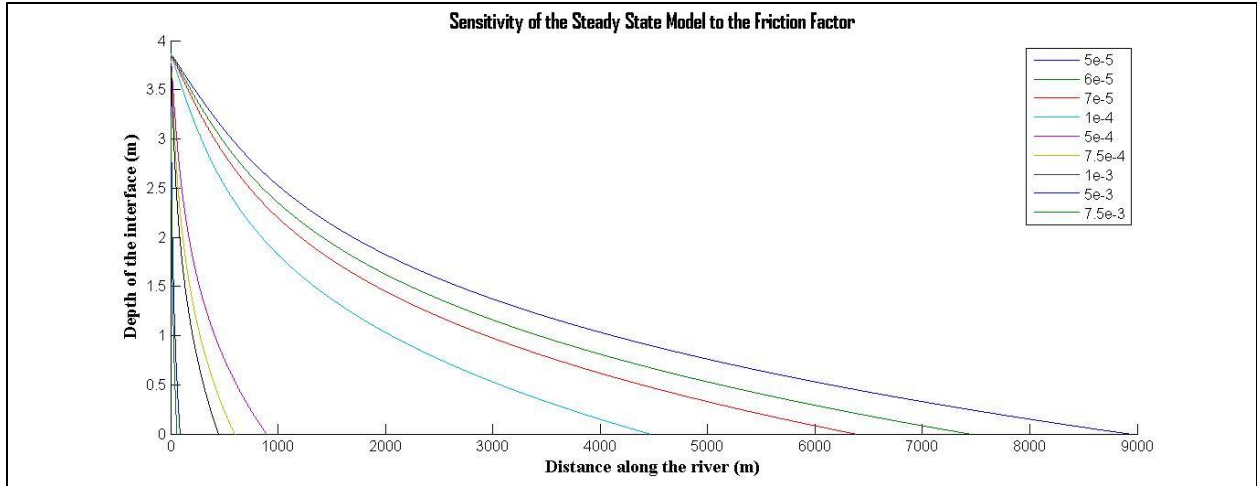


FIGURE 18: SENSITIVITY TO FRICTION FACTOR

7.2.2 Sensitivity analysis of the time-varying model

Model was run for a constant discharge of 25 cum/sec for a one-month period and the sensitivity of the model to different parameters was investigated. The intrusion length was then determined at steady-state. The results of the sensitivity analysis are shown in Figures 19-21.

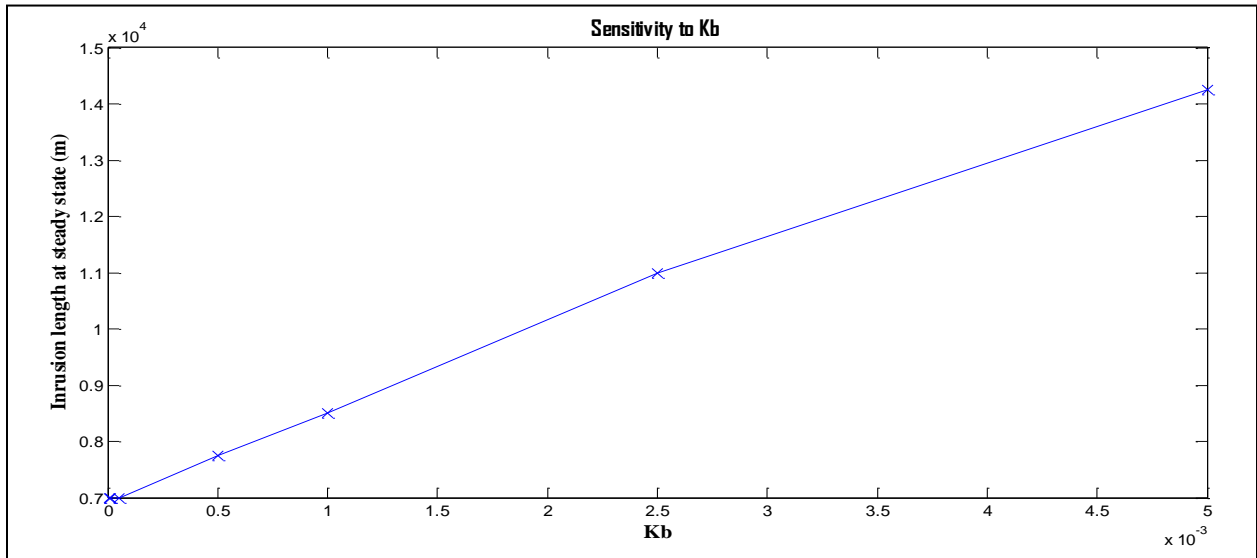


FIGURE 19: SENSITIVITY TO BOTTOM FRICTION FACTOR (KB)

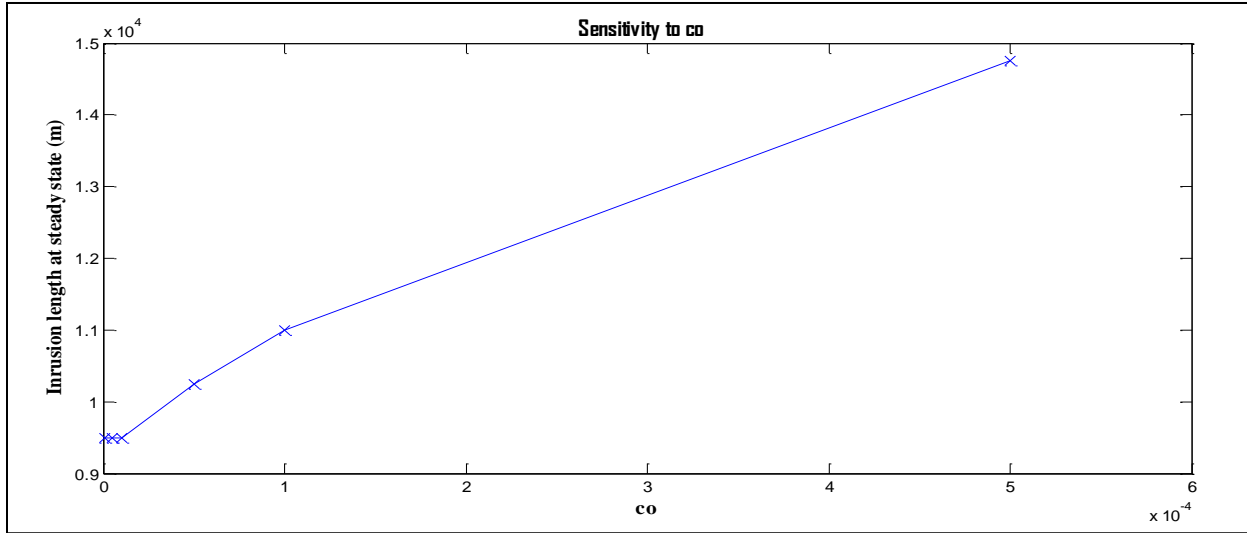


FIGURE 20: SENSITIVITY TO COEFFICIENT OF INTERFACIAL FRICTION FACTOR (CO)

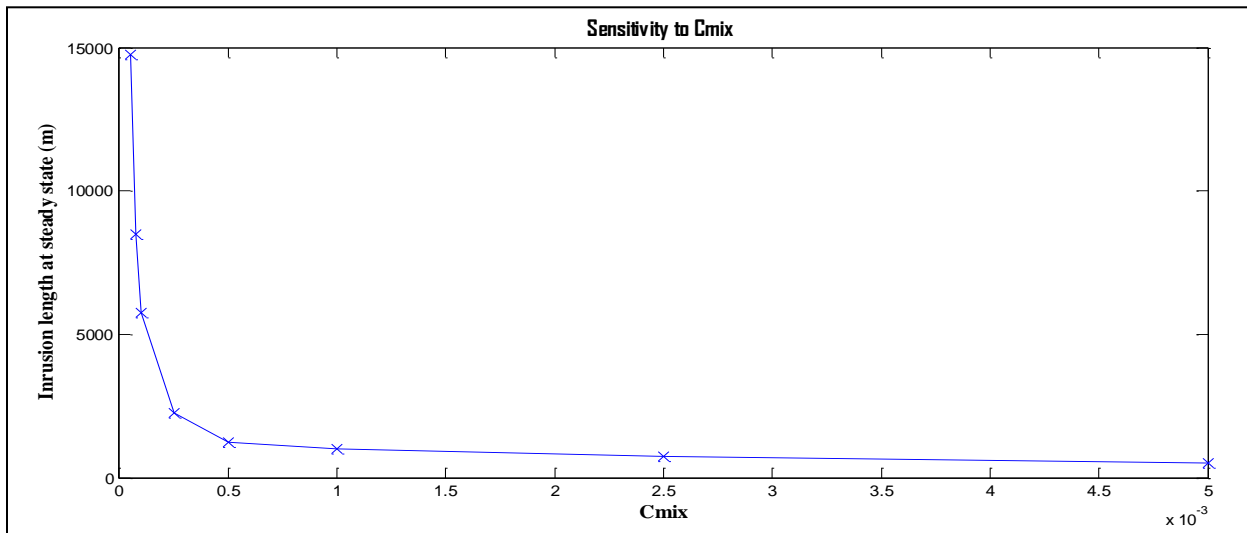


FIGURE 21: SENSITIVITY TO COEFFICIENT OF MIXING (C_{MIX})

7.3 Calibration and Validation of the Time Varying Model

7.3.1 River flow data used in calibration

Salinity measurements during the period from day 347 to 404 were employed because of the existence of the saline wedge during this period as a result of low flow conditions. Also, the initial flood condition was fulfilled.

The calibrated values for the Maha Oya according to the field conditions were:

Interfacial friction factor $co=1e-4$;

Bottom friction factor $kb=1e-3$;

Interfacial mixing coefficient $C_{mix}=6.25e-5$

$z=0.001$; $K=0.4$; (default values)

7.3.2 Calibration results

Field data for salinity and results from the model simulation have been plotted in the same figure for comparison. Calibration may be convenient if starting with the interfacial friction coefficient with reasonable value for the bottom friction factor, keeping no mixing until desirable intrusion length is achieved and then introduce the mixing for fine tuning. However in many cases the mixing coefficient plays an important role in the calibration. If no mixing exists, the results may not converge with reasonable values on the friction coefficient. Calibration is complete when the model simulation results are comparable to the set of field values. Calibration results are shown in Figure 22-25.

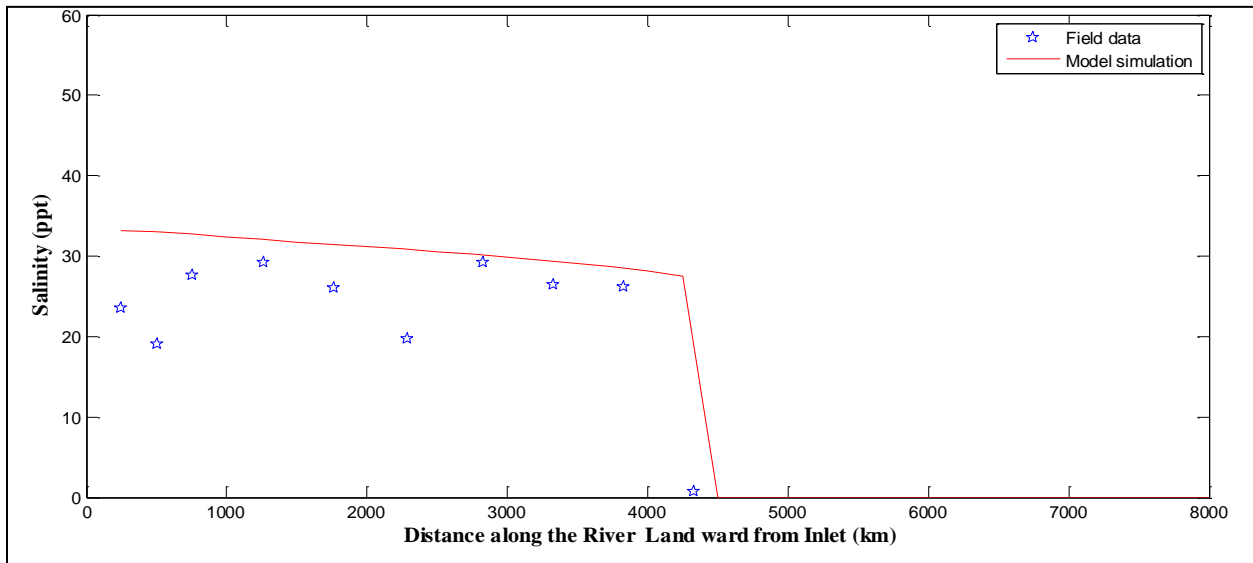


FIGURE 22: CALIBRATED MODEL SIMULATION RESULTS VERSUS FIELD CONDITION ON DAY 351 (FROM 2/10/2011)

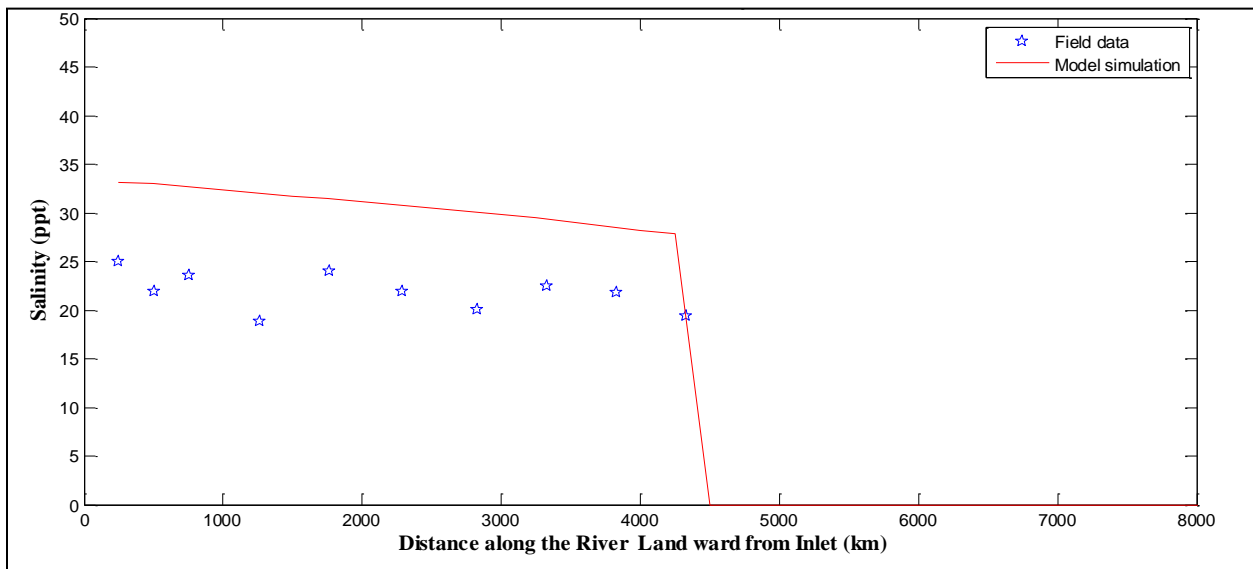


FIGURE 23: CALIBRATED MODEL SIMULATION RESULTS VERSUS FIELD CONDITION ON DAY 366 (FROM 2/10/2011)

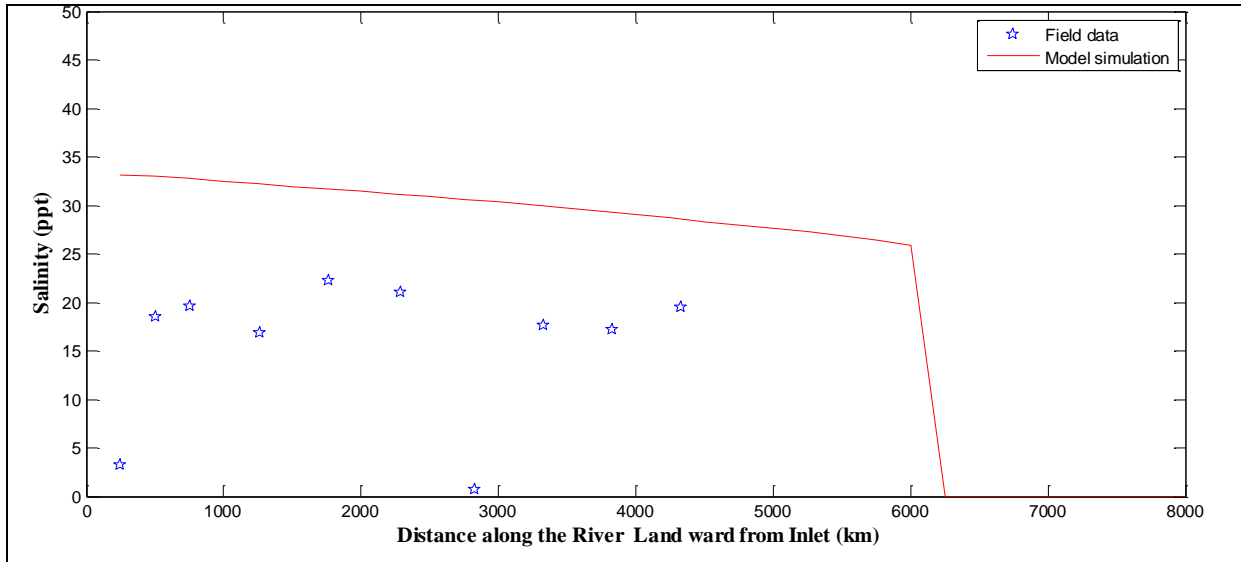


FIGURE 24: CALIBRATED MODEL SIMULATION RESULTS VERSUS FIELD CONDITION ON DAY 379 (FROM 2/10/2011)

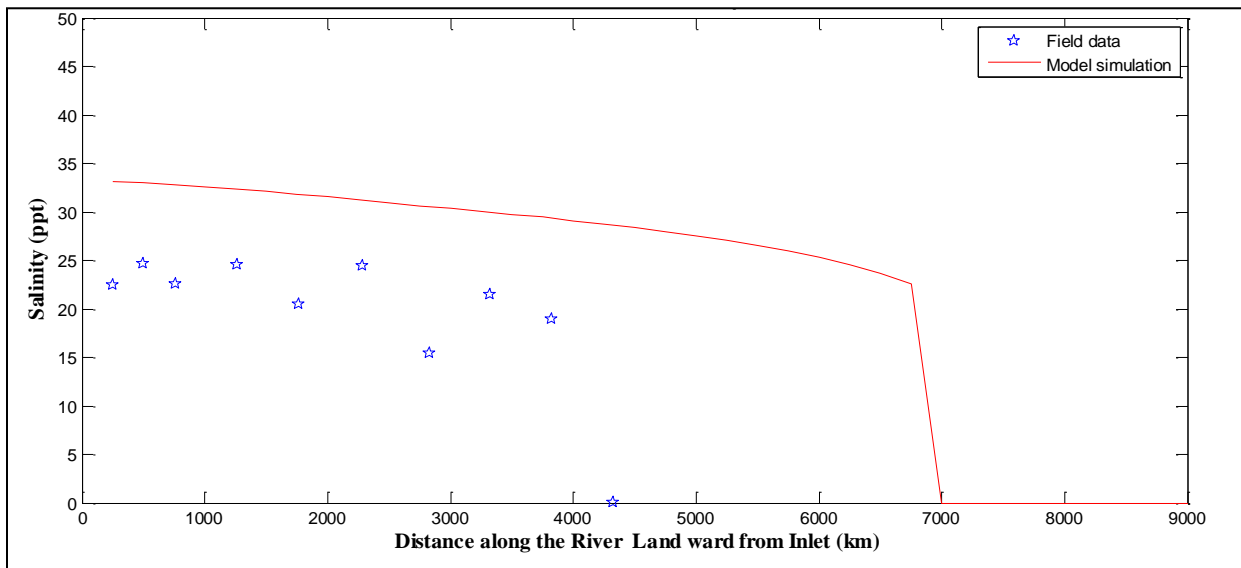


FIGURE 25: CALIBRATED MODEL SIMULATION RESULTS VERSUS FIELD CONDITION ON DAY 402 (FROM 2/10/2011)

It is seen that the results are over predicting the salinity values in comparison with the actual field conditions, because in the model boundary condition at the inlet it has been assumed the properties of sea water. Thus, the salinity of sea water was used as initial salinity and it often has higher values than the actual salinity at the inlet.

During the calibration period the river flow varied from 45 cum/s to 65 cum/s, but the field data do not show any movement of the wedge and it has stopped about 4.5 km from the inlet whereas model simulation shows movement. One reason would be the hydrodynamic effect of the artificial structure 7 km from inlet. Therefore, the calibration has been disturbed, and this causes errors in the simulation.

7.3.3 Validation Results

For the validation, another set of river discharge conditions from day 431 to 512 that fulfilled the initial and boundary conditions were selected, and at day 506 the salinity measurements were used for comparison. During the period of salinity measurements for the validation, the river had low flow compared to the calibration period. Hence it can be argued that the dynamic effects of the existing structure that created falling water over the weir was less and that the salt wedge had some free movements during the validation time. The validation results as shown in Figure 26 are in reasonable agreement with the actual situation.

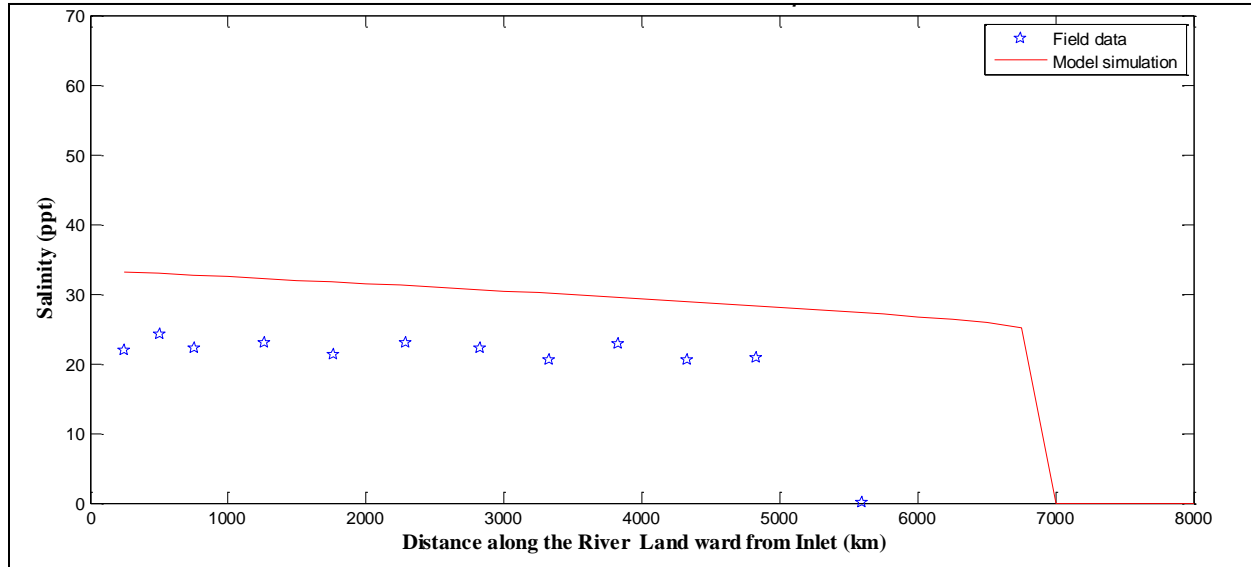


FIGURE 26: VALIDATED MODEL SIMULATION RESULTS VERSUS FIELD CONDITION ON DAY 506 (FROM 2/10/2011)

7.4 Steady-State Model application

The steady-state model may be applicable under small tidal influence and for gradually varying river discharge conditions. It may also be useful for obtaining an initial guess of the salinity intrusion length before going into details.

Discharge of the Maha Oya from day 350 to day 366 (Figure 8) can be approximated as 65 cum/s and from day 500 to day 507 as 35 cum/s (day 1 starts at 1st of March 2010). Availability of salinity measurements during these two periods facilitated calibration and validation of the model. Maximum intrusion length was the main variable in the calibration and validation.

7.4.1 Calibration results

Steady river flow of approximately 45 cum/s during the period of day 381 to day 402 was used in the model. Salinity measurements at day 402 show the existence of salt wedge up to 4.5 km from the inlet (field data in Figure 25). Steady state model can be calibrated using this intrusion length for simulation of maximum intrusion length. Having only one calibration parameter (friction factor), calibration can be done to match the maximum intrusion length exactly, using intrusion length at day 402. Figure 27 shows the calibrated

curve for river discharge of 45 cum/s. The value of the friction factor after calibration was 1.1×10^{-3} .

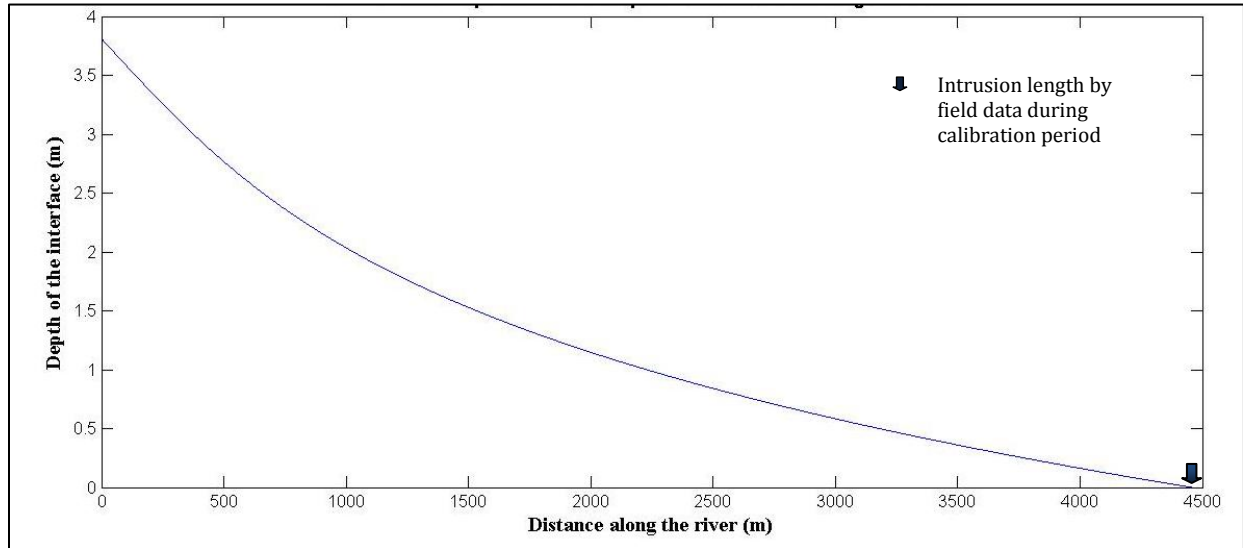


FIGURE 27: CALIBRATION CURVE OF THE STEADY-STATE MODEL

7.4.2 Validation results

Similarly during the period of day 481 to day 507, the river discharge remains almost constant at 35 cum/s (Figure 8). Therefore the model can be run for the steady state condition during this period. According to the field data in Figure 26 salinity measurements at day 506 shows that the intrusion was limited to a distance about 5.5 km from the inlet. From Figure 28, which shows the validation results, further movement upwards is obtained and almost a similar position of the salt wedge tip occurs as in the time-varying model.

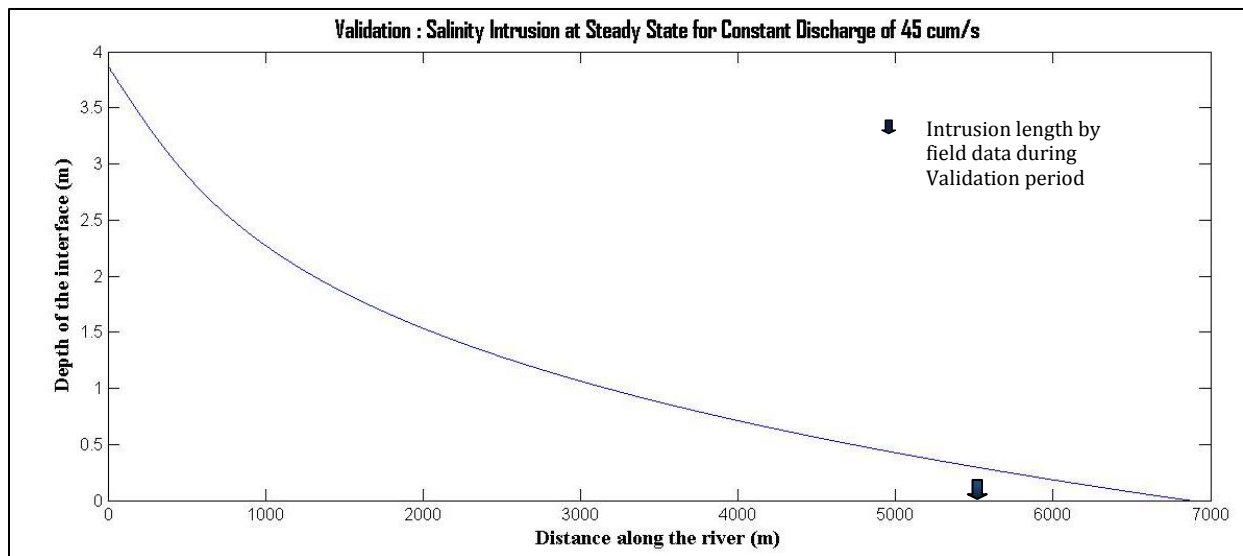


FIGURE 27: VALIDATION CURVE OF THE STEADY-STATE MODEL

8. Discussion

8.1 Results

8.1.1 Steady-state model

The steady-state model shows similar results as the time-varying model at equilibrium in terms of intrusion length under constant river discharge. Therefore, if the discharge conditions vary gradually, a steady-state model may be applicable. However, it does not provide information about possible salinity variations in either direction, vertical or horizontal. Since the salt layer hydrodynamics is ignored in the steady-state model, it only depends on the bottom friction factor as a calibration parameter and it shows high sensitivity towards this parameter.

8.1.2 Time-varying model

According to Figure 25, it can be seen from the salinity measurements that the salt wedge sometimes does not move appreciably, whereas as the model shows movement. One reason for this may be the salinity barrier at Bambukuliya. Kinetic energy of the overflowing water could provide an extra force to hold back the salt wedge propagation. During the validation period the influence of this flowing water is less and the salinity wedge is observed to move landward. In the model, the effects of the saltwater barrier are not considered and the model has infinite upstream boundary as the theoretical maximum intrusion length. Variation in bed levels along the sandy bed of the river during the study period may lead to errors in the simulations, as the model assumes unchanged bathymetry during the simulation period. Limitation of facilities in data acquisition and length of the study period are also a challenge to the accuracy.

8.2 Problems Related to the Salinity Intrusion in the Maha Oya

One of the main reasons for the increased salinity intrusion in the Maha Oya is illegal sand mining. It deepens the river, making holes in the bottom. Though the effects of these deep holes have not been investigated in detail, it is expected that stagnant salt water in these holes may contribute as a sources for the salt flux in the vertical mixing. Sand mining also leads to river bank erosion and finally change the bathymetry of the river in an unfavorable manner.

In Sri Lanka decentralized system of water supply are very popular. People dig wells individually in most part of the country for their water demands. In coastal areas these wells are often contaminated with salt water. In the Maha Oya lower reaches there is a risk of contamination of ground water due to the salinity intrusion in the Maha Oya. This is critical during the low flow seasons. During low flows the ground water table in surrounding areas tends to go deeper and salinity intrusion becomes higher. Then, this intruded salt water tends to infiltrate into the ground water and find its way to the wells. Sand mining activities also increase during the low flow seasons.

In agriculture, mainly rice is the staple food plant in Sri Lanka, and it is sensitive to the salinity of the irrigation water. Intrusion of salt into the irrigation water will adversely

affect the plant growth and reduce the crop yield. It takes more time and proper drainage systems are needed with more fresh water to wash away the accumulated salt in the paddy fields. Therefore, preventing saltwater intrusion is important to maintain low salt content in the soil.

8.3 Solutions to the Identified Problems

Salinity intrusion into the Maha Oya can be controlled by keeping human activities which adversely influence the bathymetry of the river to a minimum. Regulating sand mining activities so that the amount of sand extraction is maintained at a desired level in order to keep the river bottom undisturbed is important in this regards. Maintaining a sufficient river discharge by limiting upstream water withdrawals during the low flow season is also important to control the salinity intrusion. More detailed studies to understand the sediment transport, inlet characteristics, and sea level variation would be a valuable source of information in safeguarding this valuable ecosystem.

8.4 Simulation of Solution

The model was run in two steps for the same input data keeping all parameters fixed for two different river depths. Simulation results were plotted together in the Figure 29 for comparison.

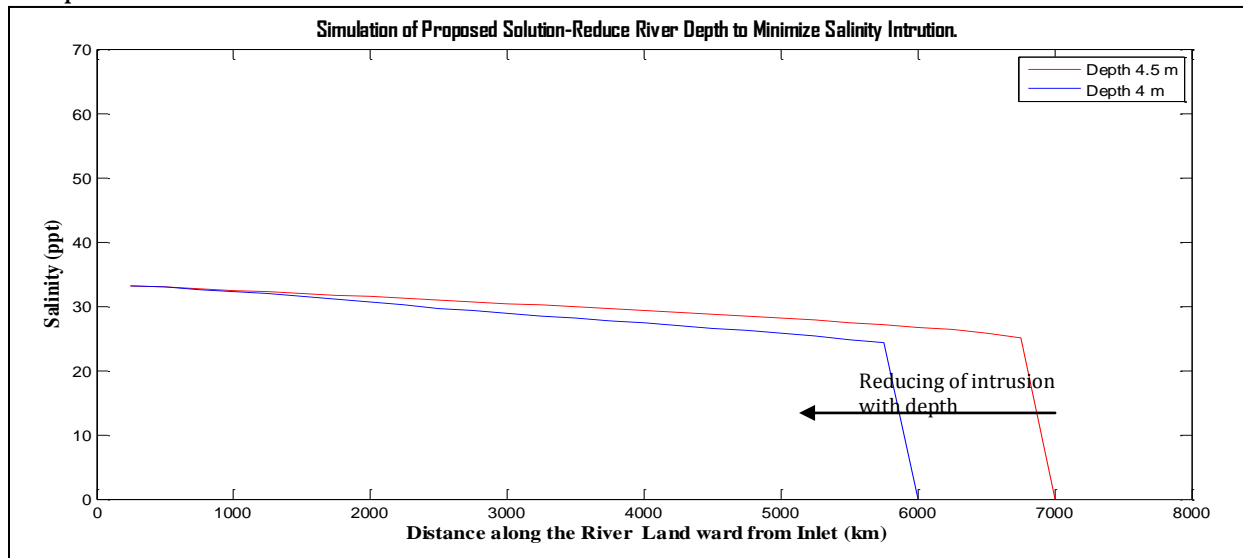


FIGURE 29: REDUCTION OF INTRUSION WITH DECREASE IN WATER DEPTH

Figure 29 shows the variation in the intrusion length with the depth of the river. According to the results, the intrusion length is reduced with a decrease in the depth. Thus, minimizing sand mining activities would probably reshape the river profile with sand infilling of the mining holes and bed level increase to desired depths.

9. Conclusions

This study was focused on understanding the situation of the Maha Oya from a salinity intrusion perspective. Field campaign and literature review were integrated parts of the study. Field works comprised salinity measurement along the river, discharge measurement at Bambukuliya, and surveying of the river. Some surveying data was provided by Environmental Foundation Limited, who was the facilitator of the project. Field works also included data collection from authorities handling the data. Due to the time restriction in the project the field campaign did not cover very low flow conditions. After getting a basic understanding about the salinity structure and governing hydrodynamics that included the tidal influence, the literature review emphasized to two-layer stratified flow system. The model was developed as a series of finite difference approximations in space (one-dimensional) and in time. Formation of salt wedge in space and time was the result. All phenomena were described by the flow equations. Continuity and momentum equations are the basis for developing the shape of the interface. Mixing at the interface was also considered in flow equations. Finally, salt transport equation was used to simulate longitudinal density variations. Boundary conditions assumed having a fresh river initially and densimetric critical flow at the inlet. As the result, the model shows existing salinity structure at the time of interest. Thickness of the stratified layers and appropriate salinity of them in space and time were the model outputs.

Time-varying models can be used for variable hydrodynamic conditions under constant bathymetry, once they are calibrated. So for long-term data during which the river bathymetry may change, the model may not be able to well simulate saltwater intrusion with fixed values on the calibration parameters. More detailed studies should then be carried out to improve the model performance. Calibration parameters may have functional dependencies that change with factors such as the bathymetry of the river, the effect of tidal oscillation in stratification, inlet characteristics and sediment transport .

Salinity intrusion in the study area is limited by the weir located about 7km upstream of the inlet. Thus, the maximum intrusion length is always less than distance between the inlet and the weir. The salinity concentration may increase during low-flow seasons in lieu of the lateral movement of the salt wedge. The model has not considered this boundary condition and it simulates a free up stream end.

The Maha Oya salinity intrusion is very sensitive to the fresh water discharge and you always have a river without residual salt after each flooding period. So it is easy to run the model having only the river discharge as the flow data. Although the bottom layer dynamics have been considered in the model, it is not necessary to have the flow data of the bottom layer to run the model if the initial flood condition is fulfilled. A sharp interface has been assumed and vertical salinity variation in each layer has not been taken in to account in flow equations. Therefore, variations in the vertical concentration of salinity are not simulated in the model. An assumption of zero lateral flow is reasonable because the river does not have any branches within the study limit except the Dutch canal, which can be ignored in comparison with the Maha Oya flow.

Inlet parameters are changing seasonally. The inlet of the Maha Oya is comparatively narrow. The width of the inlet is less than the average width of the river and during low flow season this inlet closes forming a sand barrier. The inlet parameters are the influencing factors in salinity intrusion. Thus, it seems that the inlet would be a good location for controlling the salinity intrusion in the Maha Oya. Further studies to understand the effect of the inlet on the salinity intrusion is desirable.

Bibliography

- Abeywickrama N, Lanka Jalani and IWMI .2002. basin level dialoge Sri Lanka.paper for the International water conference Hanoi,Vietnam October 14-16 2002 [pdf] available at < <http://www.bvsde.paho.org/bvsacd/dialogo/abey.pdf> > viewed on 14th February 2012.
- Alwis A.D et al 1995, Initial Environmental Examination of the Proposed Industrial Estate at Karanawa Watta (Dankotuwa).Study report:NAREPP/IRG. Colombo Sri Lanka [pdf] available at < http://pdf.usaid.gov/pdf_docs/PNABY878.pdf > viewed on 5th May 2011.
- Amarasinghe U.A, Mutuwatta L, Sakthivadivel R 1999, Water scarcity variations within a country: A case study of Sri Lanka. Research report 32.: International Water Management Institute. Colombo Sri Lanka .[pdf] available at < <http://cdm15025.contentdm.oclc.org/u?p267501ccp2.3270> >viewed on 11th of September 2011.
- Amarasinghe U. A 2010. Spatial Variation of water supply and demand in Sri Lanka, Conference Paper h042803, International water Management Institute.[pdf] available at < <http://ideas.repec.org/p/iwt/conppr/h042803.html> > viewed on 5th of October 2011.
- Arita, M. and Jirka G.H 1987.Two-Layer Model of Saline Wedge. I: Entrainment and Interfacial Friction. Journal of Hydraulic Engineering,. 113(10): p. 1229-1246.American Society of Civil Engineers[pdf]available at< [http://link.aip.org.ludwig.lub.lu.se/link/doi/10.1061/\(ASCE\)0733-9429\(1987\)113:10\(1229\)](http://link.aip.org.ludwig.lub.lu.se/link/doi/10.1061/(ASCE)0733-9429(1987)113:10(1229)) > viewed on 23rd March 2011.
- Arita, M. and G.H. Jirka 1987.Two-Layer Model of Saline Wedge. II: Prediction of Mean Properties. Journal of Hydraulic Engineering,. 113(10): p. 1249-1263 American Society of Civil Engineers[pdf]available at< [http://link.aip.org.ludwig.lub.lu.se/link/doi/10.1061/\(ASCE\)0733-9429\(1987\)113:10\(1249\)](http://link.aip.org.ludwig.lub.lu.se/link/doi/10.1061/(ASCE)0733-9429(1987)113:10(1249)) > viewed on 23rd March 2011.
- Balloffet, A. and D.K. Borah 1985. Lower Mississippi Salinity Analysis. Journal of Hydraulic Engineering,. 111(2): p. 300-315. American Society of Civil Engineers[pdf]available at< [http://link.aip.org.ludwig.lub.lu.se/link/doi/10.1061/\(ASCE\)0733-9429\(1985\)111:2\(300\)](http://link.aip.org.ludwig.lub.lu.se/link/doi/10.1061/(ASCE)0733-9429(1985)111:2(300)) > viewed on 25th March 2011.
- Benjamin, T.B. 1968. Gravity currents and related phenomena. Journal of Fluid Mechanics, 31(02): p. 209-248.Institute of Geophysics and Planetary Physics. University of California. La Jolla.[pdf] available at < <http://weather.ou.edu/~hblue/metr6223/Benjamin.68.pdf> > viewed on 9th November 2011.
- Bowen, M.M., et al. 2000. Mechanisms and variability of salt transport in partially-stratified estuaries. Cambridge, , Massachusetts Institute of Technology ; Woods Hole Oceanographic Institution. Woods Hole [pdf] available at < <http://search.proquest.com.ludwig.lub.lu.se/docview/304663034> > viewed on 17th July 2011.
- Karelse M, Vreugdenhil C.B, Delvigne G.A.L and Breusers H.N.C. 1974. Momentum and mass transfer in stratified flows: report on literature study; R 880.Delft Hydraulics Laboratory.Delft[pdf]available at < <http://www.scribd.com/doc/65826285/Momentum-and-mass-transfer-in-stratified-flows-report-on-literature-study> > viewed on 24th November 2011.
- Pugh D. T 1987: Tides, Surges and mean sea-level by : Marine and Petroleum Geology, Volume 5, Issue 3, August 1988, Page 301, John Wiley and Sons Ltd., [pdf] available at < <http://eprints.soton.ac.uk/19157/1/sea-level.pdf> > viewed on 10th July 2011

Drfumblefinger 2010.,Elephant bathing at Pinnawela[photo] Travepod [online]available at,< http://blog.travepod.com/travel-photo/dfumblefinger/1/1266238317/5_elephants-bathing-in-pinnawala.jpg/tpod.html > viewed on 15th February 2012.

Environmental Foundation limited 2010, Maha Oya under threat, Maha Oya Brochure, [pdf], available at< http://www.efl.lk/wpcontent/uploads/2011/03/MahaOyaBrochure_English.pdf > viewed 25th of July 2011

Fischer H.B, List E.J, Koh R.C.Y, Imberger J, Brook N.H 1979, Mixing in Inland and Coastal Waters. New York: Academic Press Inc

Fernando K.M.N.S 2005. Maha Oya (River) and River Basin from National Water and Sanitation Service Providers Perspective, Paper for training program. Asian Development Bank. [pdf] available at < <http://www.adb.org/Water/narbo/2005/Training-Program/pres-Fernando-NARBO-training.pdf> >viewed 5th of October 2011.

GU, L. and G.A. LAWRENCE 2005.Analytical solution for maximal frictional two-layer exchange flow. Journal of Fluid Mechanics. 543: p. 1-17.Department of Civil Engineering.University of British Columbia. Vancouver[pdf] available at < <http://journals.cambridge.org.ludwig.lub.lu.se/action/displayAbstract?fromPage=online&aid=350142> > viewed on 14th July 2011.

Institute of fundamental Studies Sri Lanka 2010,Geology of Sri Lanka,lecturenote [online]available at < <http://www.ifs.ac.lk/> > viewed on 11th of September 2011.

Keskin, M.E. and N. Ağiralioğlu1997. A simplified dynamic model for flood routing in rectangular channels. Journal of Hydrology,. 202(1-4): p. 302-314.Department of Civil Engineering.Technical University of Istanbul.Istanbul[pdf] available at < [http://dx.doi.org.ludwig.lub.lu.se/10.1016/S0022-1694\(97\)00072-3](http://dx.doi.org.ludwig.lub.lu.se/10.1016/S0022-1694(97)00072-3) > viewed on 2nd May 2011.

Masaru, Y. 2003. Observations in the Proterozoic Geology of Sri Lanka: IGCP-440 Field Workshop, March-April. Gondwana Research, 2003. 6(4): p. 942-946.Japan[pdf]available at < [http://dx.doi.org.ludwig.lub.lu.se/10.1016/S1342-937X\(05\)71043-1](http://dx.doi.org.ludwig.lub.lu.se/10.1016/S1342-937X(05)71043-1) > viewed on 11th September 2011

McCutcheon S.C, Martin J.L, Barnwell T.O.Jr 1993.Water Quality in Maidment D.R (Editor).Hand Book of Hydrology(p.11.3), MaGraw-Hill,New York,NY[excel]available at < <http://www.earthwardconsulting.com/density.xls> > viewd on 14th September 2011

Mobile Geographics LLC.2005.Tide Chart: Colombo, SriLanka[online] avialable at < <http://tides.mobilegeographics.com/locations/1319.html> > viewd on 17th February 2012.

Prandle, D 2003. Relationships between Tidal Dynamics and Bathymetry in Strongly Convergent Estuaries. Journal of Physical Oceanography. 33(12): p. 2738-2750.

Punyawardena V.B.R n.d, Climate change:Challenges and Oppertunities in Sri Lanka.l Resources management Center. Department of Agriculture, Sri Lanka [pdf] available at< http://cmsdata.iucn.org/downloads/pres_ranjith_punyawardena.pdf >viewed on 7th October 2011.

- Ranasinghe, P.N., et al 2002. Importance of Grain Size Factor in Distribution of Trace Elements in Stream Sediments of Tropical High Grade Terrains – A Case Study from Sri Lanka. *Chemie der Erde – Geochemistry*. 62(3): p. 243-253. Urban Fischer Verlag [pdf] available at < <http://dx.doi.org.ludwig.lub.lu.se/10.1078/0009-2819-00015> > viewed on 20th July 2011.
- Rastogi R.G. 1969. Lunar tidal oscillations in ionospheric absorption at Colombo. *Journal of Atmospheric and Terrestrial Physics*, 31(5): p. 759-761.[pdf] available at < [http://dx.doi.org.ludwig.lub.lu.se/10.1016/0021-9169\(69\)90134-2](http://dx.doi.org.ludwig.lub.lu.se/10.1016/0021-9169(69)90134-2) > viewed on 23rd February 2012.
- Ranatunga C 2005. Management Issues in River Basins of Sri Lanka A Stakeholders View Based on Maha Oya River Basin, Paper for training program. Asian Development Bank. [pdf] available at < <http://www.adb.org/Water/narbo/2005/Training-Program/pres-Ranatunga-NARBO-training.pdf> > viewed 5th of October 2011.
- Seim, H., J. Blanton, and S. Elston 2006. Tidal circulation and energy dissipation in a shallow, sinuous estuary. *Ocean Dynamics*. 56(3): p. 360-375. Springer Verlag [pdf] available at < <http://www.springerlink.com.ludwig.lub.lu.se/content/q5173t34035t5trj/fulltext.pdf> > viewed on 31st March 2011.
- Sargent, F.E. and G.H. Jirka 1987. Experiments on Saline Wedge. *Journal of Hydraulic Engineering*. 113(10): p. 1307-1323. American Society of Civil Engineers [pdf] available at < [http://dx.doi.org.ludwig.lub.lu.se/10.1061/\(ASCE\)0733-9429\(1987\)113:10\(1307\)](http://dx.doi.org.ludwig.lub.lu.se/10.1061/(ASCE)0733-9429(1987)113:10(1307)) > viewed on 11th September 2011
- U.S Army Corps of Engineers 1993. Control methods for salinity intrusion in well stratified estuaries and waterways: technical letter No1110-2-347, Department of the Army, Washington DC [pdf] available at < <http://www.dtic.mil/cgi-bin/GetTRDoc?AD=ADA403190> > viewed on 7th August 2011.
- Vu T.C (1996), 'Salinity Intrusion in the Red River Delta. Seminar on Environment and Development in Vietnam', paper presented at the Australian National University seminar 1996, [online], available at < http://coombs.anu.edu.au/~vern/env_dev/papers/pap08.html > viewed 11th September 2011
- William C. Seabergh 2002, Hydrodynamic of Tidal Inlets. Coastal Engineering manual, Part 2, Hydrodynamics, Chapter 6, Engineer Manual 1110-2-1100, U.S. Army Corps of Engineers, Washington DC.
- Wijeratne E.M.S and Pattiaratchi (n.d) :Sea Level variability in Sri Lanka Waters, poster. National Aquatic Resources Research and Development Agency. Colombo [pdf] available at < http://wcrp.ipsl.jussieu.fr/Workshops/SeaLevel/Posters/2_1_WijeratneRevised.pdf > viewed on 16th February 2012.
- Wijeratne E.M.S 2007. Levelling of Sri Lanka Tide Gauges for improved hydrodynamic modelling of the Palk Strait, National Aquatic Resources Research and Development Agency. Colombo [pdf] available at < http://www.nara.ac.lk/journals/nara%20journal%202007/Article_280.pdf > viewed on 16th February 2012

Appendixes

Appendix 1: Mat lab codes of the Models

Steady State Model

```
clear all
Q=28.5;
b1=45;
B=20;
H=3;
g=.02*9.81;
q=Q/(sqrt(g*H)*H^2)
hc=(Q^2/g/B^2)^(1/3)
h(1)=-1.2*hc/H
b=b1/H
x=300/H
f=input('pls enter friction factor>');
for i=1:100
h(i+1)=h(i)+f*q^2*(1/h(i)-1/(1-h(i)))*x/((1-q^2/(b^2*(h(i))^3))*(8*b^2*(h(i))^2))
    if h(i+1)<-1
        break
    end
end
plot(h)
```

Time Varying Model

```
% THEMAHAOYA
clc
clear all
% LOAD RIVER FLOW DATA
load('C:\Users\DELL\Desktop\mahaoya_salinitymodel2011\Q_calibration.mat')
z=.01;K=2.5; w=2;
% CALIBRATION PARAMETERS
co=1e-4; kb=2.5e-3; Cmix=1e-4;
% BATHOMETRIC AND BASIC DATA
b=40;H0=5;s0=1e-3;
denseaw=1027;denfrew=1000;x=250;Poya=7;DaIm=[4.5];dscharge_interval=1;
L=15000; detp=0.02; depth_ave=DaIm; H0=5; diffp=detp*denfrew;
t=3.125*3600;Ttide=6.25*3600;r=Ttide/t;Temp=27.5;maxtamp=0.35;mintamp=0.1;
amx=maxtamp;ami=mintamp;dur=7; M=L/x;
J=length(qriver); Q0=mean(qriver); M=L/x; a=.35;g1=0.02*9.81;
%TIDAL EBB OR FLOOD AT INLET MOUTH
for j=1:J;
    if mod(j,2)==0
        a1(1,j)=DaIm+a;
        else a1(1,j)=DaIm-a;
    end
end
%VELOCITIES AT UPSTREAM END
```

```

for j=J
for m=1:M
    if qriver( 1:j)>Q0
ki=co;
else ki=co.*(qriver( 1:j)./Q0).^w;
    end
so(1:J)=repmat(s0,J,1);
T=dscharge_interval*25*3600;
% DENSIMETRIC CRITICAL FLOW AT INLET
h0o(1:j)=(((qriver(1:j).^2)./(g1*B^2)).^(1/3));
h10(1:j)=(h0o(1:j));
% HEIGHT OF SALT LAYER AT INLET
a0(1:j)=(a1(1:j)-h10(1:j));
a0(a0<=0.01)=0.01;
h20(1:j)=(a0(1:j));
u10(1:j)=-qriver(1:j)./(h0o(1:j)*b);
Uriver(1:j)=(qriver(1:j)./DaIm./b);
end
end
% DETERMINE APPROPRIATE FRESH WATER VELOCITIES AT EACH TIME STEPS
qmriver=repmat ([qriver],M,1);
for j=1:J
for m=1:M;
xx=(x*(1:M));
tq(m,j)=(L-xx(m))./Uriver(j)+T*j ;
end
end
for m=1:M
for j=1:J-1
n=0;
    while t*(n)+T*j<tq(m,j+1)
n=n+1;
Q(m,n,j)=qmriver(m,j);
        continue
    end
end
end
Q=Q(:,any(Q))
siz=size(Q);
sQ=size(Q);
QQQ=Q*0;
% TO REMOVE ZERO VELOCITIES
for i=1:sQ(1)
L=find(Q(i,,:));
l=length(L);
QQQ(i,1:l)=Q(i,L);
clear l
end

```

```

MM=M;NN=J*T/t;
SQQQ(2)=int32(NN);
SQQQ(1)=M;
% FRICTION COEFFICIENT FOR ALL STEPS
kki=zeros(SQQQ(1),SQQQ(2));
for i=1:SQQQ(1)
for j=1:SQQQ(2)
    if QQQ(i,j)> Q0
kki(i,j)=co;
        else kki(i,j)=co*(QQQ(i,j)/Q0).^w;
        end
        if QQQ(i,j)==0
kki(i+1:end,j)=kki(i,j);
            end
        end
end
end
% MONTHLY TIDAL VARIATION SEMIDIURNAL LUNAR TIDES
for N=1:14
modn=mod(N,14);
    if modn< 8
a_month(N)=abs(amx-(amx-ami)/dur*(modn-1));
        else
a_month(N)=abs(ami-(amx-ami)/dur*(8-modn));
        end
end
%TIDES FOR FULL TIME PERIOD
Nt=int32(SQQQ(2));
mdays=int32(14);
avsp=idivide(Nt,mdays,'ceil');
an_month1= repmat(a_month,1,(avsp+1));
an_month=an_month1(Poya:end);
% TIDAL IMPACT FOR EACH STEP FOR BOTH FLOOD AND EBB
a1=zeros(1,SQQQ(2));
for N=1:SQQQ(2)
tide=an_month(1:N);
    if mod(N,2)==0
a1(1,N)=DaIm+tide(1,N)*2/pi;
        else a1(1,N)=DaIm-tide(1,N)*2/pi;
        end
end
% FOR TIME STEP NOT EQUAL TO HALF TIDAL PERIODS
    if r==1
aa2= a1;
    elseif r==2
c=cat(2,a1(:),a1(:));
e= reshape(c.',1,[]);
aa2=e;
    elseif r==4

```

```

c_4=cat(2,aa1(:),aa1(:));
e_4= horzcat(c_4,c_4);
f_4= reshape(e_4.',1,[]);
aa2= f_4;
else aa2=0;
end
aa2;
N=SQQQ(2);M=SQQQ(1);
for m=1:SQQQ(1)-1;
for n=1:SQQQ(2)-1;
u2(1:M,1)=zeros(M,1);
h2(1:M,1)=zeros(M,1);
h1(1:M,1)=repmat(H0,1,M);
h00o=(QQQ(1,2)^2/(g1*B^2))^(1/3);
h1(1,2)=(h00o);
a=.7;
h0(1,2:SQQQ(2))=(QQQ(1,2:SQQQ(2)).^2/(g1*B^2)).^(1/3);
a00(1,2:SQQQ(2))=(aa2(1,2:SQQQ(2))-h0(1,2:SQQQ(2)));
a00(a00<=0.01)=0.01;
h2(1,2:SQQQ(2))=a00(1,2:SQQQ(2));
u1(1:M,1)=repmat(-Q0/b/H0,M,1);
u1(1,2)=-QQQ(1,1)/(h00o*b);
ut(1,2)=sqrt((h1(1,2)+h2(1,2)).*g1./(h1(1,2).*h2(1,2))).*tide(1,2)/sqrt(2);
ud(1,2)=sqrt(h2(1,2).*g1*2);
uu(1,2)=ut(1,2)+ud(1,2);
u2(1,2)=uu(1,2).*log10(h2(1,2)/(10*z)./K);
u2(u2<=0)=.001;
Fi0=(u1(1,2)-u2(1,2))/sqrt(((h1(1,2)+h2(1,2))*g1));
si0=((Fi0^2)*(h1(1,2)+h2(1,2))^2*ki)/(h1(1,2)*h2(1,2));
u1(1:M,1)=repmat((-Q0/(b*H0)),M,1);
u1(1,2:SQQQ(2))=-QQQ(1,2:SQQQ(2))./(h0(1,2:SQQQ(2))*b);
h1(1,2:SQQQ(2))=h0(1,2:SQQQ(2));
u2(1:M,1)=repmat(.01,M,1);
ut(1,2:SQQQ(2))=sqrt((h1(1,2:SQQQ(2))+h2(1,2:SQQQ(2))).*g1./(h1(1,2:SQQQ(2)).*h2(1,2:SQQQ(2)))).*(tide(1,2:SQQQ(2))./sqrt(2));
ud(1,2:SQQQ(2))=sqrt(h2(1,2:SQQQ(2)).*g1*2);
if mod(SQQQ(2),2)==0
uu(1,2:SQQQ(2))=ut(1,2:SQQQ(2))+ud(1,2:SQQQ(2));
else uu(1,2:SQQQ(2))=ud(1,2:SQQQ(2))-ut(1,2:SQQQ(2));
end
if r==1
uu2(1,2:SQQQ(2))= uu(1,2:SQQQ(2));
elseif r==2
uu=uu(1,2:SQQQ(2));
c=cat(2,uu(:),uu(:));
e= reshape(c.',1,[]);
uu2=e;
elseif r==4
uu=uu(1,2:SQQQ(2));

```

```

c_4=cat(2,uu(:),uu(:));
e_4= horzcat(c_4,c_4);
f_4= reshape(e_4.',1,[]);
uu2= f_4;
    else uu2=ud;
uu=uu(1,2:SQQQ(2));
    end
u2(1,2:SQQQ(2))=uu2(1,2:SQQQ(2))./K.*(log10((h2(1,2:SQQQ(2))/10/z)));
u2(u2<=0)=.01;
F1(1,2)=u1(1,2)/sqrt((h1(1,2)*g1));
F2(1,2)=u2(1,2)/sqrt((h2(1,2)*g1));
Fi(1,2)=(u1(1,2)-u2(1,2))/sqrt(((h1(1,2)+h2(1,2))*g1));
si(1,2)=(Fi(1,2)*abs(Fi(1,2)))*((h1(1,2)+h2(1,2))^2)*kki(1,2)/(h1(1,2)*h2(1,2));
sb(1,2)=(F2(1,2)*abs(F2(1,2)))*kb;
sf(1,2)=(F2(1,2)*abs(F2(1,2)))*kb+kki(1,2).*(Fi(1,2)*abs(Fi(1,2))*((h1(1,2)+h2(1,2))^2)/(h1(1,2)*h2(1,2)));
F1(1:M,1)=(u1(1:M,1))./sqrt((h1(1:M,1).*g1));
F1(1,2:SQQQ(2))=QQQ(1,2:SQQQ(2))./(h0(1,2:SQQQ(2))*b)./sqrt((h0(1,2:SQQQ(2)).*g1));
F2(1:M,1)=zeros(M,1);
F2(1,2:SQQQ(2))=(u2(1,2:SQQQ(2))./sqrt((h2(1,2:SQQQ(2)).*g1)));
Fi(1:M,1)=(u1(1:M,1))./sqrt((h1(1:M,1).*g1));
Fi(1,2:SQQQ(2))=(u1(1,2:SQQQ(2))-u2(1,2:SQQQ(2)))./sqrt(((h1(1,2:SQQQ(2))+h2(1,2:SQQQ(2))).*g1));
sb(1:M,1)=(F1(1:M,1).^2).*kb;
sb(1,2:SQQQ(2))=((F2(1,2:SQQQ(2)).*abs(F2(1,2:SQQQ(2))))).*kb+(F2(1,2:SQQQ(2)).*abs(F2(1,2:SQQQ(2))))).*kb/2;
si(1:M,1)=zeros(1,M);
si(1,2:SQQQ(2))=((Fi(1,2:SQQQ(2)).*abs(Fi(1,2:SQQQ(2))))).*((h1(1,2:SQQQ(2))+h2(1,2:SQQQ(2))).^2).*kki(1,2:SQQQ(2))./(h1(1,2:SQQQ(2)).*h2(1,2:SQQQ(2)))+(Fi(1,2:SQQQ(2)).*abs(Fi(1,2:SQQQ(2))))).*((h1(1,2:SQQQ(2))+h2(1,2:SQQQ(2))).^2).*kki(1,2:SQQQ(2))./(h1(1,2:SQQQ(2)).*h2(1,2:SQQQ(2)))/2;
sf(1:M,1)=(F1(1:M,1).*abs(F1(1:M,1))).*kb+(F1(1:M,1).*abs(F1(1:M,1))).*kb/2;
sf(1,2:SQQQ(2))=sb(1,2:SQQQ(2))+si(1,2:SQQQ(2));
bita(1:M,1)=-sb(1:M,1)*9.81;
bita(1,2:SQQQ(2))=(si(1,2:SQQQ(2)).*h2(1,2:SQQQ(2))./(h1(1,2:SQQQ(2))+h2(1,2:SQQQ(2))).*g1+(2*s0-sf(1,2:SQQQ(2)))*9.81);
lamda(1:M,1)=(sb(1:M,1))*(g1-9.81);
lamda(1,2:SQQQ(2))=(sb(1,2:SQQQ(2))+si(1,2:SQQQ(2)).*h1(1,2:SQQQ(2))./(h1(1,2:SQQQ(2))+h2(1,2:SQQQ(2))))).*g1-(sf(1,2:SQQQ(2))).*9.81;
F1(m+1,n+1)=(u1(m+1,n)/sqrt((h1(m+1,n)*g1)+u1(m,n+1)/sqrt(h1(m,n+1)*g1)))/2;
Fi(m+1,n+1)=(u1(m+1,n)-u2(m+1,n))/sqrt(((h1(m+1,n)+h2(m+1,n))*g1)+(u1(m,n+1)-u2(m,n+1))/sqrt(((h1(m,n+1)+h2(m,n+1))*g1)))/2;
G(m+1,n+1)=(u1(m+1,n)-u2(m+1,n))^3*Cmix*t/(g1*(h1(m+1,n)+h2(m+1,n)))+(u1(m,n+1)-u2(m,n+1))^3*Cmix*t/(g1*(h1(m,n+1)+h2(m,n+1)));
G(m,n)=(G(m+1,n)+G(m,n+1))/2;
    if n==1
F2(m+1,n+1)=u2(m,n+1)./sqrt((h2(m,n+1).*g1));
si(m+1,n+1)=(Fi(m,n+1).^2).*((h1(m,n+1)+h2(m,n+1)).^2).*kki(m,n+1)/(h1(m,n+1).*h2(m,n+1));
sf(m+1,n+1)=(F2(m,n+1).^2).*kb+(Fi(m,n+1).^2).*((h1(m,n+1)+h2(m,n+1)).^2).*kki(m,n+1))./(h1(m,n+1).*h2(m,n+1));
sb(m+1,n+1)=(F2(m,n+1).^2).*kb;

```



```

else
F2(m+1,n+1)=(u2(m+1,n)./sqrt((h2(m+1,n).*g1)+u2(m,n+1)./sqrt((h2(m,n+1).*g1))))./2
;
si(m+1,n+1)=(Fi(m+1,n).^2.*(h1(m+1,n)+h2(m+1,n)).^2).*kki(m+1,n)/(h1(m+1,n).*h2(m+1,n))+
(Fi(m,n+1).^2.*(h1(m,n+1)+h2(m,n+1)).^2).*kki(m,n+1)/(h1(m,n+1).*h2(m,n+1)))./2;
sf(m+1,n+1)=(F2(m+1,n).^2).*kb+(Fi(m+1,n).^2.*(h1(m+1,n)+h2(m+1,n)).^2).*kki(m+1,n)/
(h1(m+1,n).*h2(m+1,n))+F2(m,n+1).^2).*kb+(Fi(m,n+1).^2.*(h1(m,n+1)+h2(m,n+1)).^2).*
kki(m,n+1)/(h1(m,n+1).*h2(m,n+1)))./2;
sb(m+1,n+1)=(F2(m+1,n).^2).*kb+(F2(m,n+1).^2).*kb)./2;
end
lamda(m+1,n+1)=(sb(2,n)+si(2,n).*h1(m+1,n)/(h1(m+1,n)+h2(m+1,n))).*g1-
(sf(2,n)).*9.81+(sb(2,n+1)+si(2,n+1).*h1(m,n+1)/(h1(m,n+1)+h2(m,n+1))).*g1-
(sf(2,n+1)).*9.81)/2;
lamdam(m,n)=(lamda(m+1,n)+lamda(m,n+1))/2;
Fim(m,n)=(Fi(m+1,n)+Fi(m,n+1))/2;
bita(m+1,n+1)=(si(2,n).*h2(m+1,n)/(h1(m+1,n)+h2(m+1,n)).*g1-
(2*s0+sf(2,n)*9.81)+(si(2,n+1).*h2(m,n+1)/(h1(m,n+1)+h2(m,n+1)).*g1-
(2*s0+sf(2,n+1))*9.81))/2;
bitam(m,n)=(bita(m+1,n)+bita(m,n+1))/2;
u1m(m,n)=(u1(m+1,n)+u1(m,n+1))/2;
u1(m+1,n+1)=(u1(m+1,n)-((u1(m+1,n)+u1(m,n+1))./2).*u1(m,n+1).*(t/x)+(bitam(m,n)-
G(m,n)*u1m(m,n)))/(1-((u1(m+1,n)+u1(m,n+1))./2).*u1(m,n+1).*(t/x)));
u2m(m,n)=(u2(m+1,n)+u2(m,n+1))/2;
u2(m+1,n+1)=(u2(m+1,n)+u2m(m,n).*u2(m,n+1).*(t/x)+(lamdam(m,n)+G(m,n)*u2m(m,n)))/(1+
((u2(m+1,n)+u2(m,n+1))./2).*u2(m,n+1).*(t/x)));
u2(u2<0)=0.01;
%MIXING CONSIDERED
h2(m+1,n+1)=(h2(m+1,n)+((3*u2(m+1,n)+3*u2(m,n+1))/4).*t/x.*h2(m,n+1)+G(m,n))/(1+
((u2(m+1,n)+u2(m,n+1))*3/4).*t/x);
if h2(m,n)>=0
h2_end(m,n)=h2(m,n);
else h2_end(m,n)=0;
h2(m,n)=h2_end(m,n);
end
if isnan(h2(m,n))==1
h2(m,n)=0;
end
H(1,2:SQQQ(2))=h1(1,2:SQQQ(2))+h2(1,2:SQQQ(2));
H(1:M,1)=H0;
H(m+1,n+1)=H(1,n+1)+(sf(2,n+1)-s0)*x*m;
h1(m+1,n+1)=H(m+1,n+1)-h2(m+1,n+1);
P1(1:SQQQ(1),1)=denfrew;
P1(1,2:SQQQ(2))=denseaw/(1+dets);
P2(1:SQQQ(1),1)=denfrew;
pt=1000*(1-(Temp+288.94)/(508929*(Temp+68.13)))*(Temp-3.986)^2;
S2(1,2:SQQQ(2))=(denseaw-pt)/(0.8245-4.1*Temp/1000);
S2(1:SQQQ(1),1)=0;
if isnan(h2(m+1,n+1))==1
h2(m+1,n+1)=.01;
end

```

```

    if u2(m+1,n+1)<=0 | h2(m+1,n+1)<=0
h2(m+1,n+1)=0.01;
u2(m+1,n+1)=0.001;
P2(m+1,n+1)=denfrew;
S2(m+1,n+1)=0;
else
h1m=(h1(m+1,n)+h1(m,n+1))/2;
h2m=(h2(m+1,n)+h2(m,n+1))/2;
%SALT TRANSPORT
P1(m+1,n+1)=(P1(m+1,n)+u1m(m,n).*P1(m,n+1).*(t/x)+G(m,n)*(p2(m,n)-
p1(m,n))/(h2m+h1m))/(1+(u1(m+1,n)+u1(m,n+1))/2).*(t/x));
P2(m+1,n+1)=(P2(m+1,n)+u2m(m,n).*P2(m,n+1).*(t/x)+G(m,n)*(p2(m,n)-
p1(m,n))/(h2m+h1m))/(1+(u2(m+1,n)+u2(m,n+1))/2).*(t/x));
P2(P2<1000)=1000;
P1(P1<1000)=1000;
S0=(denfrew-pt)/(.8245-4.1*Temp/1000);
S2(m+1,n+1)=(P2(m+1,n+1)-pt)/(.8245-4.1*Temp/1000);
S2(S2==S0)=0;
S1(m,n)=(P1(m,n)-pt)/(.8245-4.1*Temp/1000);
    end
end
end
h2_end;
n=L/x;
%GRAPH X AXIS IN TERMS OF DISTANCE X
X=(1:SQQQ(1))*x;
% GRAPH X AXIS IN TERMS OF TIME T
TDays=(1:SQQQ(2))*t/3600;
[dummy idx0] = min(abs(h2_end));
% DISTANCE AT STEADY STATE (MEAN + ONE SIGMA OF MAX DISTANCE AT TIME STEPS)
maxd_steady =mean(idx0)+std(idx0);
d_steady=mode(idx0);
distance_steady=d_steady*x;
maxdistance_steady=maxd_steady*x;
fd_steady=fix(d_steady);
[ col] = find(idx0 >=fd_steady);
time_step=col(1);
time_steady=time_step*t/24/3600;
time_steady=round(time_steady);

```

Appendix 2: Salinity measurements and GPS coordinates (local) of the sampling points

Date-29.09.2010

Sampling point		Depth to the sampling point	EC	TDS	Water temp	Environmental temp
P1	FD	2.77	17.54	8.75	29.6	28.2
	HD	1.35	2.86	1.42	29.6	28.2
P2	FD	3.53	11.87	5.94	29	
	HD	1.73	3.56	1.76	28.6	
P3	FD	3.48	7.26	3.62	30.2	
	HD	1.7	3.2	1.6	29	
P4	FD	3.81	20	10	29.3	
	HD	1.9	3.74	2.04	28.9	
P5	FD	3.81	20	10	28.8	
	HD	1.9	4.45	2.25	28.4	
P6	FD	7.01	20	10	28.8	
	HD	3.5	20	10	28.4	
P7	FD	7.98	20	10	29.4	
	HD	3.98	20	10	28.6	
P8	FD	4.11	20	10	28.6	
	HD	2.06	1.9	0.93	28.5	
P9	FD	3.2	1.65	0.82	28.7	
	HD	1.6	0.64	0.31	28.3	
P10	FD	2.72	0.09	0.04	28.3	
	HD	1.35	0.08	0.04	28.2	

Date-
23.12.2010

Sampling point		Depth to the sampling point	EC	TDS	Water temp	Environmental temp
P1	Surf		0.46	0.23	27.7	
	HD	1.73	0.7	0.35	26.7	
	FD	3.5	8.29	4.14	28.1	
P2	surf		0.21	0.1	27.2	
	HD	2.03	0.2	0.1	26.8	
	FD	4.2	0.36	0.18	27.5	
P3	surf		0.19	0.09	27	
	HD	2.06	0.19	0.09	27.2	
	FD	4.16	0.24	0.12	27.7	
P4	surf		0.18	0.09	27.4	
	in depth	1.22	0.17	0.08	27.6	
P5	surf		0.16	0.08	27.4	30.7
	in depth	2.11	0.16	0.08	27.6	
P6	surf		0.12	0.06	27.5	31.5
	in depth	1.22	0.12	0.06	27.2	
P7	surf		0.11	0.05	27.4	31.5
P8	surf		0.1	0.05	28.5	
P9	surf		0.11	0.05	27.8	

Date-5.1.2011

Sampling point		Depth to the sampling point	EC	TDS	Water temp	Environmental temp
P1	Surf		3.52	1.75	28.2	
	HD	1.8	11.31	22.62	28.3	
	FD	3.66	49.56	24.78	29	
P2	surf		2.46	1.23	27.7	
	HD	1.55	6.09	3.18	29.1	
	FD	3.12	33.06	16.53	28.3	
P3	surf		2.11	1.05	28	
	HD	2.06	10.77	5.37	29.1	
	FD	3.63	53.49	26.79	29.9	
P4	surf		1.75	0.88	28.3	
	HD	2.36	13.29	6.63	29.7	
	FD	4.75	51.54	25.77	29.4	
P5	surf		1.23	0.61	27.8	
	HD	3.86	38.43	19.2	29.3	
	FD	7.75	54.3	27.39	29.6	
P6	surf		0.56	0.26	28	
	HD	1.7	5.55	2.85	29.9	
	FD	3.43	25.8	12.81	29.4	
P7	Surf		0.29	0.14	27.8	
	HD	1.9	11.67	5.82	29.1	
	FD	3.81	23.55	11.79	29.7	
P8	surf		0.19	0.09	27.6	
	HD	3.4	3.1	1.55	27.2	
	FD	6.83	17.39	8.69	27.5	
P9	surf		0.27	0.13	27.9	
	HD	1.8	0.28	0.14	27.6	
	FD	3.6	2.23	1.11	27.7	
P10	surf		0.13	0.06	28.3	
	HD	1.98	0.12	0.06	27.8	
	FD	3.96	0.13	0.06	28	
P11	surf		0.05	0.11	28.2	
	HD	1.27	0.05	0.11	27.4	
	FD	2.56	0.11	0.05	27.6	
P12	surf		0.11	0.06	27.5	
	HD	2.18	0.11	0.05	27.3	
	FD	4.37	0.12	0.06	27.4	
P13	surf		0.11	0.05	27.6	
	HD	1.22	0.11	0.05	27.2	
	FD	2.46	0.11	0.05		
P14	surf		0.12	0.06	27.9	
	HD	0.86	0.11	0.05	27.4	
	FD	1.73	0.11	0.05	27.4	

Date-02.02.2011

Sampling point		Depth to the sampling point	EC (ms)	TDS(ppt)	Water Temp
P1	Surf		4.53	2.26	26.1
	HD	2.08	12.24	6.09	24.9
	FD	4.16	40.35	20.13	24.9
P2	surf		3.79	1.9	26.4
	HD	1.7	9.37	4.68	26.5
	FD	3.4	43.59	21.81	25.1
P3	surf		3.9	1.95	26.5
	HD	1.7	12.09	6.03	26.6
	FD	3.4	25.92	12.9	25.1
P4	surf		3.4	1.7	26.6
	HD	2.8	24.69	12.3	24.7
	FD	5.59	46.14	23.01	25.2
P5	surf		3.02	1.51	26.5
	HD	2.43	5.09	2.54	26.7
	FD	4.88	53.7	26.88	25.4
P6	surf		1.98	0.98	26.1
	HD	2.13	3.66	1.78	26.8
	FD	4.27	42.18	21.06	25.4
P7	Surf		1.54	0.76	26.7
	HD	1.83	3.1	1.54	26.8
	FD	3.66	42.9	21.45	25.8
P8	surf		0.84	0.41	26.6
	HD	3.66	32.4	16.17	26.1
	FD	7.31	54.36	27.33	26.1
P9	surf		0.73	0.36	26.9
	HD	2.08	5.13	2.55	26.6
	FD	4.16	40.83	20.37	25.6
P10	surf				
	HD				
	FD				
P11	surf		0.21	0.11	26.7
	HD	1.35	0.27	0.13	26.7
	FD	2.69	0.53	0.26	26.7
P12	surf		0.14	0.07	26.8
	HD	2.39	0.13	0.06	26.8
	FD	4.8	0.16	0.08	26.7
P13	surf		0.15	0.07	27
	HD	1.75	0.13	0.06	26.5
	FD	3.5	0.13	0.06	26.9
P14	surf				
	HD				
	FD				

Date-14.02.2011

Sampling point		Depth to the sampling point	EC (ms)	TDS(ppt)	Water Temp
P1	Surf		2.07	1.03	29.4
	HD	1.68	48.93	24.45	29.4
	FD	3.35	47.34	23.49	29.4
P2	surf		2.15	1.05	27.3
	HD	1.75	4.32	2.16	28.2
	FD	3.5	37.77	18.99	28.8
P3	surf		1.84	0.92	28.2
	HD	2.05	8.74	4.47	27.8
	FD	4.14	55.26	27.63	29.2
P4	surf		1.63	0.81	28
	HD	2.99	50.28	25.14	29.3
	FD	6.02	58.59	29.25	29.2
P5	surf		1.74	0.87	29
	HD	3.15	31.47	15.78	29.8
	FD	6.3	52.02	26.04	29.6
P6	surf		1.17	0.57	29.6
	HD	1.83	51.93	25.92	30.7
	FD	3.66	39.57	19.77	30.4
P7	Surf		1.08	0.52	29.7
	HD	2.01	39.69	19.89	30.2
	FD	4.04	58.2	29.16	30.3
P8	surf		0.66	0.32	28.4
	HD	1.93	6.11	3.04	27.9
	FD	3.86	52.92	26.46	29.6
P9	surf		0.35	0.18	29.1
	HD	4.09	1.31	0.64	28.4
	FD	7.67	52.41	26.22	29.9
P10	surf		0.21	0.1	29.5
	HD	1.8	0.57	0.29	28.4
	FD	3.61	1.51	0.75	28.9
P11	surf		0.15	0.07	29.3
	HD	2.39	1.29	0.6	30.2
	FD	4.77	16.85	8.49	28.8
P12	surf		0.16	0.07	30.4
	HD	1.42	0.15	0.07	29
	FD	2.89	0.31	0.15	28.6
P13	surf		0.13	0.06	29.2
	HD				
	FD	3.27	0.14	0.07	29.4
P14	surf				
	HD				
	FD				

Date-1.3.2011

Sampling point		Depth to the sampling point	EC (ms)	TDS(ppt)	Water Temp
P1	Surf		1.62	0.8	30.1
	HD	1.85	7.63	3.8	32.8
	FD	3.71	50.04	24.99	31.4
P2	surf		0.87	0.45	28.7
	HD	1.52	6.5	3.24	28.6
	FD	3.05	43.77	21.9	27.8
P3	surf		1.3	0.66	28.4
	HD	1.93	3.23	1.62	28.4
	FD	3.86	47.22	23.61	28
P4	surf		1.25	0.62	27.5
	HD	2.28	14.66	7.32	28.7
	FD	4.65	37.77	18.84	28
P5	surf		1.33	0.65	28.5
	HD	1.78	2.01	1	28.9
	FD	3.61	48	24	29.1
P6	surf		0.86	0.43	29.4
	HD	1.77	2.41	1.2	29.1
	FD	3.48	43.98	21.96	29.8
P7	Surf		0.68	0.34	29.2
	HD	1.7	1.68	0.84	29.2
	FD	3.45	38.73	20.01	30.8
P8	surf		0.56	0.28	28.8
	HD	3.61	45	22.5	30.6
	FD	7.24	44.43	28.26	30
P9	surf		0.42	0.21	30
	HD	1.73	1.36	0.68	29.2
	FD	3.45	43.65	21.81	30
P10	surf		0.3	0.15	29.9
	HD	2.23	10.09	5.05	29.6
	FD	4.48	38.58	19.35	29.9
P11	surf		0.21	0.1	29.9
	HD	1.12	0.81	0.4	29.4
	FD	2.23	4.18	2.8	29.7
P12	surf		0.16	0.08	30.2
	HD	1.52	0.14	0.07	29.8
	FD	3.05	0.16	0.08	29.6
P13	surf		0.13	0.06	31.7
	HD	1.47	0.14	0.07	29.8
	FD	2.95	0.14	0.07	29.4
P14	surf		0.15	0.07	31.1
	HD	1.04	0.14	0.07	29.4
	FD	2.08	0.14	0.07	29.6

Date-14.3.2011

Sampling point		Depth to the sampling point	EC (ms)	TDS(ppt)	Water Temp
P1	Surf		1.16	0.58	32.6
	HD	1.05	2.22	1.11	32
	FD	2.1	6.48	3.24	32.6
P2	surf		1.12	0.55	31.8
	HD	1.7	5.12	2.56	31
	FD	3.5	36.93	18.54	33.1
P3	surf		1.01	0.51	31.8
	HD	1.5	1.88	0.94	30.4
	FD	3.1	39.21	19.62	33.2
P4	surf		1.09	0.55	30.4
	HD	2.8	2.78	1.39	30.5
	FD	5.67	33.93	16.92	32.7
P5	surf		0.74	0.37	30.9
	HD	3.11	35.97	18.15	32.4
	FD	6.22	44.49	22.26	31.8
P6	surf		0.67	0.34	31.3
	HD	1.8	1.43	0.71	30.6
	FD	3.77	41.91	21.06	32.7
P7	Surf		0.46	0.23	31.2
	HD	1.8	1.38	0.69	30.4
	FD	3.7	40.02	20.07	32.9
P8	surf		0.41	0.2	30.7
	HD	3.7	26.67	13.32	31.4
	FD	7.52	35.52	17.64	31.8
P9	surf		0.4	0.2	32.8
	HD	2.8	1.36	0.72	30.7
	FD	5.68	34.26	17.16	32.4
P10	surf		0.25	0.12	31.4
	HD	2.2	10.59	5.3	30.6
	FD	4.45	39.15	19.56	33.6
P11	surf		0.3	0.14	31.9
	HD	1.4	1.21	0.61	31.1
	FD	2.92	28.68	14.37	33.2
P12	surf		0.16	0.08	32
	HD	1.7	0.14	0.07	31.1
	FD	3.41	0.16	0.08	31.2
P13	surf		0.14	0.07	31.3
	HD	1.8	0.14	0.07	30.5
	FD	3.72	0.15	0.07	30.9
P14	surf				
	HD				
	FD				

Date-6.4.2011

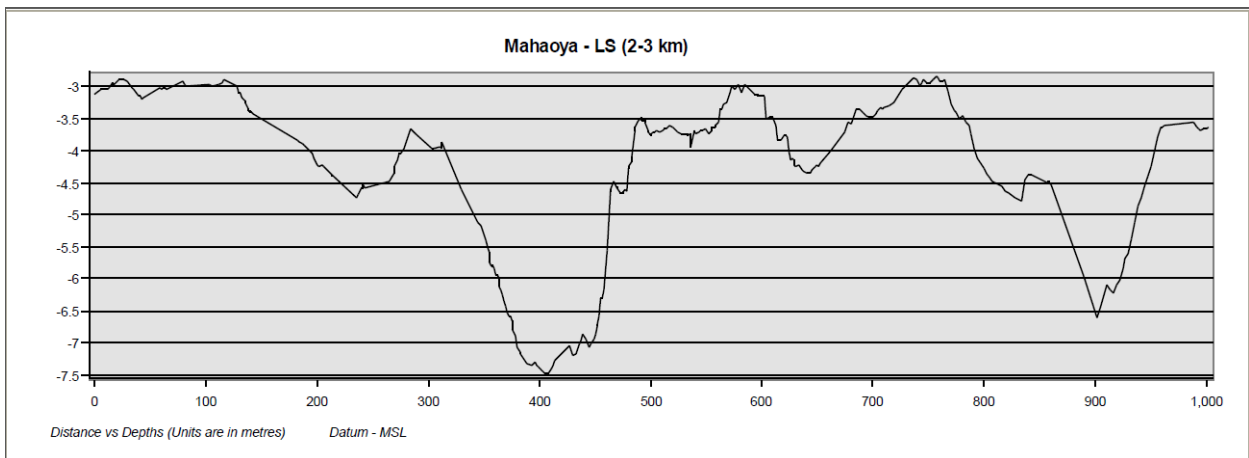
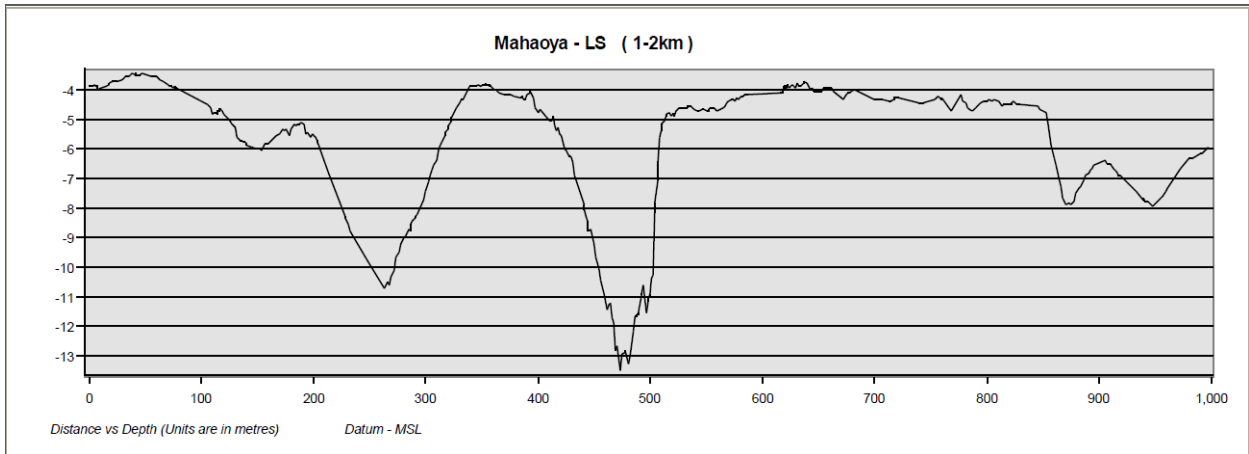
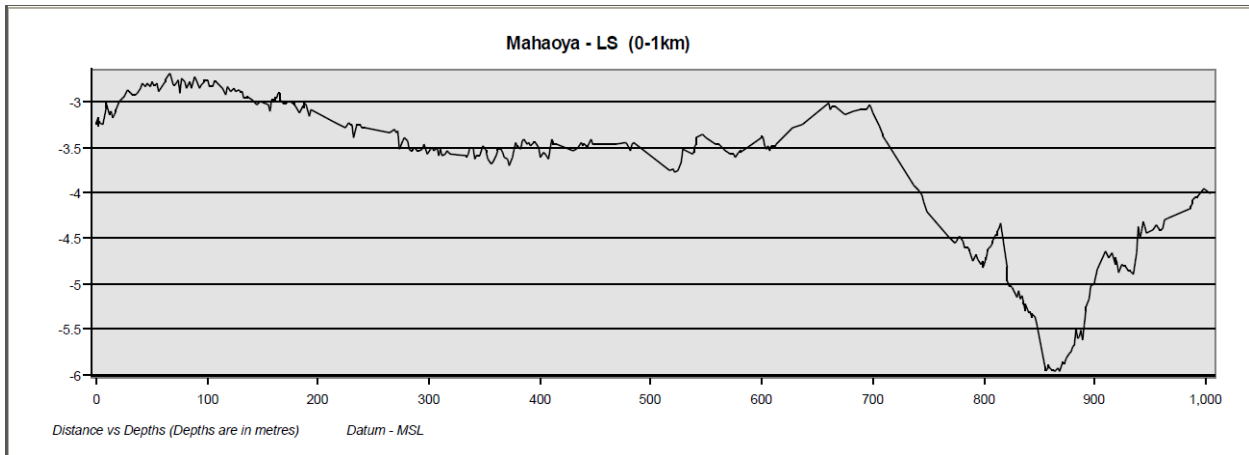
Sampling point		Depth to the sampling point	EC (ms)	TDS(ppt)	Water Temp
P1	Sur		4.75	2.37	32.5
	0.5m from surface	0.5	8.62	4.3	31.3
	1m from surface	1	24.96	12.51	32.2
	1.5m from surface	1.5	35.31	17.64	32.6
	FD	2.13	45.03	22.47	32.1
P2/2	surf		4.95	2.47	32.1
	0.5m from surface	0.5	6.55	3.28	32.3
	1m from surface	1	14.41	7.2	31.6
	1.5m from surface	1.5	29.37	14.7	33.2
	FD	2.62	49.29	24.66	32.8
P2	surf		5.22	2.61	31.6
	0.5m from surface	0.5	6.76	3.38	31.3
	1m from surface	1	18.9	9.45	33.1
	1.5m from surface	1.5	26.7	13.32	32.9
	FD	2.78	45.21	22.56	32.9
P3	surf		3.37	1.69	32.6
	0.5m from surface	0.5	4.73	2.42	31.2
	1m from surface	1	25.8	12.84	32.3
	1.5m from surface	1.5	33.93	16.95	32.6
	FD	5.62	49.26	24.6	33.2
P4	surf		2.56	1.26	33.2
	0.5m from surface	0.5	3	1.54	32.1
	1m from surface	1	17.39	8.69	32.1
	1.5m from surface	1.5	32.64	16.32	33.5
	FD	5.95	40.98	20.49	33.7
P6	surf		1.5	0.75	35
	0.5m from surface	0.5	3.22	1.61	32.4
	1m from surface	1	7.04	3.5	31.9
	1.25m from surface	1.25	10.72	5.35	35.1
	1.5m from surface	1.5	36.18	18.12	34.9
FD	3.94	48.84	24.42	35	
P8	Surf		0.98	0.5	33.9
	1m from surface	1	2.08	1.04	31.6
	1.1m from surface	1.1	10.85	5.48	31
	1.25m from surface	1.25	18.43	9.22	31.3
	1.5m from surface	1.5	25.74	12.87	32.9
FD	7.26	30.33	15.39	32.3	
P10	surf		0.69	0.35	33.9
	1m from surface	1	2.49	1.22	32.7
	1.1m from surface	1.1	17.28	8.63	32.5
	1.5m from surface	1.5	36.72	18.39	34.6
	FD	4.35	43.05	21.51	34.6
P12	surf		0.21	0.1	33.5
	1m from surface	1	1.23	0.61	33.5
	1.25m from surface	1.25	1.56	0.77	31.2
	1.35m from surface	1.35	3.44	1.72	
	1.5m from surface	1.5	19.91	9.64	31.9
FD	1.9	37.8	18.96	35	
P13	surf		0.23	0.11	31.1
	FD	4.78	0.2	0.1	31.5
Between P12 and P13	surf		0.18	0.09	34
	FD	6.84	3.62	1.8	31.6
Table continue Midpoint between P12/2 and	surf		0.23	0.11	

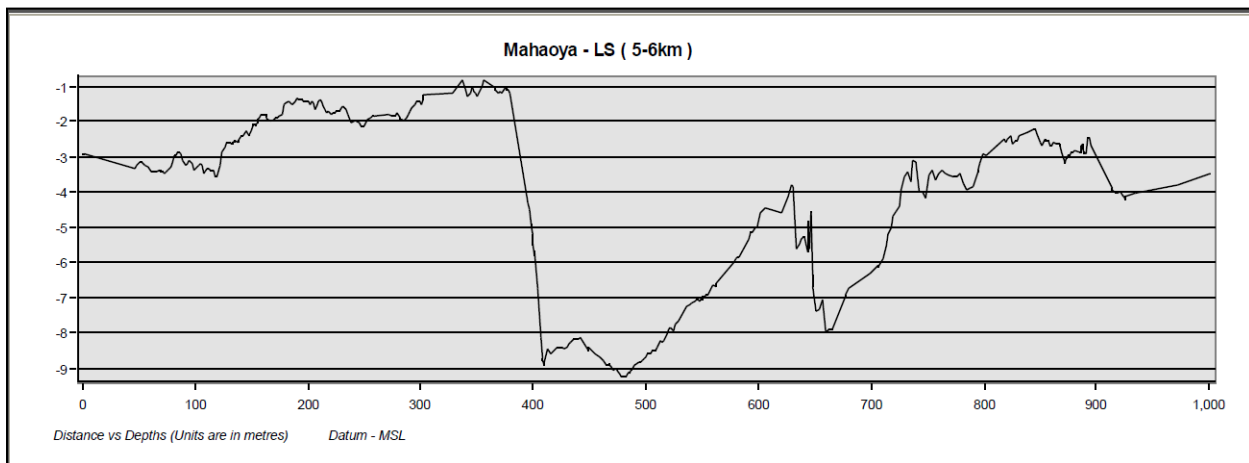
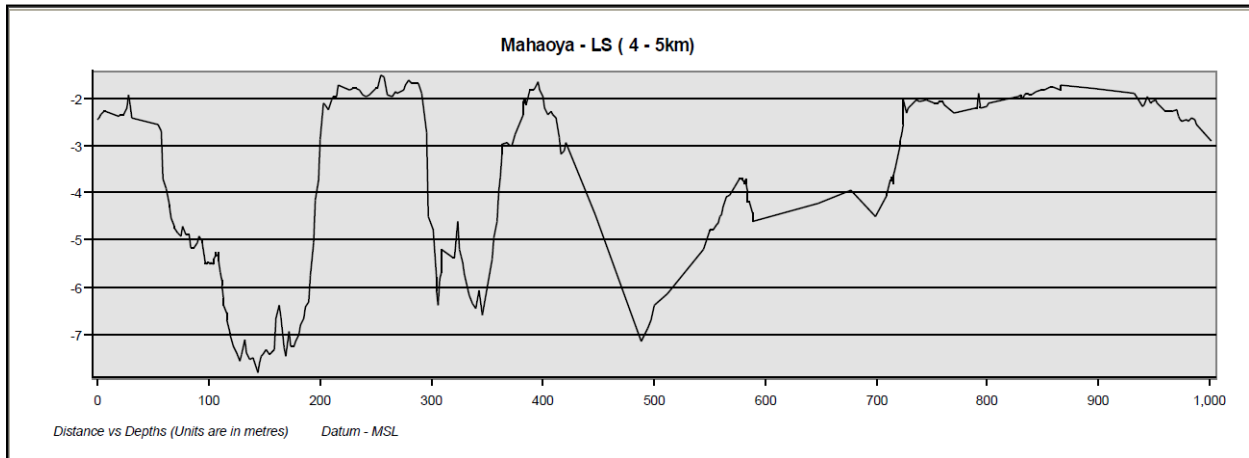
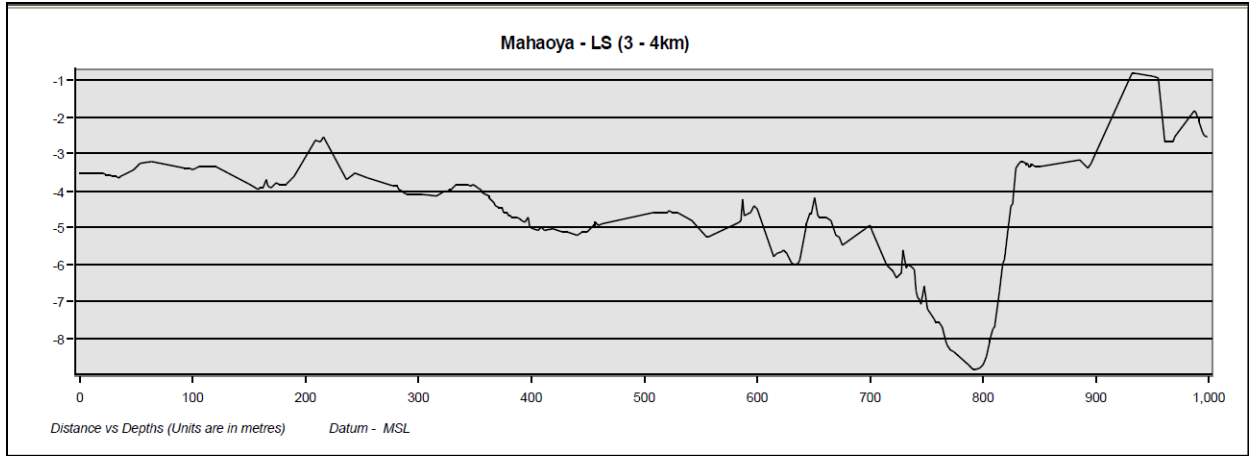
P12	1m from surface	1	1.53	0.76	32.1
	1.25m from surface	1.25	1.16	0.57	32
	1.5m from surface	1.5	7.61	3.8	31.5
	FD	1.92	37.29	18.66	33.1
Midpoint between P12/2 and P13	surf		0.17	0.08	32.2
	HD	3.95	0.51	0.25	30.9
	FD	7.9	3.64	1.81	31.6

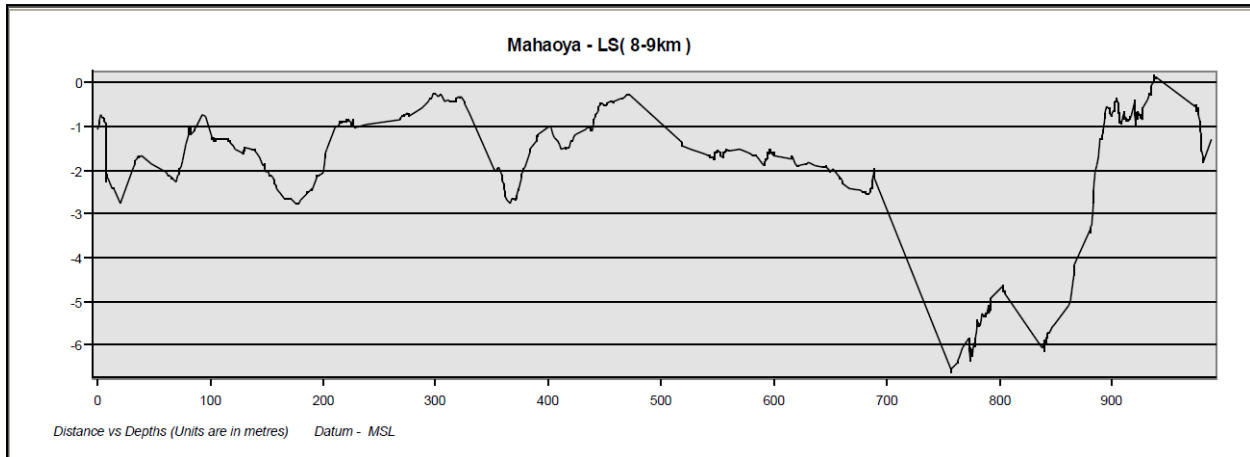
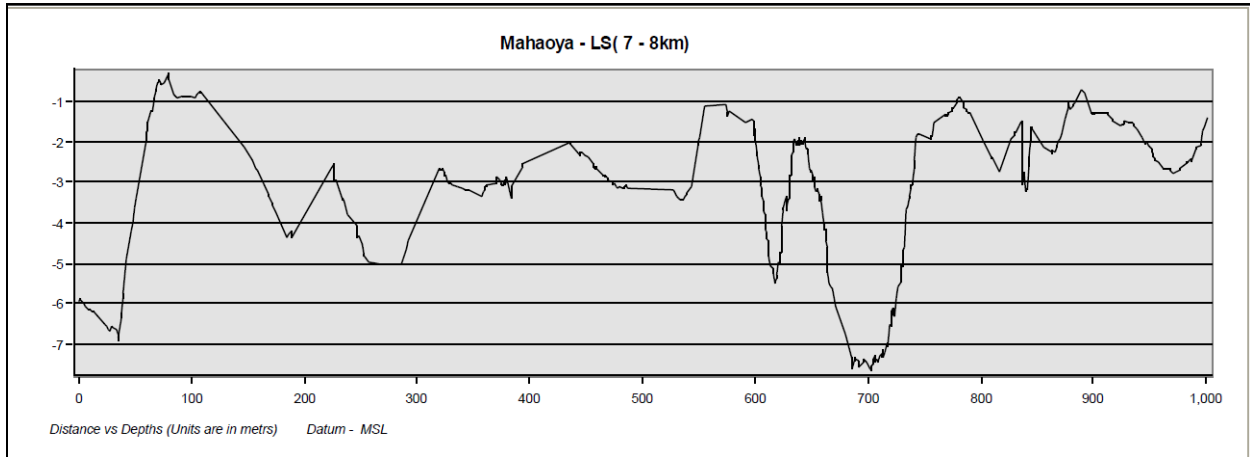
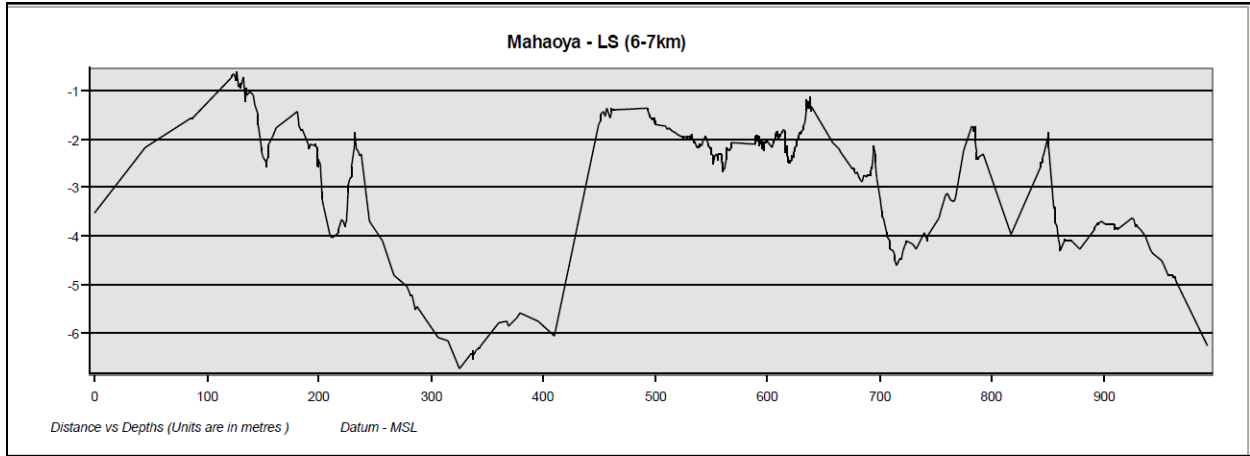
GPS coordinates (Local) of the measuring points

Point	Location	
	x coordinates	y coordinates
P2	97574	604129
P3	97822	604119
P4	98075	604123
P5	98279	604279
P6	98781	604289
P7	99055	603871
P8	99575	603947
p9	100033	604237
P10	100224	604696
P11	100449	605142
P12	100945	605225
P13	101399	605007
P14	101783	604349

Appendix 3: Longitudinal sections of the Maha Oya







Appendix 4: Current meter readings and flow calculation at gauge reading 1.62 m

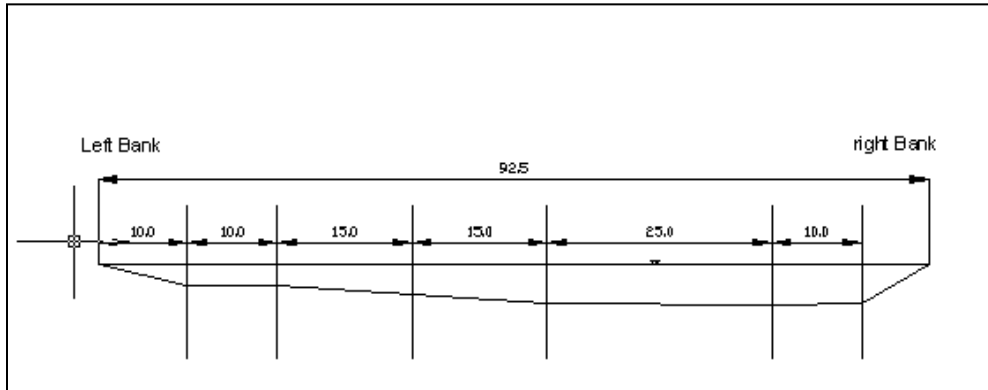


FIGURE 4A: CROSS SECTION OF THE RIVER WHERE CURRENT METERING WAS DONE AT BAMBUKULIYA

10m from the left bank				20m from the left bank				35m from the left bank			
depth	velocity	area	discharge	depth	velocity	area	discharge	depth	velocity	area	discharge
30	0.066	8.18	0.53988	45	0.056	8.44	0.47264	65	0.12	14.63	1.7556
90	0.075	5.57	0.41775	90	0.171	5.62	0.96102	130	0.165	10.13	1.67145
130	0.086	4.04	0.34744	135	0.102	6.63	0.67626	200	0.131	9.75	1.27725
180	0.106	4.37	0.46322	180	0.035	10.09	0.35315	260	0.112	14.33	1.60496
			1.76829				2.46307				6.30926

50m from the left bank				75m from the left bank				85m from the left bank			
depth	velocity	area	discharge	depth	velocity	area	discharge	depth	velocity	area	discharge
85	0.03	26	0.78	90	0.039	23.62	0.92118	85	0.055	14.49	0.79695
170	0.119	16.75	1.99325	180	0.14	15.75	2.205	170	0.06	8.05	0.483
255	0.126	17	2.142	270	0.15	15.75	2.3625	255	0.045	6.76	0.3042
340	0.148	24.33	3.60084	360	0.093	20.56	1.91208	340	0.053	7.75	0.41075
			8.51609				7.40076				1.9949

Total flow = 28.5 cum/s

